A feasibility study into the application of low-fidelity models for the prediction of the shell modes of a wind turbine tower with a slip joint.

Jeroen Seegers
4219473

June 2022

Alessandro Cabboi
Alice Cicirello
Oriol Colomes Gene
Sergio Sánchez Gómez

Offshore Engineering
Delft University of Technology

Abstract

The slip joint connection is a relatively new alternative method for connecting offshore wind turbine towers to prior installed monopiles. It consists of two overlapping conical sections that together form a connection. There are several challenges left to be solved before the slip joint can be applied on a commercial scale. One of those challenges lies in the decommissioning process of the slip joint connection. It is proven that build-up settlement can increase the friction force within the joint over its lifetime and complicate its disconnection. One potential method for reducing the friction force in the slip joint is the excitation of one of the structures shell modes localized around the slip joint. Good estimations of the shell modes of the structure are therefore essential. Models for precise estimation of the shell modes of a wind turbine with a slip joint are difficult and expensive to develop due to the complexity of the joint. This thesis is a study into the possibility of using simplified finite element models to estimate the shell modes of a wind turbine connected with a slip joint. This is done by estimating the shell modes of the structure using a reference model and seven simplified models in a modal analysis. The estimated shell modes are compared based on their eigenfrequency and mode shape. Based on this comparison, conclusions about the applicability of simplified models are drawn. The first 300 eigenmodes of the structure are estimated with both the reference model and simplified models. Of these eigenmodes, ten shell modes of interest are selected based on their eigenfrequency and location at which the modes are localized. The modes of interest are than compared for their eigenfrequency and mode shape. The mode shapes are compared based on the Modal Assurance Criterion (MAC), which is calculated at a specific location of interest. In addition to this, the angle in which the modes are orientated is measured and compared, as this can be useful information for the decommissioning process. Results showed that three out of seven simplified models studied resulted in a estimation of the shell modes which was sufficiently accurate. The simplifications used for these models consist of the averaging of wall thickness for the upper and lower slip joint and a simple model for the upper slip joint. From these results it can be concluded that some of the simplifications can be applied when estimating shell modes of a wind turbine tower connected with a slip joint, as they lead to only a small decrease in accuracy of the shell mode estimation. However, using these results to make predictions about other potential simplifications is challenging as each different simplification has a unique influence on the estimation of the shell modes.

Preface

This thesis marks the end of my adventure studying at the Technical University of Delft. It not only tested my engineering skills, but also my skill in researching. During my time studying at this university I always had special interest in finite element modelling and vibration analysis. This is also the reason I chose my thesis subject to be the estimation of shell modes using finite element models. Solving problems which are too difficult to be solved using analytical equations always seemed interesting and challenging to me. Also, the slip joint is a relatively new concept with many unanswered questions. Efforts are being made to research and develop the slip joint concept and apply it to offshore wind turbines. With the ever growing demand in sustainable energy, it is good to know that the efforts put into this thesis might have a ever so small contribution towards a more sustainable future. This thesis is meant for anyone with an interest in the slip joint concept, the shell modes of a wind turbine tower or the finite element modelling process of an offshore wind turbine tower.

I want to thank my committee for the good guidance I have received during my thesis. Many times have they provided useful information to help guide me in the right direction. Special thanks go out to my supervisor, Alessandro Cabboi, with whom I have had many meetings and provided me with excellent guidance and advice during the entirety of the thesis.

I also want to thank family and friends, who were always ready to help me in whatever way they could. Special thanks go out to Nick Dekkers, who has put in a lot of effort to motivate me until the thesis was complete.

Contents

List of Figures

List of Tables

Chapter 1

Introduction

With the ever growing demand in energy and increasing awareness of its environmental impact, the need for renewable energy is increasing rapidly. One of the many possible sources of renewable energy are wind turbines. Wind turbines can be installed on land, but due to their large size this option is becoming less preferred. An alternative is to install them offshore, where they are less obstructing to our society. Offshore wind turbines are often installed onto monopiles which are embedded in the seafloor. The structures can be connected using various methods. A relatively new method in development for connecting the wind turbine tower and the monopile is the slip joint. An example of a slip joint used for connecting a wind turbine can be seen in Figure 1.1.

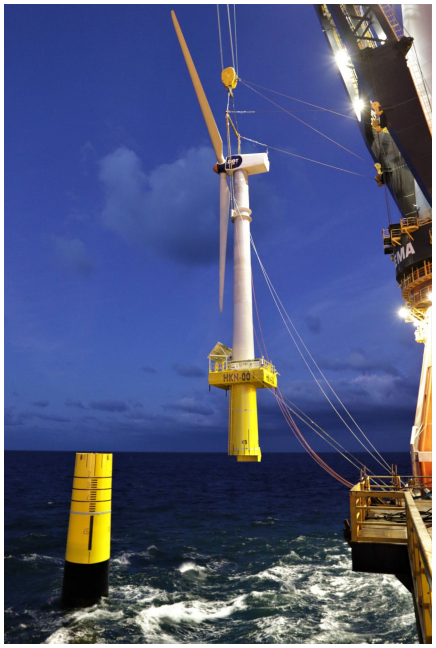

Figure 1.1: Example of a slip joint. [28]

Two important events in the lifecycle of a wind turbine are the installation and decommissioning phase. Both events allow little room for error and need to be well prepared. Decommissioning a wind turbine connected with a slip joint brings forth new challenges. One of those challenges is to overcome the high friction force within the joint to achieve disconnection. One potential solution to reduce the friction force within the joint is the introduction of vibration into the structure. Especially the excitation of high frequency shell modes of the structure is of interest. The estimation of high frequency shell modes can be a challenging task. High-fidelity models for the prediction of vibration and friction force in the slip joint are difficult and expensive to develop due to the complexity of the problem. The possibility of using simplified models to make predictions about the behaviour of the slip joint is therefore of interest. In this thesis, the shell modes of a wind turbine tower with a slip joint are estimated using the finite element method and modal analysis. The goal of this thesis is to study how much the estimation of shell modes is influenced by simplifications applied to the finite element model.

1.1 The slip joint connection

One of the most common methods to install offshore wind turbines is placing them onto pre-installed monopiles which are embedded in the seafloor. Conventionally, the tower and monopile are connect using either a grouted connection or bolted flanges. Over time, both connections have shown drawbacks [13, 20]. The grouted connections can experience wear during its lifetime, which decreases the axial capacity of the structure. In some cases this even lead to failure of the wind turbine. The bolted flanges can experience loss of tension and require increased monitoring and maintenance. An alternative solution in development for connecting the wind turbine to the monopile is the slip joint connection.

A slip joint consists of two conical sections that overlap each other, forming a connection solely based on the contact and friction between them, see Figure 1.2. The simplicity of the connection and its installation makes it a very interesting alternative for connecting a wind turbine to a monopile.

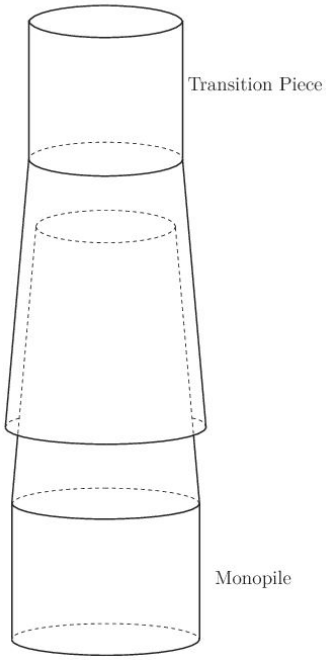

Figure 1.2: The slip joint concept. [26]

The slip joint is not a new concept as it was already applied in an onshore wind turbine, which was installed in 1995 [29]. However, it has never seen wide commercial use and needs to be research extensively before they can be regularly applied in offshore wind turbines. Efforts in developing the slip joint connection for offshore applications are being made by DOT (Delft Offshore Turbine) and TUD (Delft University of Technology).

1.2 Slip joint decommissioning

A wind turbine is decommissioned at the end of its lifecycle. For a wind turbine tower connected with a slip joint this can be achieved by disconnecting the slip joint and removing the tower from the monopile. The weight of the tower and the friction force present in the slip joint have to be overcome for disconnection of the joint. However, due to the build-up of settlement and corrosion, the friction force within the joint increases over the lifetime of the wind turbine. The simplest solution to overcome the friction force is to increase the force applied to the slip joint until disconnection. Previous research into the decommissioning of slip joints is provided by A. Cabboi et al.[12]. This paper provides an estimation for the force required to achieve disconnection, see Figure 1.3. Decommissioning tests showed that the required force can attain values equal to several times of the self weight of the structure. Applying this level of force to the tower and slip joint can lead to unsafe situations and can possibly damage the joint and/or equipment. Measures for reducing the friction force present in the joint are therefore practically essential for the decommissioning of wind turbine connected with a slip joint.

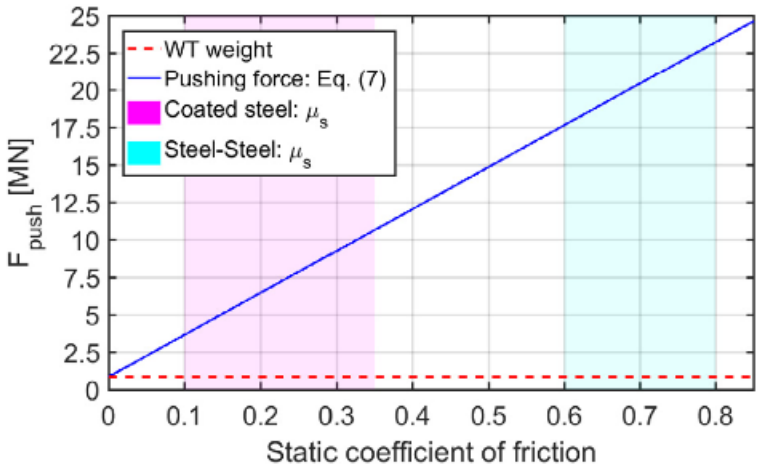

Figure 1.3: Estimation of the required pushing force. [12]

1.2.1 Vibration assisted reduction of friction

One method considered for reducing the friction force in the slip joint is the introduction of vibration to the system. Reducing friction force by introducing vibration is not a new phenomenon and can even be a bit intuitive. For example, an object on a tilted surface that is initially at rest can be made to slide down by vibrating the surface slightly, without further increasing the angle of the surface. Experiments from as early as the '60s [15] have shown that friction can be reduced by applying vibration. Multiple attempts to explain this phenomenon have been made but a general consensus on how this phenomenon should be addressed does not yet exist. Nonetheless, facilitating the decommissioning of a slip joint by introducing vibration and thus reducing friction force in the joint promises to be an interesting option, as was also presented in the paper by Cabboi et al. [12].

This paper describes the decommissioning of a 500 kW DOT500 wind turbine that was assisted by introducing vibration to the structure, with the goal of reducing the friction force in the slip joint and therefore reducing the force required to disconnect the joint. In this study, the eigenfrequencies and mode shapes of the wind turbine tower were identified by a field hammer test and experimental modal analysis. The results were compared with numerical results obtained from a finite element model of the wind turbine tower. During the decommissioning test a vertical force was applied with jacks and the estimated resonance frequencies were excited one by one. The excitation was caused by shakers which were placed on the structure. The pushing force, applied by the hydraulic jacks, was measured during the experiment. Disconnection of the slip joint occurred around a excitation frequency of 53 Hz. Figure 1.4 shows the pushing force and excitation frequency of a decommissioning attempt.

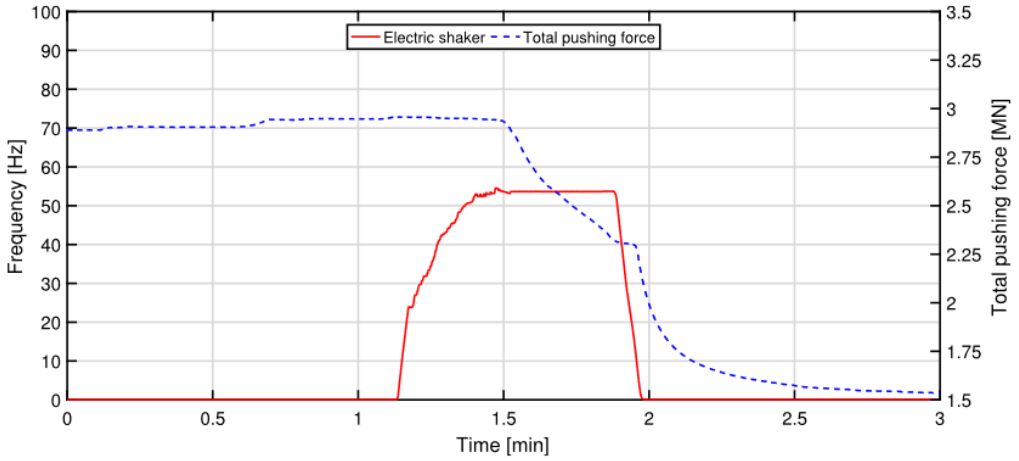

Figure 1.4: Pushing force and frequency of a successful decommissioning attempt. [12]

This figure clearly shows a constant pushing force that reduces after vibration was introduced. The reduction in pushing force is caused by displacement of the slip joint. These results show that the introduction of vibration can reduce the friction force in the slip joint and can be a potential tool in facilitating the decommissioning phase of a slip joint.

1.2.2 Shell mode estimation

The reduction of friction by the introduction of vibration is a phenomenon that is not yet fully understood, as will be discussed in Section 2.4. Further research is required if vibration is to be utilized for the decommissioning of wind turbines with a slip joint. The most effective way to vibrate a structure is by trying to excite one of its eigenmodes, as resonance will amplify the motion of the structure. The structure can be excited by installed shakers. Excitation of specific eigenmodes requires precise shaker placement and tuning. In this case it is essential to have good estimations of the eigenmodes of the structure. In theory, a wind turbine has infinite eigenmodes. Usually, only the first few eigenmodes are of interest. This is due to these eigenfrequencies being close to environmental excitation frequencies. However, it is not yet known which type of eigenmodes would

be most effective in reducing the friction force present in the joint. A hypothesis by A. Cabboi [11] predicts that shell modes which are localized around the slip joint are the most effective for reducing the friction force within the joint. This hypothesis is based on the idea that exciting a high frequency shell mode, localized right above the slip joint, could significantly alter the contact stress distribution within the slip-joint, facilitating a decrease of the friction force within the surfaces in contact. The decommissioning tests discussed by A. Cabboi et al.[12] showed that the slip joint disconnected at a frequency of 53 Hz, which supports this hypothesis. To assist future efforts towards studying this hypothesis, this thesis will mainly focus on the estimation of the high frequency shell modes of a wind turbine tower with slip joint connection.

1.2.3 Finite Element Method (FEM)

There are several methods to estimate the eigenmodes of a structure. The eigenmodes of simple structures can often be estimated using simple analytical models. However, analytical models quickly get complicated when the complexity of the structure increases, as governing equations quickly become to difficult to be solved. In this case, the problems are usually studied with experimental and/or numerical methods, as these methods are usually better in dealing with complicated problems. Experimental methods provide a good representation of reality but can be difficult and expensive, depending on the problem analysed. For example, studying the decommissioning of a slip joint is difficult to do with solely experimental methods. The decommissioning of a wind turbine tower with slip joint is a big and costly operation and therefore can't easily be repeated. Besides, the same experiment can only be executed once due to the internal stresses within the joint, which were build up over its lifetime and can't be easily reproduced. Therefore, experimental research is often assisted by numerical methods. Numerical methods provide approximations for mathematical problems. These models can be solved with computers and often quicker and cheaper than experimental methods. One of the most popular numerical approaches is the Finite Element Method (FEM). With FEM, a model of the structure is created and discretized into smaller elements, which can be solved individually. Combining these individual results provides an estimation of the results of the complete structure. FEM can also be used to analyse the vibration properties of a wind turbine tower connected with a slip joint.

1.2.4 Low fidelity FE models

There are many choices to be made during the development of an finite element model. Each choice can potentially have a large effect on the accuracy of the results. One important choice in the development of FE models is the level of detail that should be applied in the model. Not every single detail present in the wind turbine needs to be included in the FE model, as they might hardly/not have any influence on the results of the analysis. The level of detail which is sufficient depends on the goal of the analysis and is not always known in advance. Development of a high fidelity FE models can be very difficult and expensive and might not always be the best approach. Low fidelity models can often provide sufficiently accurate results. A high fidelity model to analyse the decommissioning of a wind turbine connected with a slip joint assisted by vibration would likely be difficult and costly to developed due to the complex behaviours of the slip joint. It therefore is interesting to consider the option of using low fidelity models to aid in studying this problem. High and low fidelity finite element models will be further discussed in Section 2.1. This thesis aims

to assess the applicability of simplified FE models for the estimation of the shell modes of a wind turbine tower with slip joint.

1.2.5 Modal analysis

The eigenmodes of a structure can be estimated using modal analysis. Modal analysis also stands at the base of many other types of vibration analysis. The estimation of shell modes with a modal analysis is not the final goal of the vibration analysis of the wind turbine. Modal analysis is an extremely useful type of analysis but also has limits, mostly due to it being a linear analysis. Some of the properties of the slip joint can therefore not be included in this analysis. For example, modelling the contact within the joint results in a non-linear model, which can't be used in a modal analysis. More precise vibration analysis requires a more complicated model and another type of analysis, like a transient vibration analysis. These other methods often require far more computational power, due to the inclusion of the non-linearities in the FE model. The use of low fidelity models would be especially beneficial for these types of methods, as much computational time might be saved. This thesis is an initial study into whether or not simplified models can be applied when the shell modes of a wind turbine connected with a slip joint are of interest. Showing how the use of simplified models can affect the results of a modal analysis is a first step into the study of using simplified models in one of the other types of vibration analysis.

1.3 DOT6000FOX - Offshore wind turbine

The offshore wind turbine studied in this thesis is provided by Delft Offshore Turbines (DOT). The wind turbine is shown in Figure 1.5.

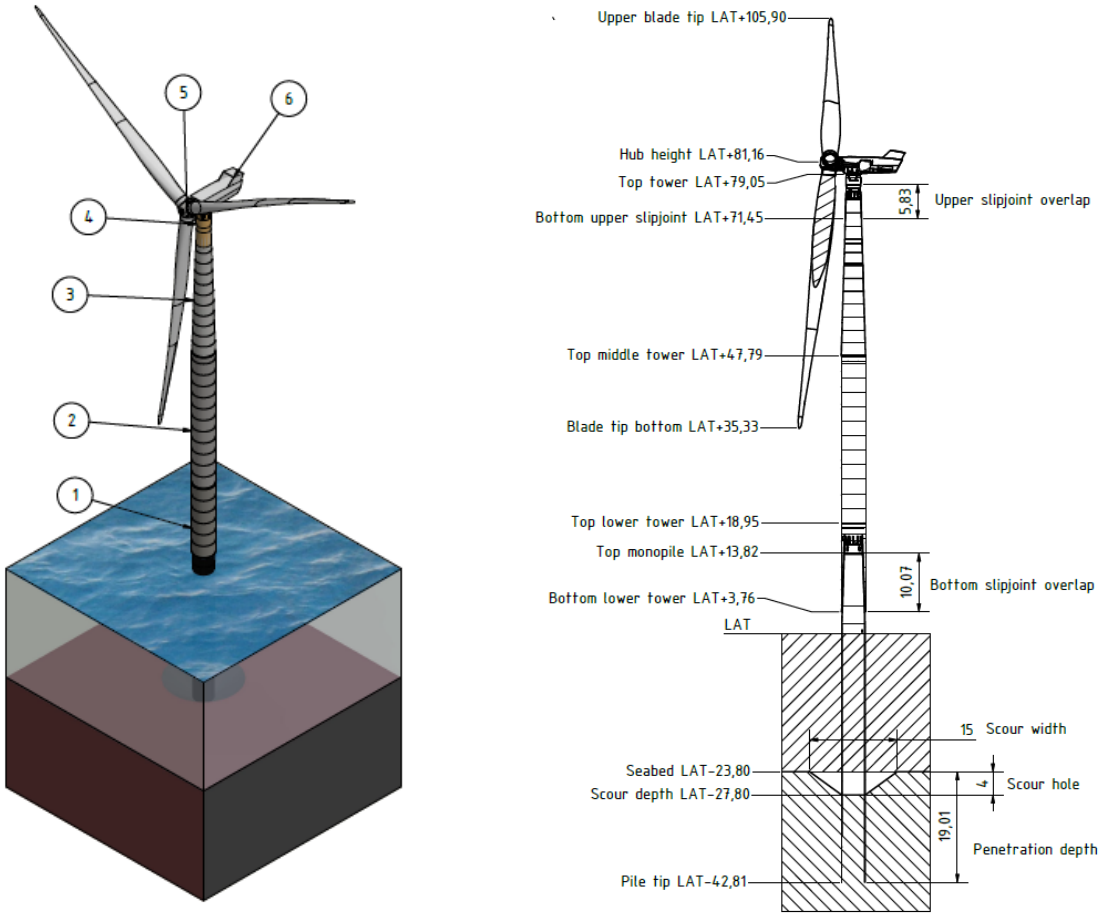

(a) 3d model of the offshore wind turbine.

(b) Side view of the offshore wind turbine.

Figure 1.5: DOT6000FOX offshore wind turbine.

The wind turbine tower includes two slip joints, indicated with numbers 1 and 4 in Figure 1.5a. One is located just above sea level and the other is located below the hub of the turbine. Detailed views of the slip joints are shown in Figure 1.6.

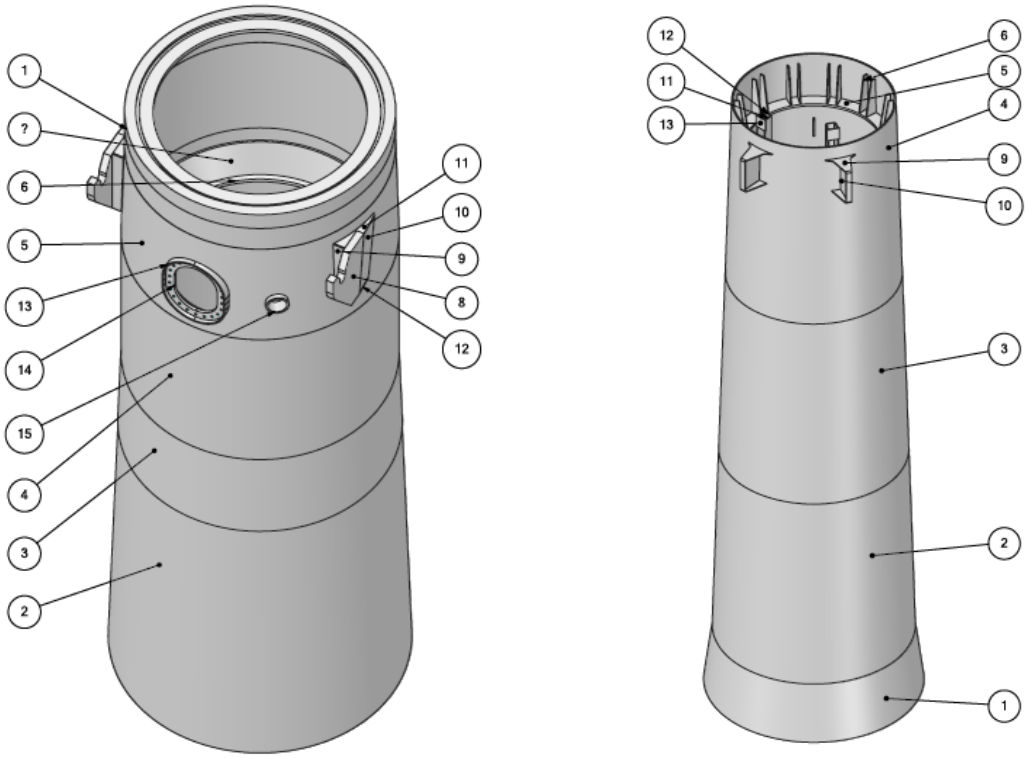

(a) Upper slip joint geometry.

(b) Lower slip joint geometry.

Figure 1.6: DOT6000FOX offshore wind turbine

This is a good wind turbine for this study since it includes two slip joints. Each slip joint has a unique geometry and is located in a unique location, meaning that they are likely to also provide unique results in regard to the estimation of the shell modes.

1.4 Scope and research questions

The previous section introduced the research opportunities for this thesis. The decommissioning of a wind turbine tower with a slip joint is complicated by high friction force within the joint. This can potentially be solved by exciting one the structures shell modes localized around the slip joint. The shell modes can be estimated with the finite element method using modal analysis. It is not known which level of detail needs to be applied to the finite element model to obtain a reasonably accurate estimation of the shell modes. Being able to use a simplified finite element models to estimate the shell modes of the wind turbine tower is also potentially beneficial for further studies in regard to the vibration of slip joints. The main research question for the thesis reads a follows:

How do simplifications applied to a finite element model of a wind turbine connected with a slip joint affect the estimation of the structures high frequency shell modes using modal analysis?

This question can be divided into multiple sub-questions, which are meant to help answer the main question.

- *How can the higher fidelity reference model be developed to provide a good estimation of the shell modes of the wind turbine tower connected with a slip joint?*
- *What are the eigenmodes of the wind turbine tower and which of these are the most interesting for comparing the reference model and simplified models?*
- *Which sort of simplifications are most interesting to be applied to finite element model of the wind turbine tower with slip joint?*
- *How can the results of the higher fidelity reference model be compared to the results of the low fidelity simplified models?*

1.5 Research strategy

This section will discuss the strategy deployed to answer the main and sub research questions. The first step taken is a review of modelling strategies. This review discusses common strategies for modelling offshore wind turbines. Then, it is studied how certain modelling choices in the development of the reference model might influence the results of a modal analysis. This preliminary study provides a first insight into the modelling process and how the modelling choices can affect the estimation of the eigenmodes. The next step is the development of the reference FE model of the wind turbine with slip joint. This model will be used as a reference point for comparing the results of the simplified FE models. Then, a method for comparing the results of different FE models is be developed. Each finite element model will estimate the first 300 eigenmodes of the structure. It is discussed which of these modes will be selected for the comparison to follow and how these modes will be compared to the eigenmodes of the simplified models. To aid the comparison, a Modal Assurance Criterion (MAC) script is developed for the quantitative comparison of the estimated mode shapes. The next step is the development and comparison of the simplified models. Seven simplified models are developed and the shell modes resulting from these models are compared to the shell modes obtained with the reference model. The comparison of the different models can provide insights in the applicability of simplified FE models for the estimation of high frequency shell modes of a wind turbine connected with a slip joint.

1.6 Chapter overview

Chapter 2 reviews common modelling strategies for wind turbine towers when estimating the eigenmodes of the structure. Chapter 3 consists of a preliminary study into the modelling of wind turbine towers and slip joints. This study aims to provide an initial overview into which details and parameters can be important when evaluating the eigenmodes of a wind turbine tower. Chapter 4 introduces the reference model for the comparison. It explains how this model is developed and which modelling choices were made. Chapter 5 discusses how the estimated eigenmodes can be compared with each other. It includes the development of the MAC script which will be used to compare the mode shapes of the different eigenmodes. It also explains which of the eigenmodes will be used for comparison. Chapter 6 shows and discusses the results of the comparison of the reference model and the simplified models. Chapter 7 is the final chapter and includes the conclusion which can be drawn based on the results. It also includes a discussion of the results and the methods used to obtain these results. Lastly, this chapter provides a few recommendations for future research.

Chapter 2

Review of modelling strategies

Modelling a offshore wind turbine (OWT) is not a new phenomenon and is an essential part of the design cycle of these systems. OWT's are complex structures that consist of multiple sub-parts and are affected by various environmental loads. There are several papers and guidelines available which describe common approaches for modelling of OWT's [24][30][7]. Depending on the goal of the model some details can be simplified. This section discusses the modelling choices described in literature and describes how they will be applied in the FE model of the wind turbine used in the thesis.

2.1 High and low fidelity models

Highly detailed FE models or simplified FE models are also known as high and low fidelity models. High fidelity models are accurate but expensive models, which can be used to analyse problems. A high fidelity model, which estimates high frequency shell modes of a wind turbine connected with a slip joint, is very likely to be complex and costly. An alternative would be the use of low fidelity models, which are inexpensive and less accurate. Depending on the goal of the analysis the use of low fidelity models can be a good substitute for the expensive high fidelity models. One simple example of high and low fidelity models is the estimation of the first few natural frequencies of a wind turbine tower, as shown in Figure 2.1.

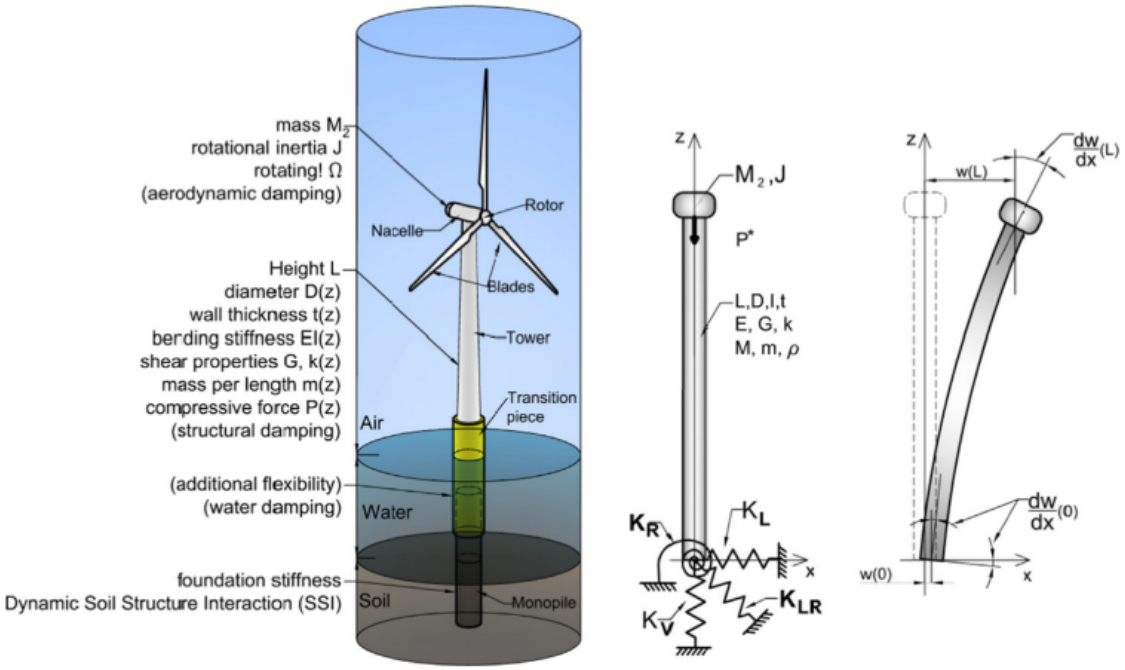

Figure 2.1: Offshore wind turbine vs. low fidelity model. [6]

This figure shows an illustration of a offshore wind turbine with multiple important parameters. A high fidelity model of this wind turbine can be complex. Instead, the natural frequencies are estimated with a fast and reasonably accurate low fidelity model. For example, the wind turbine can be approximated as a Euler-Bernoulli beam with three springs to model the soil structure interaction [6].

A more direct example of the difference between high fidelity and low fidelity models of an offshore wind turbine is studied in a paper by A. Jacomet et al.[17]. This paper studies the difference in the results of three wind turbine tower models, each with a different level of detail. The first model assessed is a simple 3D model of the tower, see Figure 2.2a. The geometry of the tower is simplified and the soil-structure-interaction is ignored by clamping the tower at its lowest point. In the second model, the soil-structure-interaction is included by also modelling the surrounding soil. In the third model, the geometry of the transition piece of the tower is modelled in high detail, as shown in Figure 2.2b. The grouted connection and bolted flanges are modelled to represent reality as close as reasonably possible.

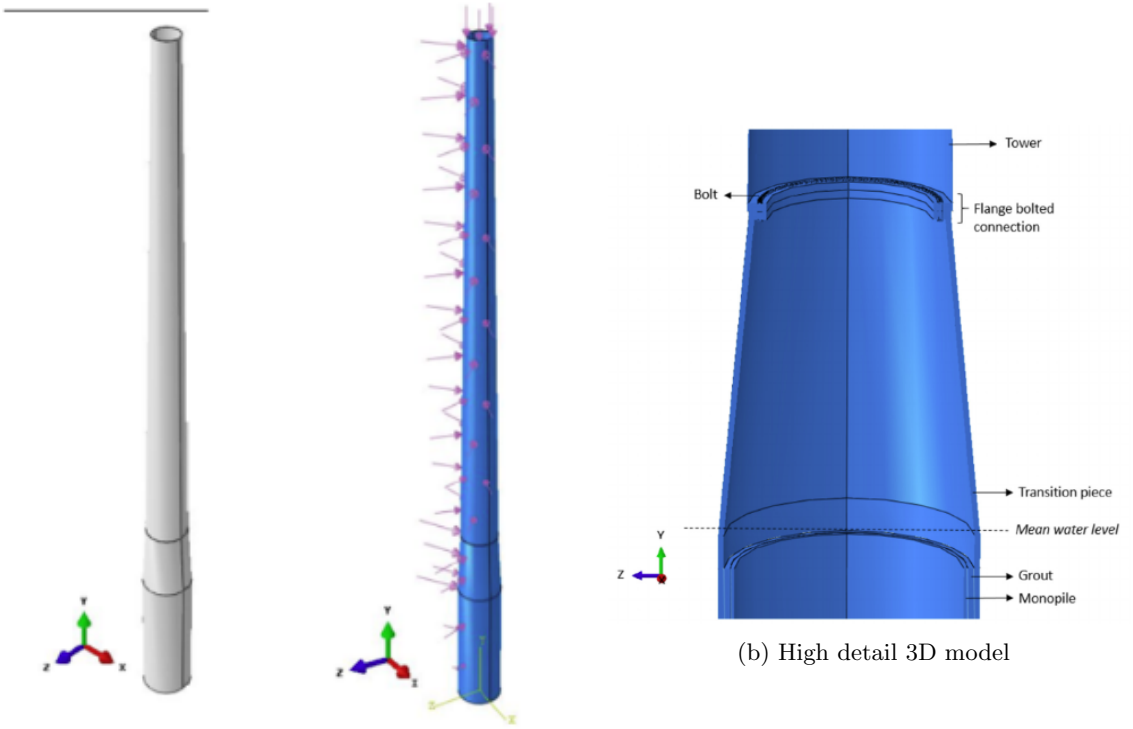

(a) Simple 3D model

(b) High detail 3D model

Figure 2.2: Simple and detailed model of a wind turbine. [17]

These models were used to estimate results like the deflection of the top of the tower under environmental forces, the first natural frequency and von Mises stresses for the tower. A summary of the results is shown in Table 2.1.

	Design 1		Design 2						Design 3	
			Soil 1		Soil 2		Soil 3			
	NC	EC	NC	EC	NC	EC	NC	EC	NC	EC
Maximum Lateral Displacement (m)	0.2914	1.097	0.3203	1.208	0.3529	1.335	0.3284	1.24	0.2680	1.012
Maximum Von Mises Stress (MPa)	58.61	189.3	*	*	*	*	*	*	102.7	490.2
Natural Frequency (Hz)	0.31051		0.31051		0.28330		0.29371		0.31051	

* In design 2, the maximum von Mises stress in both models with soil and without soil was negligible and, therefore, the soil did not have any influence on the variation of this parameter.

Table 2.1: Results of the three models. [17]

The results show that the first model gives a reasonable estimation for the deflection and natural frequency of the tower, but the estimated von Mises stresses were inaccurate. The third model included far more details and likely gave more accurate results. The main difference between these two models were the von Mises stresses. Due to the modelling of small details like bolts high local

stresses were estimated, which were not present in the simplified model. This study shows that low fidelity models can be sufficient for the estimation of some of the results, based on the required accuracy and goals of the analysis.

2.2 Eigenmodes of a wind turbine tower

The following sections will contain a lot of different eigenmodes of multiple models. For this reason, it is very useful to first define a method for describing each eigenmode in a unique way. Complex systems will result in complicated eigenmodes, which can be difficult to describe with words or parameters. Nowadays, the most common support structures for wind turbines are tubular steel towers. So is the wind turbine provided by DOT. These towers consist of large tubular sections, which also include smaller details like the transition piece, ladders or door openings. These structures are extensively studied since they are commonly used. Figure 2.3a shows a real wind turbine for which a finite element model was developed to estimate its mode shapes and natural frequencies. In the FE model some smaller details like bolts and ladders were ignored to reduce calculation times. The FE model is shown in Figure 2.3b.

(a) Real picture (b) FE model of the tower

Figure 2.3: Real picture and FE model of GAMESA G52. [14]

The FE model is used to estimate the eigenmodes of the structure. The estimated eigenmodes can be seen in Figure 2.4.

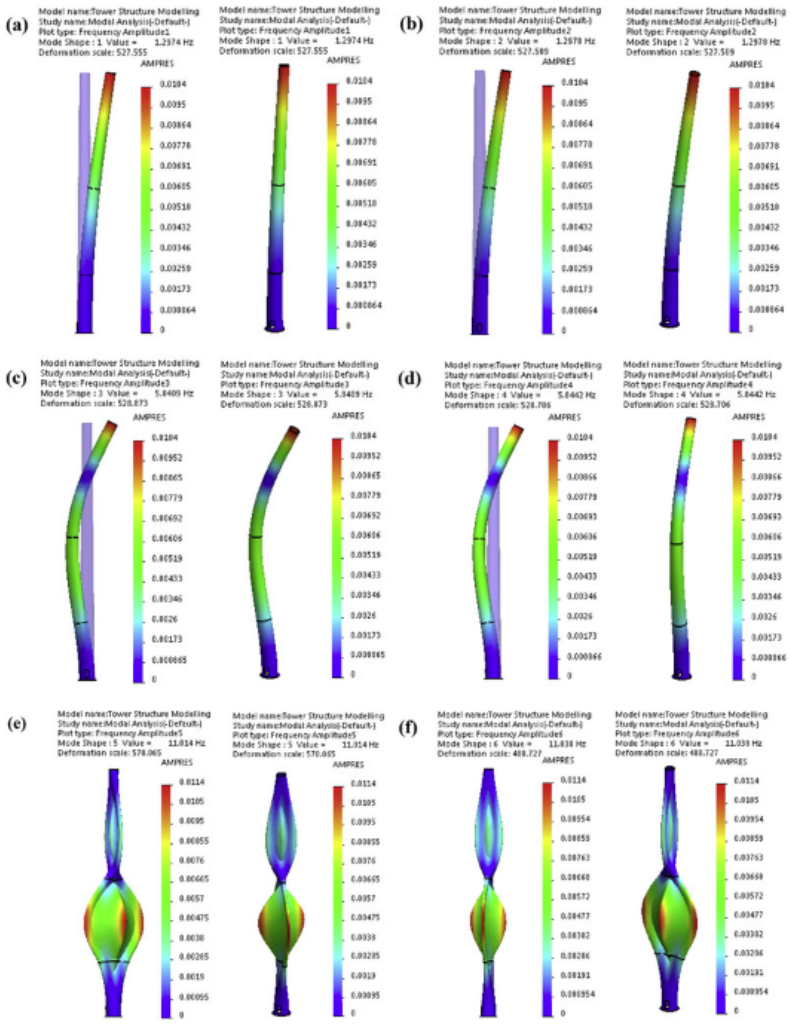

Figure 2.4: Estimated eigenmodes of the tower. [14]

In this thesis many similar eigenmodes will be estimated and discussed. Therefore, it is very useful to provide a method to describe each estimated eigenmode in a unique way. Figure 2.4 shows that the eigenmodes of the wind turbine tower might be similar to the eigenmodes of a cylinder.

2.3 Cylinder mode shape classifications

The mode shapes of a cylinder of finite length are presented in a paper by Wang and Williams [32]. Six different categories of mode shape types are presented, for which descriptions are provided in Table 2.2. Illustrated examples of the mode shapes are given in Figure 2.5. This method of describing the eigenmodes can also be useful when describing the eigenmodes of a wind turbine

tower.

Category	Description
A. Pure radial modes	Constant cross-section and the cross-sections remain plane.
B. Radial motion with radial shearing modes	Non-constant cross-section, the cross sections do not remain plane.
C. Extensional modes (breathing mode)	Cross-section that is stretched in the circumferential direction along its length.
D. Circumferential modes (thick shells)	Adjacent segments of the cross-section expand or contract.
E. Axial bending modes	Segments of the cross-section bend in the axial direction.
F. Global modes	The cylinder behaves as: a beam in a transverse vibration, a bar in torsional vibration or a rod with longitudinal vibration.

Table 2.2: The six mode shapes categories. [32]

Especially the distinction between the local modes and global modes is important for this research. Global modes are described as modes where the cylinder behaves as either a beam, bar or rod and vibrates in the transverse, torsional or longitudinal direction. In these types of vibration, every part of the structure oscillates and is therefore called a global mode. For local modes only a part of the structure is oscillating, the vibration is localized. This distinction is important because local vibrations around the slip joint connection are the main point of interest for this research.

Besides the six different types of mode shapes there are two additional parameters to describe the mode of vibration for a cylinder. These parameters are 'm' and 'n'. They describe the number of nodes in the longitudinal and circumferential direction of the cylinder, respectively. An example of these two parameters can also be found in Figure 2.5.

Classification of vibrational modes of thick cylinders

Mode shape	*n*	*m*	Frequency
A	2	0	1251
	3	0	3266
	4	0	5720
	5*	0	8445
B	2	1	1451
	3	1	3520
	4*	1	5960
	5	1	8653
	2	2	3240
	3*	2	4632
	4	2	6844
	5	2	9371
	2*	3	6216
	3	3	7875
	4	3	8524
	5	3	10771
C	0	0	3918
	0	1	4129
	0	2	4282
	0*	3	5616
	0	4	8847
D	1	1	6140
	1*	2	8219
	1	3	9933
	2	1	8605
	2	2	9173
	3	1	8867
E	1	1	3038
	2*	1	4741
	3	1	6597
	4	1	10259
	1	2	4788
	2*	2	6211
	3	2	8040
	4	2	10132
F	1*	2	3515
(a)	1	3	5621
	1	4	9103
	1	5	out of range
(b)	0*	1	3090
	0	2	6391
	0	3	10106
	0	4	out of range
(c)	0	1	5603
	0*	2	10908
	0	3	out of range
	0	4	—

*: The mode shape illustrated.

Figure 2.5: Illustrations showing the six mode shapes categories. [32]

2.4 Friction reduction by vibration

This section provides a small introduction in friction reduction by introducing vibration. This mechanism is not the main topic of research for this thesis, but, since it is the main motivation for the estimation of shell modes, it still is interesting to provide some background and present early experiments.

One of the first papers discussing this phenomenon is by H. Fridman and P. Levesque [15]. They explored the effect of vibration on the static friction between metallic surfaces. Their results show that a significant reduction in the static friction coefficient is possible and is dependent on the frequency and amplitude of the vibration. They also set up an initial framework to try and explain the reduction in friction force by vibration. They visualize the contact areas between two surfaces as consisting of a certain number of welds. For the possibility of movements the welds would have to be broken. The welds can be broken by introducing a force, either lateral or transverse direction. This can be done by introducing a external force that is large enough the overcome the static friction, which will results in sliding of the two surfaces. The forces introduced by vibration can help break these welds and therefore reduce the external force required, lowering the apparent friction coefficient. A reduction of friction force in the presence of vibration was also confirmed in tests by D. Godfrey [16]. With these tests Godfrey researched the effects that lubrication had on the friction reduction by vibration. Both lubricated and not lubricated tests showed a reduction in friction force when vibration was introduced. In his research Godfrey noted that friction reduction only started when the accelerations of the vibrations reached the acceleration due to gravity. He suggested that friction reduction between two bodies starts to occur when one of the body is accelerating faster than the other body is able to follow, which was the acceleration by gravity in the case of these tests.

2.5 Common excitation forces and boundary conditions

Modal analysis is common practice in the design of OWT's. It is used to assess the eigenfrequencies and eigenmodes of the system in order to avoid the possible excitation of resonance frequencies by present loads. The most important environmental loads that can excite the structure come from the wind, waves or rotation of the rotor. These loads are often plotted in a graph to have a simple overview of which frequencies regions should be avoided, see Figure 2.6.

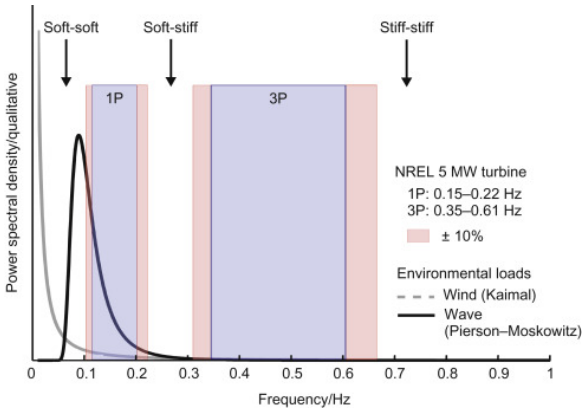

Figure 2.6: Frequency regions which are excited by environmental loads. [19]

The exciting frequencies are relatively low, which means that the modes that are of greatest interest are the first few modes present in the structure. Commonly, the first two eigenmodes of a wind turbine are the first two global bending modes of the tower[24]. For this reason, the only eigenmodes of interest are usually the global bending modes. When only the global bending modes are of interest the model of the tower is often modelled as a cantilever beam or modelled with simple beam elements. This simplifies the model, while still providing fairly accurate estimates for the first few global eigenmodes [7].

However, in this thesis the interest lies in the shell modes of the structure. The model has to be able to capture all the eigenmodes of the structure within the first 300 eigenmodes. A simplified model using beam elements will not be able to capture the local shell modes. The tower has to be modelled with solid or shell elements. Recommendation for the development of the FE model is given by F. Petrini et al. [24]. Four levels of modelling are described, which are summarized in Table 2.3.

Model level	Scale	Maximum detail level	Main adopted Finite Elements
Systemic level	wind farm	approximate shape of the structural components	BLOCK elements
Macro level	single turbine	approximate shape of the structural components, correct geometry	BEAM elements
Meso level	single turbine	detailed shape of the structural components	SHELL, SOLID elements
Micro level	individual components	detailed shape of the connecting parts	SHELL, SOLID elements

Table 2.3: Four levels of development for the FE model a wind turbine. [24]

The meso level is the most appropriate lever of development for the FE model.

2.5.1 Rotor Nacelle Assembly (RNA)

The rotor and nacelle assembly of a wind turbine are often represented as a point mass when assessing the tower of the structure [3]. Doing so reduces the complexity of the model significantly. The eccentricity of the RNA can also be included in the point mass. The weight and the eccentricity of the RNA are also provided by DOT. The weight is estimated to be 138912 kg and the eccentricities are shown in Figure 2.7.

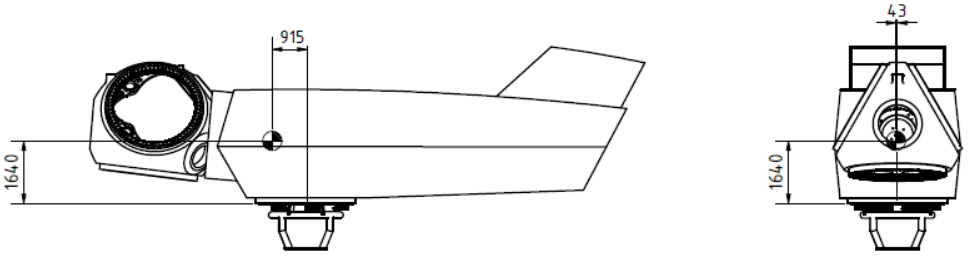

Figure 2.7: Centre of gravity of the RNA.

The moments of inertia of the RNA should also be included in the point mass. These properties are unfortunately not known or provided by DOT and need to be approximated. The moments of inertia of a RNA of a similar wind turbine are provided by [8]. The mass and mass moments of inertia are shown in Table 2.4.

Total mass	134300 [kg]
I_{xx}	$7.43 * 10^6$ [kg m2]
I_{yy}	$1.21 * 10^7$ [kg m2]
I_{zz}	$7.34 * 10^6$ [kg m2]

Table 2.4: Mass and mass moment of inertia for RNA. [8]

2.5.2 Added mass

When a body accelerates in a fluid it also has to accelerate part of the fluid surrounding it. The extra mass that has to be accelerated is known as added mass. This effect is extensively described in literature [10],[22]. Part of the monopile is located underwater and vibrations essentially are repeated acceleration. The added mass of the water could affect the eigenmodes of the structure and has to be included in the reference model of the wind turbine. The amount of added mass is dependent on the geometry of the body and the density of the surrounding fluid. The added mass can be estimated with the help a table given in [10], see Figure 2.8.

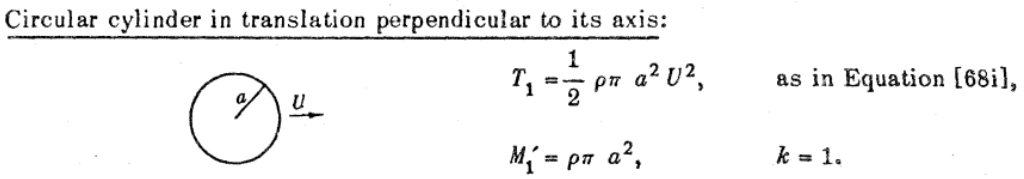

Figure 2.8: Added mass per unit length of a cylinder. [10]

The added mass per unit length for a circular cylinder can be estimated with Equation (2.1).

$$M_a = \rho\pi\alpha^2 \tag{2.1}$$

Here ρ is the density of liquid and α is the radius of the cylinder. The monopile has a constant diameter below sea level equal to 4 meter. The density of seawater is approximately 1025 kg/m^3. The added mass per unit length can therefore be estimated as 12880.5 kg/m.

2.5.3 Soil boundary condition

Another important modelling choice to be made is how the structure to soil boundary condition is included. Modelling the monopile as clamped at the mud line is often too simple and can lead to inaccurate results. The behaviour between the monopile and the surrounding soil is called the soil-structure interaction. There are several approaches to model the soil-structure interaction [4, 25]. The method that is most recommended by the design guides DNV [30] and API [5] is the p-y method. This method is based on Winkler's approach[33], which models the soil with non-linear springs along the length of the monopile. This method was originally developed for smaller diameter piles and is less accurate for piles with a diameter of more than 4 meter. However, it still is a commonly applied method due to its simplicity and the absence of other widely accepted methods [34]. Alternatively, the soil-structure interaction can be modelled using a finite element model. This method provides more accurate results, but is a lot more complex to apply. It is chosen to use the p-y method to model the soil-structure interaction due to its simplicity and the assumption that the soil boundary condition will have limited influence on shell modes located in other regions of the tower.

The p-y method, partially developed by [1][2], provides estimate curves for the relationship between the soil resistance (p) and the pile deflection (y). The ratio between these parameters is known as the coefficient of subgrade reaction (k) [27]. A typical p-y curve is shown in Figure 2.9.

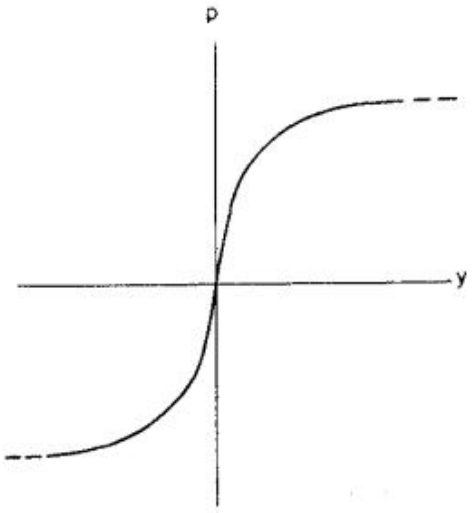

Figure 2.9: Typical p-y curve. [1]

At low deflection, the soil resistance reacts linearly. As the deflection increases it starts to act non-linear. At a certain point the soil resistance reaches a maximum, the ultimate soil resistance. The curves are dependent on the properties of the surrounding soil and on the soil depth, and can be estimated experimentally, numerically or analytically. It is not necessary to evaluate the whole p-y curve. It is assumed that vibrations of the monopile can be regarded as small deflections only, which means that only the initial slope of the curve is of interest. The slope equals the coefficient of subgrade reaction. The soil profile of the location of the wind turbine is unknown and has to be assumed. Estimates for the coefficient of horizontal subgrade reaction are provided by Terzaghi [27]. Table 2.5 shows estimates of the value n_h for submerged sand. When dense sand is assumed as the soil type this value equals 34 ton/ft^3.

Relative density of sand	Loose	Medium	Dense
Range of values of A	100–300	300–1,000	1,000–2,000
Adopted values of A	200	600	1,500
Dry or moist sand, values of n_h	7	21	56
Submerged sand, values of n_h	4	14	34

Table 2.5: Recommended values for n_h $[ton/ft^3]$. [27]

The coefficient of horizontal subgrade reaction (k_h) can be determined with Equation (2.2).

$$k_h = \frac{p}{y} = n_h \frac{z}{B} \tag{2.2}$$

Where z is the depth below surface and B is the width of the pile. The width of the monopile equals 4 meter. Equation (2.2) results in a linearly increasing coefficient of horizontal subgrade reaction. It is equal to 0 at mud line and the maximum value at the bottom of the monopile equals 161.59 ton/ft^3, which equals $55.96 * 10^6 N/m^3$.

2.6 Eigenmode comparison

Before the eigenmodes of two different models can be compared they need to matched to one another. Matching the eigenmodes means pairing an eigenmode of one model to the 'corresponding' eigenmode of the other model. It is possible for the order of the eigenmodes to shift, since the eigenfrequencies of the modes can change. The 10th eigenmode of a model will not always remain to be the 10th eigenmode if that model is changed. It therefore is necessary to match the shell modes to ensure the correct modes are compared to one another. A commonly used method for matching the eigenmodes is the Modal Assurance Criterion (MAC).

2.6.1 Modal Assurance Criterion

The Modal Assurance Criterion (MAC) is a popular tool for a quantitative comparison of mode shapes. Pastor et al.[23] provide exemplary cases in which mode matching is essential. One of the cases mentioned is before and after a change in the physical structure caused by wanted modification. This is essentially also the case for this thesis. The MAC is an indicator that compares two mode shapes. It can take any value between 0 and 1. A value of 1 indicates that the mode shapes are equal and a value of 0 indicates that there is no correspondence between the mode shapes. Any value in between indicates that the mode shapes are only partially matching. Commonly, a MAC value of higher than 0.9 is regarded as a positive match between two mode shapes. The MAC is most sensitive to large differences and less sensitive to small differences in the mode shapes. The MAC can be calculated with Equation (2.3)

$$MAC(r,q) = \frac{|\{\phi_A\}_r^T \{\phi_X\}_q|^2}{\left(\{\phi_A\}_r^T \{\phi_A\}_r\right)\left(\{\phi_X\}_q^T \{\phi_X\}_q\right)} \tag{2.3}$$

Here $\{\phi_A\}$ and $\{\phi_X\}$ are two mode vectors, which contain the two discrete mode shapes to be compared. The MAC is often presented in a 2D matrix, with the mode vectors of one model along its first axis and the mode vectors of the second model along its second axis. This provides an easy overview for comparing the several possible combinations of the mode vectors. An example of this matrix is shown in Figure 2.10.

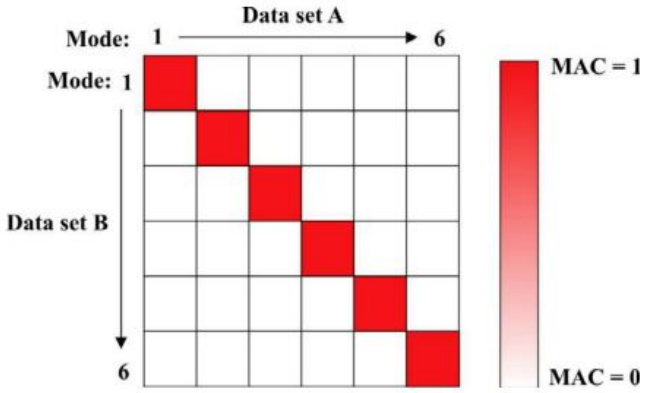

Figure 2.10: Example of a 2D MAC matrix. [23]

If the mode shapes of both models are equal and are in the same order this matrix will contain a MAC value of 1 on it diagonal and a value of 0 on its off-diagonals. If the modes are different or in a different order it will be reflected by the MAC matrix.

Chapter 3

Preliminary study of modelling decisions

The goal of this chapter is to highlight and analyse some of the decisions that are important for the development of a finite element model of a wind turbine that is to be used in a modal analysis. It is meant as an initial study into how finite element modelling can be used to estimate the shell modes of a structure. For example, the choice of element type or model discretization are studied using simple models. By using simple models instead of a complete model of the wind turbine effects of the different modelling choices are like to be more clear. Things learned during this initial study can be applied during the development of the reference model or simplified models.

3.1 Finite element types

Probably one of the most important decisions to be made when developing a FE model is what type of elements should be used. There are many different types of elements, which are generally grouped into 1D, 2D or 3D elements. 1D elements are line elements which can be used for a simple representation of rods, bars or beams, etc. 2D elements are surface like elements that can be used to model plate or shell like structures. 2D elements consist of a mid-surface and assigned a thickness which is constant over that surface. The stresses present in the element are considered constant through its thickness. 3D elements are solid elements and can be used to model most objects. Which type of elements to use is dependent on the geometry of the model and on the goal of the analysis. It is almost always possible to model a geometry using 3d elements, which may look like a simple solution. However, 3D elements also require the most computational power. For large structures this can become a significant amount. It is therefore useful to use simpler 2D or 1D elements when possible.

Modelling the tower of the OWT with only 3D elements is a nearly impossible task as this would require a lot of computational power. Since the tower mostly consists of thin-shelled cylinders it can be very beneficial to look at the use of 2D elements. There are 3 main types of 2D elements:

Membranes, plates and shells [9]. Membranes only resist loads applied in the direction of the mid-surface and can be used to analyse plane stress and strain. Plate elements are 2D elements that only resists transverse loads and only assess the bending of the structure. Shell elements combine the membrane stresses and bending stresses. Also, shell elements may consist of curved surfaces and are therefore sometimes considered as 2.5D elements. This can make the use of shell elements an attractive option when modelling the tower. There is no standard definition when shell elements can be used but a general rule of thumb is that they can be considered when the wall thickness is at least 20 times less than the length of the body.

Next, an example cylinder will be assessed. It is used to study the difference between using solid or shell elements to model the cylinder and are also compared to experimental values. The experimental eigenfrequencies are provided in a paper by C. Wang and J.C.S Lai [31]. In this paper experimental and theoretical eigenfrequencies are compared. One table in this paper includes multiple eigenfrequencies for a clamped-clamped cylinder, see Table 3.1. The cylinder has a thickness of 2.54 mm, an inner radius of 48.51 mm and a length of 394.42 mm. The paper doesn't provide the Young's modulus or density of the cylinder, but states that regular steel is used. Therefore a Young's modulus of 2E11 Pa and a density of 7850 kg/m^3 are assumed.

Mode number (m)	Source	Mode number (n)					
		2	3	4	5	6	7
1	Experiment [14]	1240	2150	3970	6320	9230	12 600
	Koval and Cranch's equation	1569	2326	4092	6419	9251	12 566
	Yu's equation	1756	2460	4246	6615	9522	12 959
	Morley's equation	1611	2206	3982	6351	9257	12 695
	Equation (23)	1729	2541	4334	6704	9611	12 048
	Equation (13)	1386	2159	3942	6308	9212	12 647
2	Experiment [14]	2440	2560	4160	6475	9380	12 750
	Koval and Cranch's equation	3605	2782	4185	6444	9259	12 569
	Yu's equation	4036	2943	4342	6641	9530	12 962
	Morley's equation	3975	2734	4085	6376	9266	12 698
	Equation (23)	3417	3060	4572	6885	9776	13 209
	Equation (13)	2938	2672	4171	6481	9372	12 803
3	Experiment [14]	–	3380	4540	6720	9540	12 900
	Koval and Cranch's equation	6883	3918	4474	6524	9286	12 580
	Yu's equation	7706	4144	4642	6723	9558	12 974
	Morley's equation	7674	3998	4402	6463	9295	12 709
	Equation (23)	5460	4019	5016	7186	10037	13 456
	Equation (13)	4806	3613	4606	6773	9624	13 043
4	Experiment [14]	–	4480	5130	7100	9890	13 220
	Koval and Cranch's equation	11310	5759	5087	6708	9349	12 605
	Yu's equation	12662	6092	5278	6913	9623	12 999
	Morley's equation	12643	5994	5068	6660	9362	12 736
	Equation (23)	7422	5266	5688	7627	10401	13 792
	Equation (13)	6670	4828	5268	7204	9979	13 372
5	Experiment [14]	8020	5740	5910	7710	10310	13 570
	Koval and Cranch's equation	16862	8233	6104	7051	9471	12 653
	Yu's equation	18879	8709	6333	7267	9748	13 050
	Morley's equation	18866	8641	6160	7027	9490	12 787
	Equation (23)	9135	6625	6553	8213	10876	14 223
	Equation (13)	8382	6157	6125	7782	10445	13 794

Table 3.1: Eigenfrequencies of a clamped-clamped cylinder. [31]

This table shows the natural frequencies of the cylinder resulting from an experiment and the natural frequencies which are estimated with different equations. Equations (23) and (13) are novel equations which C. Wang and J.C.S Lai are comparing to the other estimated natural frequencies. The table shows that there can be relatively large differences between the natural frequencies determined with the various methods. The difference become especially large for modes with a high m parameter. From this table it can be concluded that the estimation of high frequency shell modes using analytical equations is complicated and can include relatively large errors.

Two FE models are created of this cylinder, one with solid elements and one with shell elements. The resulting eigenfrequencies are shown in Table 3.2. Parameters m and n are the longitudinal and circumferential wave numbers, as explained in Section 2.3. It was chosen to only include the experimental results of Table 3.1 because these values were most comparable to the eigenfrequencies estimated by the FE models.

m	n	Experimental	FE shell	FE solid	FE difference [%]
1	2	1240	1270.8	1269.7	0.1
1	3	2150	2011.4	1998.6	0.6
2	3	2560	2473.3	2461.3	0.5
2	2	2440	2600.1	2597.9	0.1
3	3	3380	3331.1	3317	0.4
1	4	3970	3697.5	3650.5	1.3
2	4	4160	3893	3847.9	1.2
3	4	4540	4289.2	4245.4	1.0
4	3	4480	4454.2	4434	0.5
4	4	5130	4906.9	4862	0.9
5	5	7710	7278	7166.5	1.5

Table 3.2: Eigenfrequencies [Hz] estimated experimentally and with FEM.

This results show that there is a small difference between the eigenfrequencies estimated by the shell FE model and the solid FE model. This error is very small in comparison to the error between the experimental data and the FE models. The benefit of shell elements can be seen when looking at the total nodes in the FE models. Both models were given same mesh size and therefore have a similar amount of elements. The shell model consisted of 7722 elements with 23322 nodes and the solid model consisted of 8100 elements with 55897 nodes. The solid model had more than twice the amount of nodes of the shell model. The solid FE model used even had only a single element along the thickness of the shell. It is generally recommended to have multiple solid elements along the thickness of the model, which greatly increases the amount of elements and nodes. For the analysis of a simple model the amount of nodes is not a big concern but when the model becomes more complex shell elements should be applied when possible.

3.2 Mesh size convergence

The mesh size used in a FE analysis influence the accuracy of the results and the speed at which the results are obtained. A finer mesh provides more accurate results but requires more computational power, a courser mesh does the opposite. The results of the FE analysis convergence to a solution as the mesh size decreases. After a certain point further decreasing the mesh size has little influence on the accuracy of the results. A mesh size can be selected based on the allowable error in the results and the preferred computational requirements.

The mesh convergence of the example model is performed manually by changing the mesh size and comparing the results given by Ansys. The study was started off with an element size of 3 meters, which resulted in a rough model. The frequencies of interest were chosen to be the first

10 eigenfrequencies. The 10th modes eigenfrequency was close to 200 Hz, meaning that the chosen eigenfrequencies covered the interesting frequency ranges. The eigenfrequencies of this model were calculated and noted down. Then, the mesh size was decreased in steps of 0,5 meter. The results were recalculated and compared with prior results. This was done several times and the results of this study are plotted in Figure 3.1.

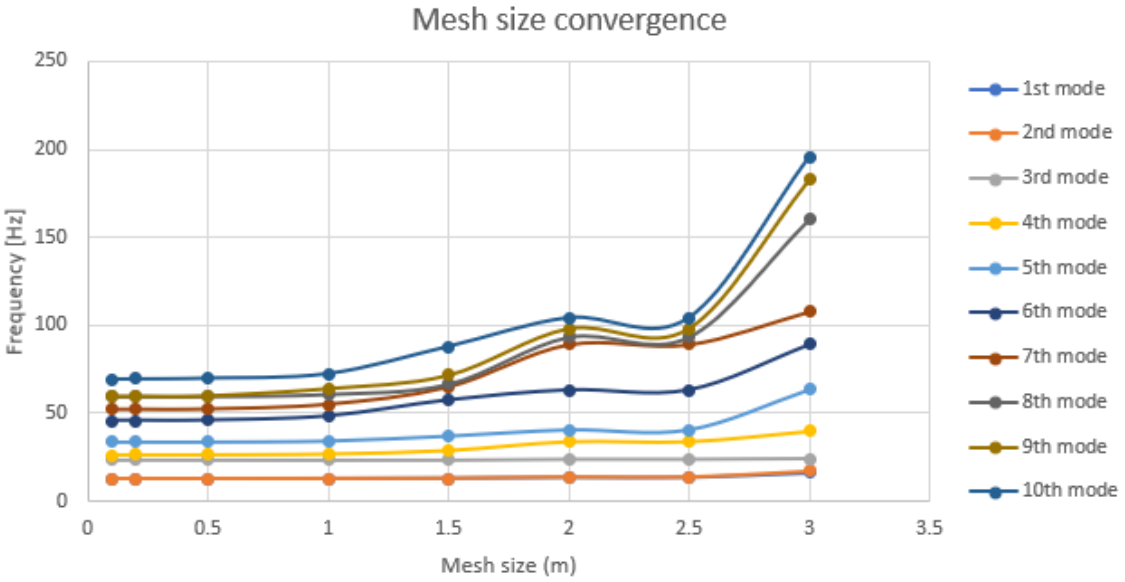

Figure 3.1: Mesh size vs. frequency of 10 modes.

This figure shows a clear reduction in the found eigenfrequencies for decreasing mesh sizes. Especially higher modes show that a finer mesh is required for accurate results. The reason higher modes are more sensitive to the mesh size is because higher modes have shorter wavelengths. A shorter wave length requires smaller elements to properly resemble the mode shape of the model. The estimated eigenfrequencies stabilize around a mesh size of about 0.8 meters. The mesh size of 0,8 meters is only valid for this model and these eigenmodes, for more advanced models or higher eigenmodes a a new mesh convergence study is required.

3.3 Shell thickness effect

Shell elements can be very useful and efficient, but also introduce new difficulties into the model. One of those difficulties is how to deal with the thickness of the elements. This difficulty can best be explained by a illustration, which is shown in Figure 3.2. The figure shows a simple geometry consisting of a middle plate (*blue*) with a certain body (*orange*) attached to each of its sides. This sort of geometry reoccurs multiple times in the detailed model of the wind turbine. If the plate is modelled as a solid geometry the nodes of the bodies and plate line up and are in contact, see Figure 3.2a. However, when the plate is modelled with shell elements the nodes of the orange bodies

do not line up with the nodes of the plate any more, the bodies and plate do not seem to be in contact, see Figure 3.2b.

(a) True geometry of the model

(b) Nodes of the model

Figure 3.2: Example of the shell thickness effect.

From now on this phenomenon will be referred to as the shell thickness effect. It occurs when a body is to be in contact with the side of another body that is modelled with mid-surface shell elements. Since a large part of the wind turbine is modelled with shell elements it is important to figure out how to deal with this effect. There is little information available regarding this effect, which is why it will be studied in this section.

The example model to study this effect is shown in Figure 3.3.

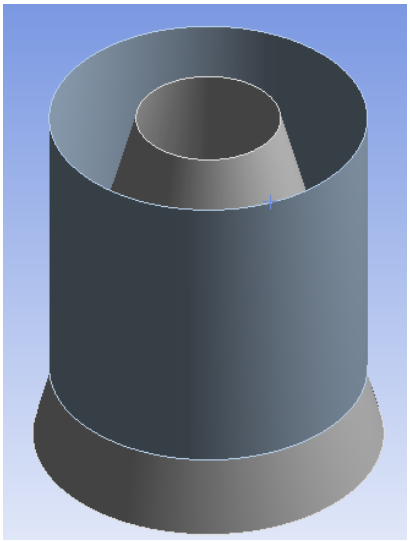

Figure 3.3: Mesh size vs. frequency of 10 modes.

This model consist of two surfaces, that of a cylinder and a cone, which are intersecting. The total height equals to 10 meters, the diameter of the cylinder is 4.125 meters and the wall thickness applied is 50 millimeter. This is model is similar to geometry that occurs in the slip joints. Two separate models of this model are created. In the first model the cylindrical surface runs up to the conical surface. When shell elements are applied to the surface the mesh intersects, as shown in Figure 3.4a. In the second model the cylinder runs op to the point were the edge of the shell would touch the elements applied to the cone, see Figure 3.4b.

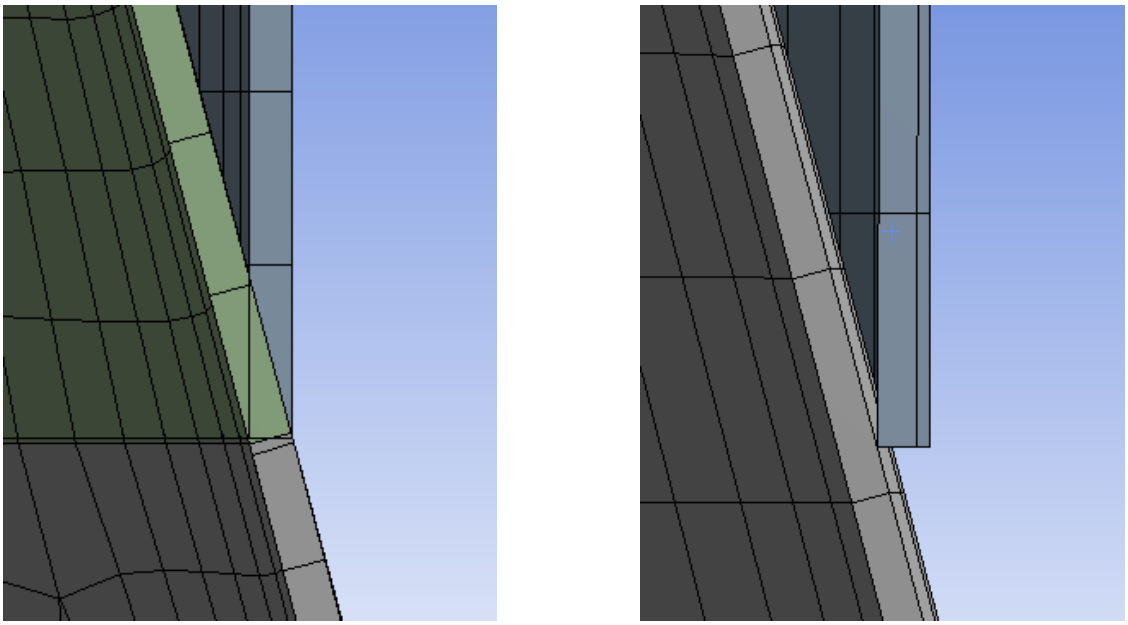

(a) Intersecting shell elements

(b) Touching shell elements

Figure 3.4: The two models used to study shell thickness effect.

In the intersecting model the cylinder has a length of 8.4 meters and in the touching model the cone has a length of 8.2 meter. The first 10 eigenmodes of this structure are now calculated using both models. The resulting eigenfrequencies are shown in Table 3.3.

Eigenmode	First model	Second model	Difference (%)
1	6.08	5.88	-3.31
2	6.31	6.23	-1.40
3	11.03	10.93	-0.93
4	15.44	15.28	-1.01
5	17.49	17.30	-1.07
6	20.97	20.47	-2.39
7	22.04	21.55	-2.24
8	24.78	24.37	-1.67
9	25.57	24.98	-2.33
10	25.66	25.21	-1.75

Table 3.3: Eigenfrequencies of both shell thickness models.

These results show that the difference in modelling approach can lead to an error of approximately 3 percent in the eigenfrequencies. This difference is seen acceptable as this phenomenon occurs only in less severe cases for the reference model. The intersecting surfaces are far easier to model and will therefore be applied during the development of future FE models.

3.4 Shaker positioning

The shell modes of the wind turbine will be excited by shakers which are placed on the structure. A good estimation of the eigenmodes is required to be able to excite the correct mode. Why the eigenfrequency is required is obvious. It might be less obvious why an estimation of the mode shape is also important. This section will study the importance of the shaker positioning on the excitation of specific eigenmodes. This is done by regarding the conical cylinder as shown in Figure 3.5a. The eigenmodes of the cylinder can be estimated easily. Specific eigenmodes can be excited by placing shakers on the structure that vibrate in the eigenfrequency of the mode. This can also be simulated in Ansys with a harmonic response analysis. For example, we can try to excite the mode shown in Figure 3.5b.

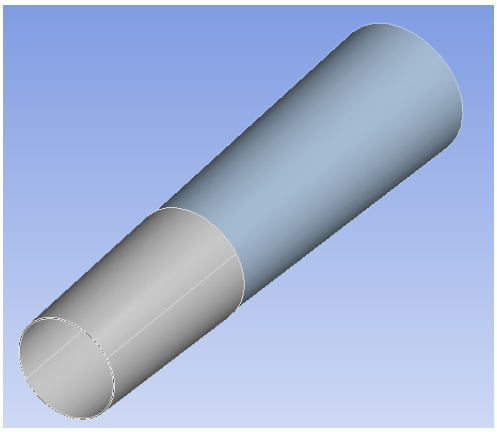

(a) Conical cylinder

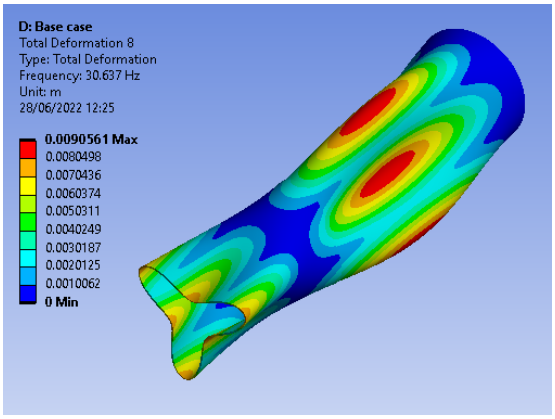

(b) Eigenmode to be excited

Figure 3.5: Example cylinder and eigenmode.

This mode has an eigenfrequency of 30.6 Hz. This eigenmode can be excited by placing a source of excitation in the model. This is done by introducing a harmonic load at one of the nodes of the model. The harmonic load is given the same frequency is the eigenfrequency of the desired mode. The resulting vibration is shown in Figure 3.6.

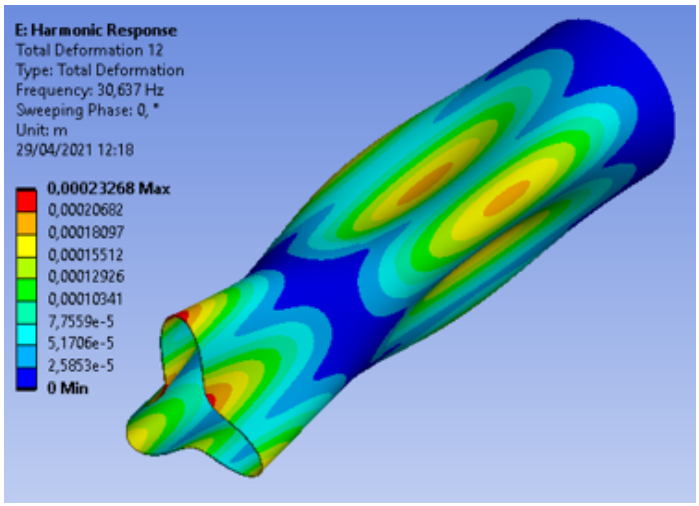

Figure 3.6: Resulting mode of vibration.

This shows that the correct eigenmode is excited. However, structures like these are usually excited by more than one shaker to have a better distribution of the introduced forces. When multiple shakers are used problems can occur. Now, the same analysis is ran with four equally divided shakers instead, as shown in Figure 3.7.

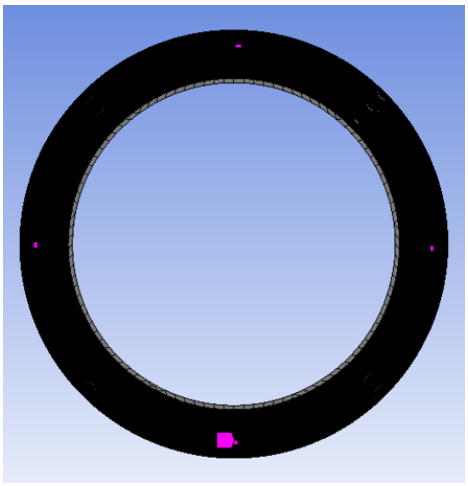

Figure 3.7: Four equally divided shakers.

Using this model results in the mode of vibration as shown in Figure 3.8.

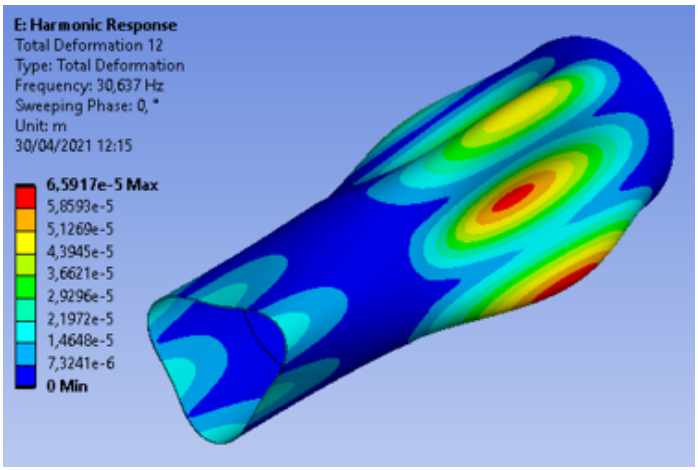

Figure 3.8: Mode of vibration with four shakers.

This figure shows a vibration with four wave lengths in the circumferential direction when there were supposed to be only three. This happened because the position and synchronization of the shakers do not correspond to the mode shape of the eigenmode. The shakers force the structure into this mode shape to fit the motion of the shakers. To obtain the correct mode shape the shakers need to given the correct phase angle. In the case of four equally divided shakers the correct phase angles would be 0, 90, 180 and 270 degrees. Now the shakers excite the correct mode shape, as shown in Figure 3.9.

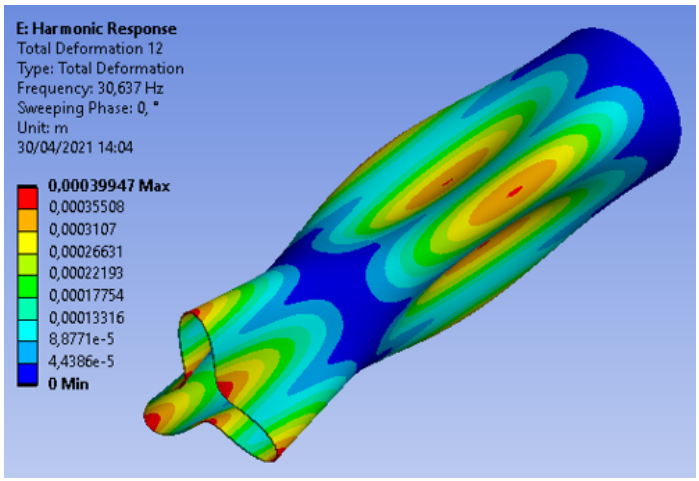

Figure 3.9: Corrected mode of vibration.

Notice that, even though the shakers introduce the same force, the amplitude is higher. This happens because the structure is now excited in an eigenmode resulting in a more effective excitation. This simple study shows that the correct placement and synchronization of the shakers is important when exciting eigenmodes. This is one of the reasons why it is important to be able to make a good estimation of the mode shapes of the eigenmodes of the wind turbine tower.

Chapter 4

The reference model

The full-detail model to be created is based on the geometry of a real wind turbine, which was provided by DOT. The CAD-model of the wind turbine is shown in figure. This model is an accurate representation of the wind turbine. Unfortunately it is not possible to directly import this model into Ansys and use it to run a modal analysis. The model was not created for this purpose and contains several details that make it unusable for a finite element analysis. For example, the model exists of only solid parts. While this represents reality, it will result in a FE model consisting of only solid elements. In the case of thin shell-like structures it can be beneficial to make use of shell elements, as discussed in Section 3.1. Shell elements require the geometry to exist out of surface areas instead of solid parts. Another example is the presence of a lot of small holes and gaps. These inaccuracies are not a big problem when the model is only used as a geometrical representation since they cannot be seen directly by the eye. However, these small holes and gaps provide problems when the model is to be used in a FE analysis, as they can result in meshing difficulties and errors in the results. It is clear that the provided model of the wind turbine requires a lot of updating and changes to be usable for FEA. For this reason it was chosen to create the full-detail model from scratch, using the provided model only as a reference model. This chapter discusses how the reference model was developed and which choices were made during the development.

4.1 Modelling choices

4.1.1 Defeaturing

Most structures are full of holes, fillets, slots, and other relatively small features. All these features can complicate the model creation and meshing process while usually providing little to no extra accuracy to the results. It is therefore common practice to not include those features in the model [18]. This process is known as defeaturing the model and has a very similar goal to this thesis, as its goal is to simplify features of an FE model without having large influences on the results of the analysis. The difference between defeaturing and this thesis is that this thesis aims to assess larger features which leads to a far greater uncertainty in the results. An example of an defeatured

object is shown in Figure 4.1. In this example the amount of nodes present in the meshed model was reduced significantly after defeaturing.

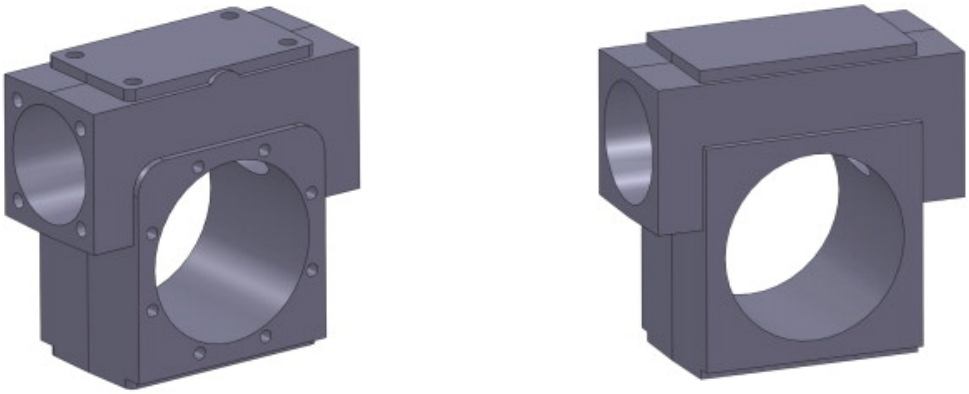

(a) Original object (b) Defeatured object

Figure 4.1: Example of defeaturing. [18]

While defeaturing is a very useful tool when creating FE models there do not yet exist clear rules on when it can be applied. Even though there are many papers available that study the effects of defeaturing [18, 21] and many FEA softwares provide automated defeaturing options there are no set rules and it remains a process that is dependent on engineering judgement. There are multiple smaller features present in the wind turbine tower, like bolting holes and fillets. Not every defeatured part will be mentioned in this section as this would result in a fairly extensive list. Features are included in the model if there existed any doubt about the influence they would have on the results.

4.1.2 Connections

The complete FE model is constructed using multiple smaller parts, which are all made individually. These parts have to be connected to form a rigid structure. Two different connection options were used for the development of the reference model. The first option used is a direct mesh connection. With this options the parts are connected in the meshing process of the model. If parts are sufficiently close they can be meshed using shared nodes at the shared boundary of the parts, which connects the mesh of the two parts. This process can be applied in multiple ways. In the reference model it is applied by applying shared topology between parts.

After the assembly of the wind turbine was created in Solidworks it was imported into Ansys. Before it was meshed and analyzed it was imported into SpaceClaim, which is a CAD software provided by Ansys. In SpaceClaim the assembly was preprocessed and prepared for the meshing process. One of the preparations was applying shared topology between connected parts. SpaceClaim provides tools that evaluate the proximity of objects and gives the option to apply shared topology between them. When applied, these parts will be given shared nodes in the meshing process. An example of shared topology will now discussed.

Assume there are two cylinders with a different thickness, as shown in Figure 4.2a. Because they have a different thickness they have to be made as individual parts. The bottom of the lower cylinder is given an fixed boundary condition. In Figure 4.2a it looks like the cylinders are connected. Performing a modal analysis on this model provides Figure 4.2b. It is obvious that the cylinders are not yet connected.

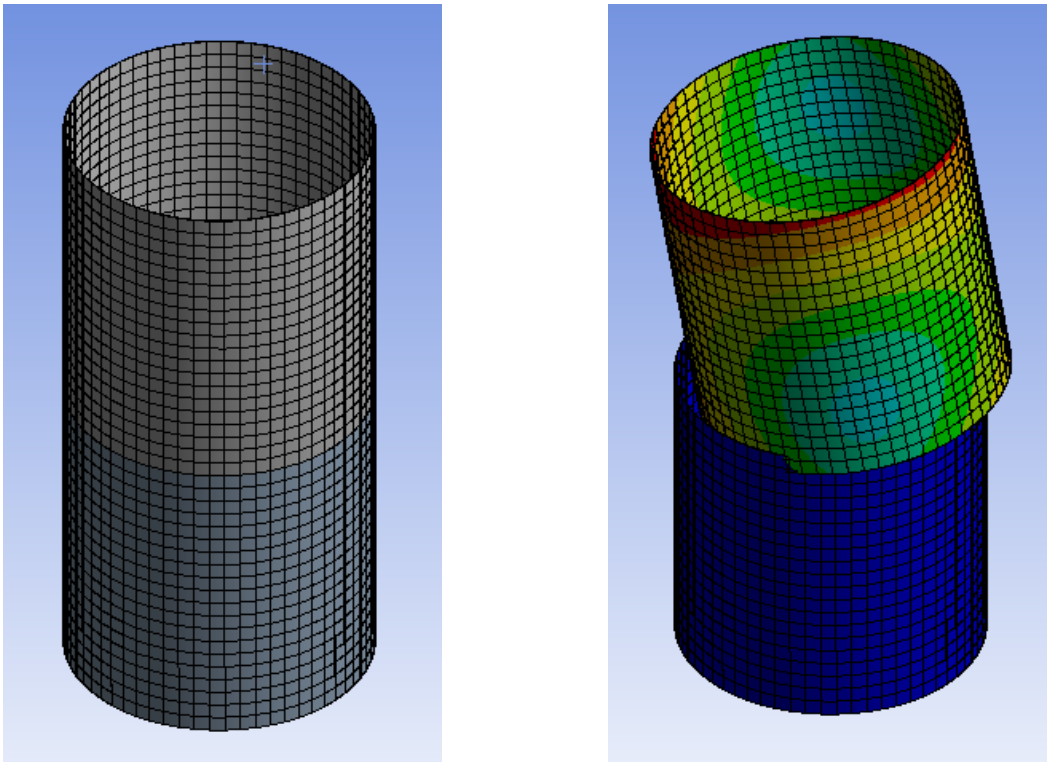

(a) Mesh of the cylinders

(b) An eigenmode of the model

Figure 4.2: Two cylinders without connection.

The cylinders can be connected by sharing their topology. SpaceClaim can search for coincident geometry based on a definable tolerance. Using this option for the example provides Figure 4.3a. The red line shows the coincident edges of both cylinders two which shared topology can be applied. After this is done the cylinders are meshed and the eigenmodes of the model are estimated. One of them is shown in Figure 4.3b, which shows that the cylinders are connected.

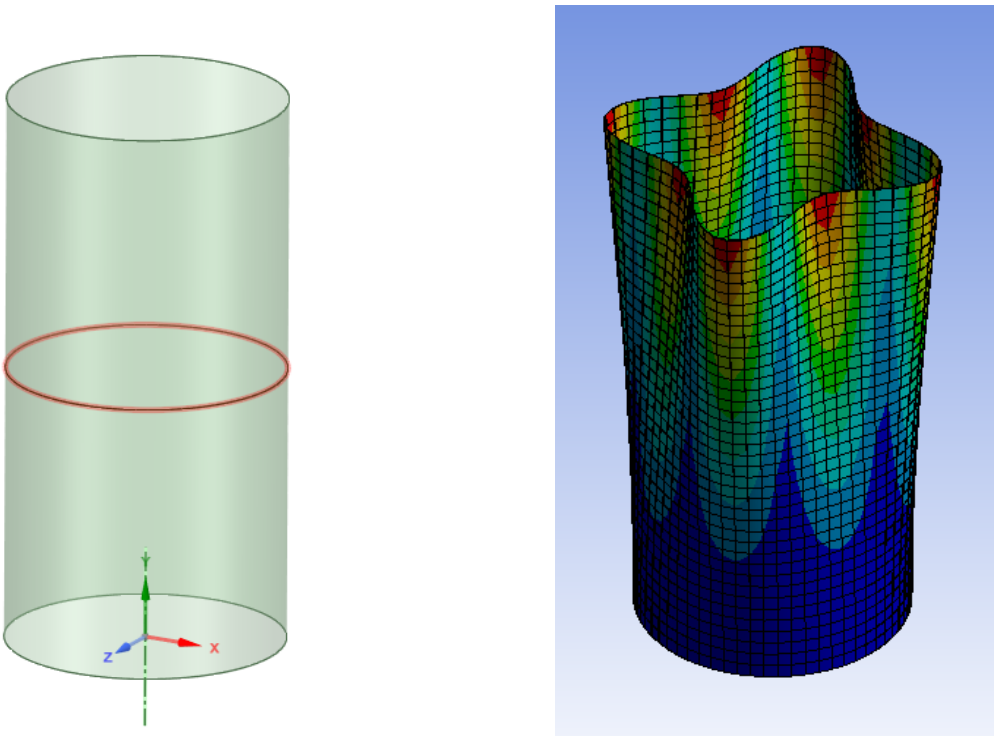

(a) Shared topology in SpaceClaim

(b) An eigenmode of the connected model

Figure 4.3: Two cylinders connected.

Some benefits of using shared topology is that it is simple to use and able to deal with small errors within the geometry and provides a continuous mesh of the model. However, for some parts a continuous mesh can also result in difficulties. Due to the mesh continuity two connected parts are required to have similar element sizes. If parts require different sized elements shared topology should not be used. Instead a bonded contact can be used to connect those parts.

4.1.3 Applying boundary conditions

Three separate boundary conditions are applied to the model, which consist of the RNA mass and inertia, the hydrodynamic added mass and the soil boundary condition, as discussed in Section 2.5. The RNA mass and inertia are applied by introducing a point mass at the top of the tower. The point mass is connected to the yaw bearing and is positioned with respect to its centre, as shown in Figure 4.4a.

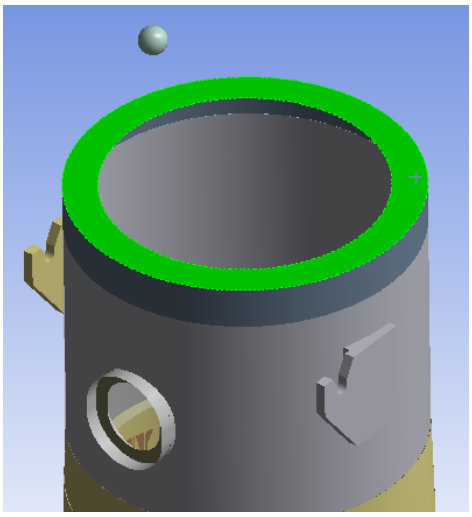

(a) Yaw bearing and point mass

Scoping Method	Geometry Selection
Applied By	Remote Attachment
Geometry	2 Edges
Coordinate System	Global Coordinate System
X Coordinate	7.738 m
Y Coordinate	85.953 m
Z Coordinate	22.524 m
Location	Click to Change
Definition	
Mass	1.3891e+005 kg
Mass Moment of Inertia X	7.43e+006 kg·m²
Mass Moment of Inertia Y	7.34e+006 kg·m²
Mass Moment of Inertia Z	1.21e+007 kg·m²

(b) Point mass settings

Figure 4.4: Point mass resembling the RNA.

The hydrodynamic added mass is included by applying a distributed mass to the section of the tower between sea level and the mud line. This section has a length of 23.8 meter. In Section 2.5.2 the added mass per unit length was estimated to be 12880.5 kg/m. Therefore, the total distributed mass applied equals 306555.9 kg.

Scope	
Scoping Method	Geometry Selection
Geometry	3 Faces
Definition	
Mass Type	Total Mass
Total Mass	3.0656e+005 kg
Suppressed	No

Figure 4.5: Distributed mass settings.

The soil structure interaction is applied with an elastic support at the section of the tower below mud line, which represents the coefficient of horizontal subgrade reaction. The stiffness of the support should increase linearly with the depth, however this is not an option provided by Ansys. Instead the increasing stiffness of the elastic support is applied stepwise, as shown in Figure 4.6.

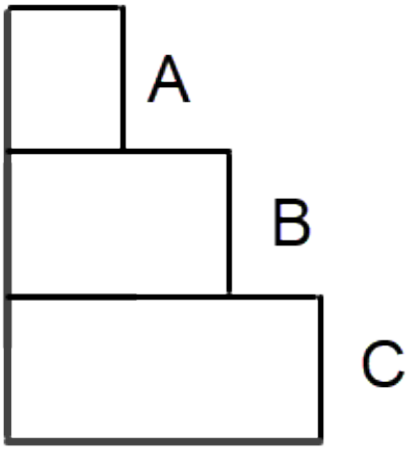

Figure 4.6: Stepwise increase of spring stiffness.

The maximum spring stiffness at the bottom was estimated to be $55.96 * 10^6 N/m^3$, see Section 2.5.3. The average spring stiffnesses are calculated for their respective sections and are shown in Table 4.1.

Section	Spring stifness $[N/m^3]$
A	$9.33 * 10^6$
B	$27.98 * 10^6$
C	$46.63 * 10^6$

Table 4.1: Applied spring stiffnesses.

4.1.4 Global mesh size convergence

The mesh size applied to the model can have a large influence on the accuracy of the results, as was also shown in Section 3.2. This section discusses the mesh size convergence of the reference model. A few modes are selected for the convergence study. These modes are five modes which are of interest for the lower slip joint, see Appendix A.2. The modes selected are mode 14, 37, 131, 203 and 255. These modes were selected to cover a large range of eigenfrequencies. The results of an initial rough convergence study are shown in Table 4.2

Mesh size [m]	0.8	0.7	0.6	0.5	0.4	0.3	0.28	0.26
Mode								
14	6.57	6.55	6.54	6.53	6.53	6.51	6.51	6.51
37	-	17.522	17.09	17.02	16.77	16.47	16.41	16.37
131	-	41.31	40.47	39.91	39.58	38.77	38.69	38.58
203	-	-	-	52.74	51.96	51.27	51.04	50.88
255	62.66	61.7	60.98	60.32	60.37	60.04	60.09	60.12

Table 4.2: Initial convergence study - Eigenfrequencies [Hz] vs. mesh size.

Some of the eigenfrequencies in this table were not able to be computed since the mesh size was too large and the modes could not be recognized. The table shows some convergence but it is difficult to select an acceptable mesh size. The mesh size step is too large and not consistent. A more refined convergence study is necessary. The step in mesh size will be held constant, decreasing the mesh size with 10 percent each step. Looking at Table 4.2 a mesh size of 0.3 meter was chosen as the central point of this study. The more refined convergence study is shown in Table 4.3.

Mesh size [m]	0.564	0.508	0.457	0.412	0.37	0.333	0.3	0.27	0.243	0.219
Mode										
14	6.53	6.53	6.53	6.53	6.51	6.5	6.51	6.51	6.5	6.51
37	16.95	17.01	16.78	16.76	16.48	16.5	16.47	16.41	16.32	16.3
131	39.64	39.11	39.4	39.55	38.39	38.66	38.77	38.56	38.16	38.22
203	52.19	52.82	52.07	51.65	51.69	51.51	51.27	50.95	50.94	50.72
255	60.35	60.51	60.28	60.33	59.91	59.65	60.04	60.08	59.81	59.96

Table 4.3: Refined convergence study - Eigenfrequencies [Hz] vs. mesh size.

It looks like only mode 14 is fully converged in this mesh size range. However, further refinement of the mesh size is very difficult. The analysis with a mesh size of 0.219 meter already took about 10 hours. The next step in mesh size would be approximately 0.197, which is expected to require multiple days for computation. Plotting the eigenfrequencies of mode 255 shows that the results do not convergence to a single value and does more resemble oscillatory convergence, see Figure 4.7.

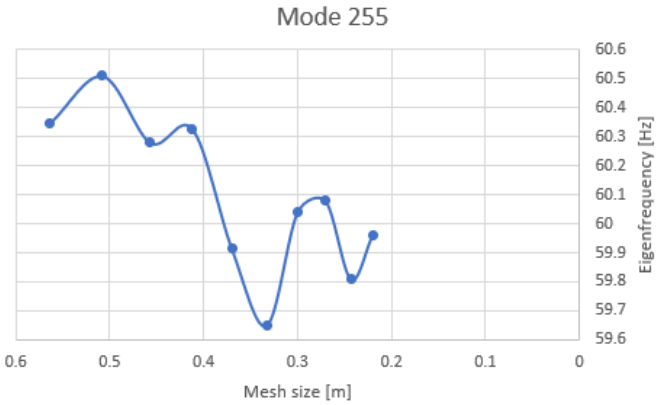

Figure 4.7: Eigenfrequency vs mesh size for mode 255.

Because it is difficult to refine the mesh further one of these mesh sizes has to be selected. A converged solution is not available which means it is difficult to select a mesh size based on expected error in the eigenfrequencies. From Table 4.3 it can be seen that the error is relatively large for element sizes larger than 0.4 meter. The error looks to stabilize around the mesh size of 0.3 meter. The results do not show whether further refinement of the element size will decrease the error any further. The mesh size selected for the reference model is 0.3 meters, because the required computational time increases rapidly at this mesh size and it is not known whether further

refinement of the mesh size increases the accuracy of the results.

4.1.5 Local mesh refinement

A mesh size convergence study is not the only option to check whether the quality of the applied mesh is acceptable. Ansys can also provide information about the individual elements, known as mesh metrics. These metrics can be used to check the quality of the elements. For example, it includes the aspect ratio or skewness of the elements. These values tell something about the shape of the element. Poorly shaped elements can cause inaccuracies or errors in the results of the analysis.

One mesh metric available is called "Element Quality". This metric ranges from 1 to 0, where 1 means that the element has a proper shape and 0 that it has a very poor shape. Which element quality is acceptable depends on the goal of the analysis, but elements with an quality close to 0 should be avoided if possible. Assessment of the element quality of the created FE model reveals that it includes some poorly shaped elements located around the lower slip joint, as shown in Figure 4.8. This figure shows there are elements with an element quality of 0.04. How these poorly shaped elements will affect the results is difficult to say. However, it still is good practice to try to increase the quality of these elements, especially because they are located at an area of great interest.

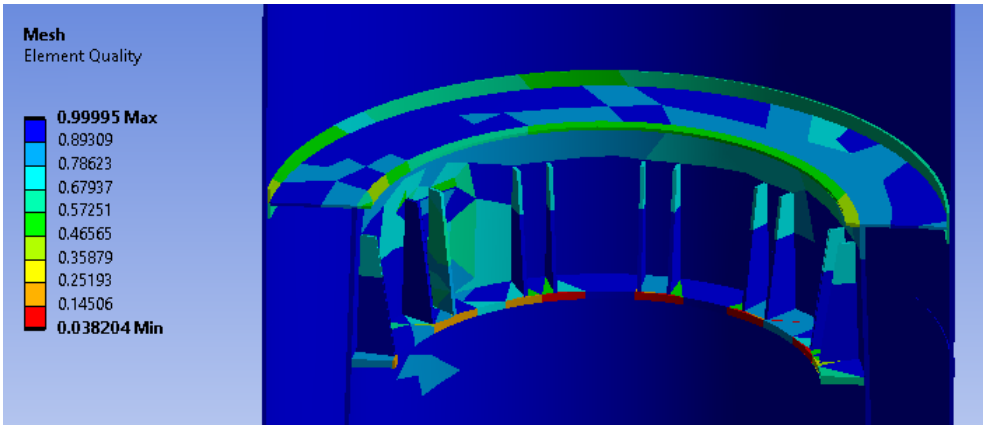

Figure 4.8: Element quality at the lower slip joint.

The poor elements can also be seen in the mesh of the model, as shown in Figure 4.9. The mesh in this area is relatively poor because it is an assembly of multiple smaller parts. The connections of these parts and relatively large mesh size create a poor mesh at this location.

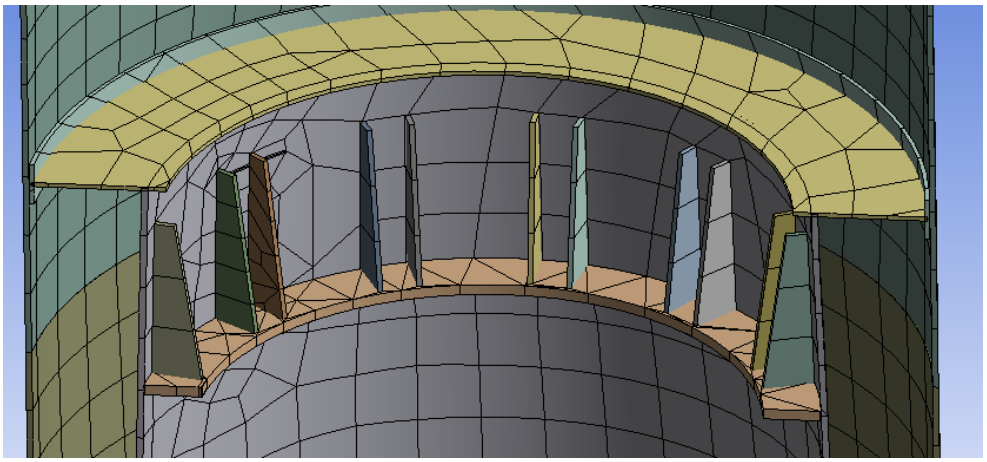

Figure 4.9: Mesh at the lower slip joint.

The quality of the mesh can be improved by refining the mesh locally, as it allows for smaller and better shaped elements. The refined mesh is shown in Figure 4.10.

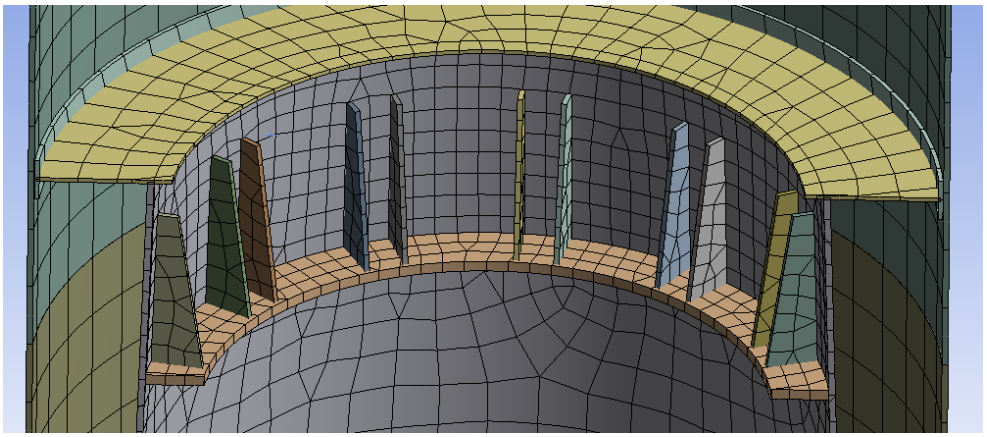

Figure 4.10: Refined mesh.

This refined mesh looks to have better shaped elements. The new element quality is shown in Figure 4.11. The lowest element quality in this location is now approximately 0.6. This shows that the local mesh refinement greatly improved the elements in this location.

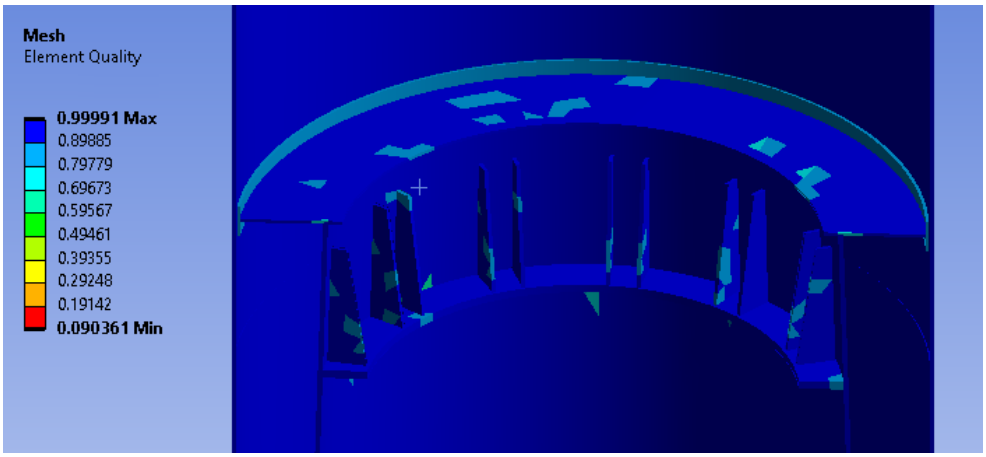

Figure 4.11: Element quality of the refined mesh.

4.2 Complete reference model

The reference model is created by connecting four separate sub-assemblies. These sub-assemblies are the monopile, lower slip joint, tower section and upper slip joint. They mainly exist out of shell elements with a few solid elements.

Monopile

The monopile is the simplest model as it includes very little details or features. It exists out of multiple cylinders and cones with individual wall thicknesses. The soil boundary condition and hydrodynamic added mass are applied to the correct sections of the monopile, see Figure 4.12.

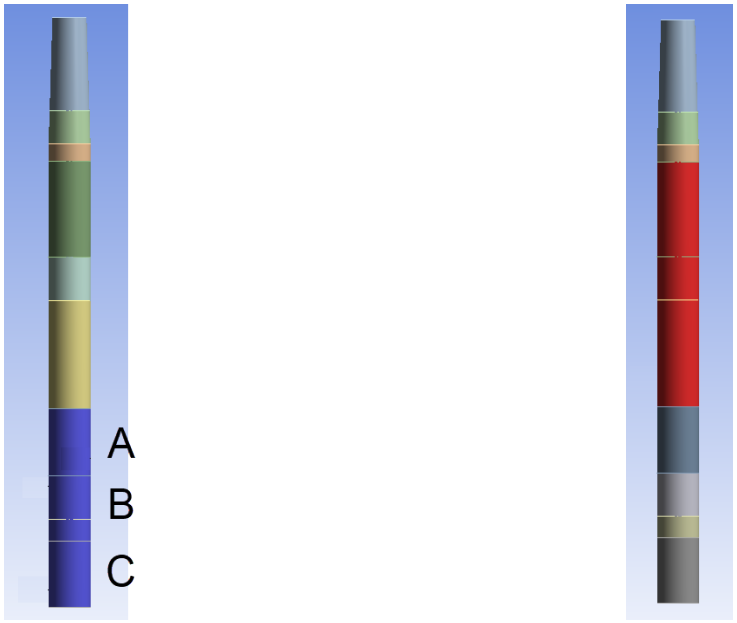

(a) Applied soil boundary condition

(b) Hydrodynamic added mass

Figure 4.12: Boundary conditions applied to the monopile.

Lower and upper slip joint

The models of the slip joints are the most complex of the four sub-assemblies. They include many details and features like stiffeners, sled plates and skirts. Most of these features are shown in Figure 4.13.

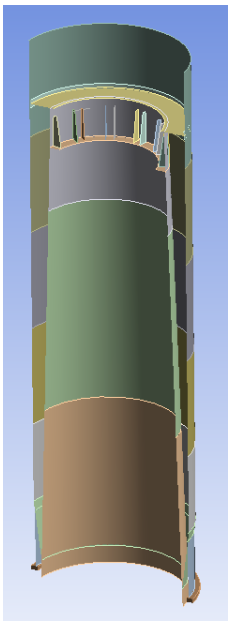

(a) Lower slip joint model

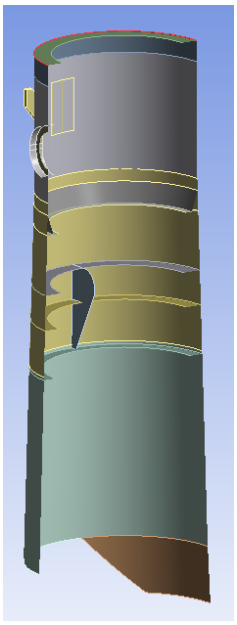

(b) Upper slip joint model

Figure 4.13: Section view of the slip joint models.

Tower section

The tower section of the reference model does not include many details or features. It mainly consists of multiple cylinders with an individual wall thickness, which is also the reason a figure of this section will not be included.

4.2.1 Slip joint simplification

How to model the connection between the two cones of the slip joint is probably one the most interesting and important choices to be made when assessing vibration assisted friction reduction within the joint. There are several physical aspects that could influence the vibration and friction of the joint. A good example is how the friction and contact within the joint is modelled. Correctly including these physical aspects in the model of the joint is important as they influence the accuracy of the results. However, there is a problem with including these kind of physical aspects in the reference model of the wind turbine. The reference model is developed to be used in a modal analysis to estimate the eigenfrequencies and mode shapes of the structure. A modal analysis requires the FE model to be linear, meaning that the relationship between force and displacement in the model is linear. Most of the physical aspects are difficult to include without introducing non-linearity in the FE model. For example, Ansys provides several options for modelling contact in the model. One option is frictional contact, which allows sliding and separation of the contacting surfaces. This could potentially be a good option to model the contact within the slip joint, but creates non-linearities in

the FE-model and can therefore not be used in modal analysis. There are only two contact options with which the FE model remain linear, a bonded contact and a no-separation contact. Either type of contact provides a poor representation of reality.

This essentially leads to two options. Use a simplified model of the slip joint which can be used for modal analysis or create a more detailed model of the slip joint which can't be used for modal analysis. In Ansys, modal analysis is a pre-requisite for many other types of vibration analysis. There might exist alternative methods for the estimation of eigenfrequencies and eigenmodes, but it is chosen to use modal analysis due to its simplicity and common use. This means that the FE model is required to be linear. This results in a large simplification of the slip joints, as the contacting surfaces in the joint have to be modelled as bonded, which is better fitting than the no-separation contact which allows frictionless sliding. As a result the eigenfrequencies and mode shapes estimated in this thesis ignore the possibility of sliding or separation of the joint. However, these results are assumed to still provide a useful initial estimate of the eigenmodes of the structure. At the start of the decommissioning process the slip joints are connected and no sliding or separation occurs, which is resembled by the bonded contact. Once the slip joint starts to slide and separate the system changes and the eigenfrequencies and mode shapes change. A more advanced model and a different type of analysis is required to study the vibrational characteristics of the slip joint during actual disconnection and will not included in this thesis.

4.2.2 Eigenmodes of the reference model

Now that the reference model is developed it is used to estimate the first 300 eigenmodes of the wind turbine tower with slip joint. The first two global modes are shown in Figure 4.14.

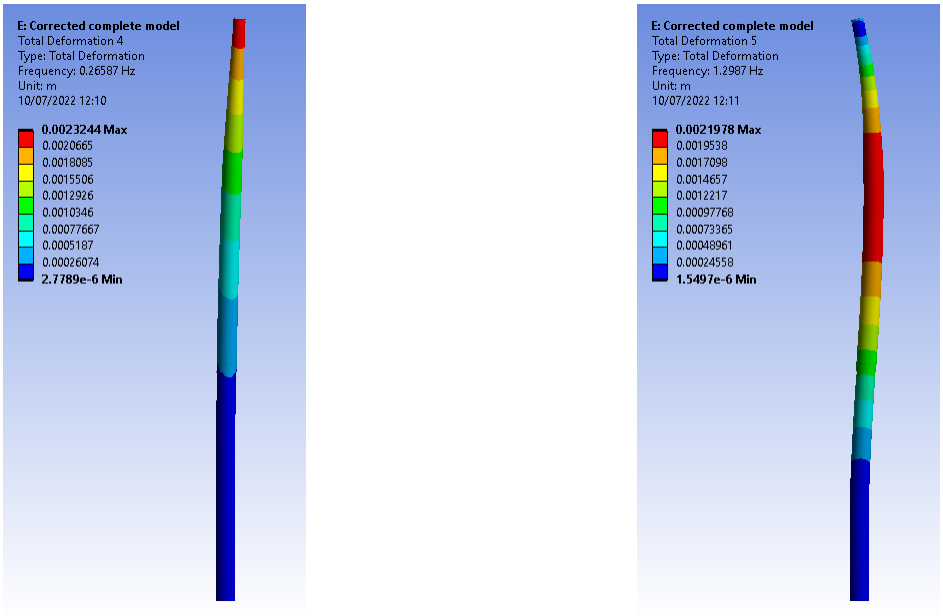

(a) Intersecting shell elements

(b) Touching shell elements

Figure 4.14: The first two global modes of the reference model

They have an eigenfrequency of approximately 0.27 Hz and 1.30 Hz. The first natural frequency lies within an acceptable range, compared to eigenfrequencies found in literature [4]. The 300th eigenmode is found to have a eigenfrequency of 65.3 Hz. The estimated eigenmodes will not be shown in this thesis, as there simply are too many. The modes selected for the comparison to follow will be shown in their respective sections.

Chapter 5

Comparison of the eigenmodes

The goal of this chapter is to explain how the estimated eigenmodes can be compared to one another. This chapter is added because the comparison of the eigenmodes is not a straight forward task and several decision are made during this process. The first section discusses how the Modal Assurance Criterion is used to compare the mode shapes of the shell modes. Section 5.2 explains how the shell modes are matched for the comparison to follow. Section 5.3 discusses which of the 300 eigenmodes will be selected for comparison. Section 5.4 tells how the results of the comparisons will be evaluated. This evaluation is meant to help judge the applicability of the studied simplifications.

5.1 Modal Assurance Criterion (MAC)

5.1.1 Implementing the MAC

This section will discuss how the MAC value is used for comparing two individual mode shapes. Ansys Mechanical does not provide build-in function for the estimation of the MAC. There are individually created add-ons available which at first sight promise to be an easy solution. The function works fine for simple FEM models but is easily broken after a more extensive robustness check. This is mainly caused by the complexity of FE model. The add-on function is not always able to properly handle the differences between the reference and altered model and therefore provides unreliable results. A different approach has to be taken if the MAC is to be used. Since the MAC is one of the most useful tools for comparing mode shapes, it is important that it is implemented in another way. Instead of using the build-in functions, the MAC is implemented with a script written in Python. One can extract the mode shape data from Ansys Mechanical and use it to calculate the MAC. Because of the robustness check of the add-on function it was already known which pitfalls the script had to deal with. The creation of this script will now be discussed in the following sections.

Obtaining the mode vector

The calculation of the MAC requires two mode vectors which contain the deformation of the model at discretized points within the FE model. The first step is extracting the mode shape vectors from the results in Ansys Mechanical. The mode shapes can be exported by Ansys, which provides a text or excel file containing the information. The first column contains all the node numbers of the nodes used by the FE model, which are in numerical order. The second column contains the nodal deformation of the eigenmode, which is the mode vector. The next three columns contain the coordinates of the node. Once obtained, these values can not simply be inserted into Equation (2.3). To be able to compare the mode shapes the nodes in the first mode vector needs to match those of the second mode vector. If the nodes do not match the MAC will compare the nodes from different locations in the FE models, which produces wrong results. The data provided by Ansys includes every single node of the FE model. Even small changes to the FE model alter the total amount of nodes and also affects their order. This makes matching every single node between two separate FE models a complicated task. For this reason, it was chosen to not include all the nodes of the system when assessing the MAC. The nodes that will be used are the nodes that are located in an area of interest. Each eigenmode has an unique mode shape which often is localized around a specific part of the model, an example is shown in Figure 5.1. Nodes outside of this area are less relevant for the comparison. The mode shape shown in Figure 5.1 will be used as a test case for developing the MAC script.

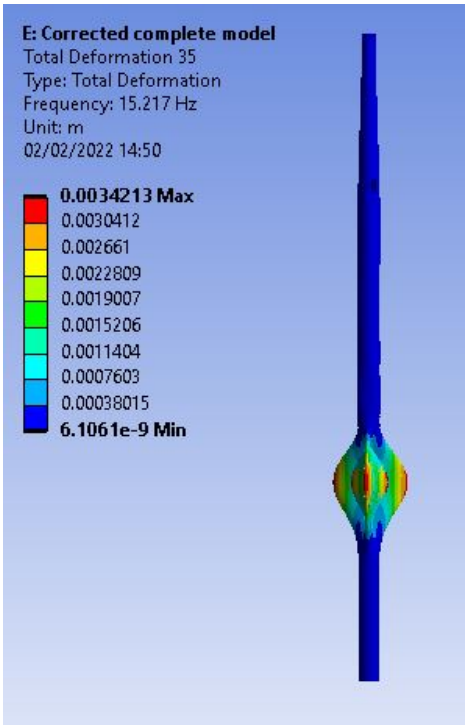

Figure 5.1: Example of a localized eigenmode

Matching the nodes of both models is still a challenging task, even when a smaller part of the FE model is regarded. It was chosen to select cross sections of the FE models as the nodes of interest. The main advantage of using nodal cross sections is that they are easier for matching the nodes of both models and they provide a clear view of the mode shape at that height. The nodes of the cross section also need to matched before the MAC can be calculated. The nodal cross sections of two mode shapes need to be altered to have a matching order and length. The nodal cross sections can be selected in Ansys with the use of a named selection. A named selection has an option to only select the nodes that comply with specified conditions. One of the conditions is to select the nodes located on a specific height level. This option provides the nodes at a given height, which essentially is the nodal cross section of the structure, as shown in Figure 5.2. This method gives the option to only compare the nodes that are excited by the eigenmode and ignore the others. For the test mode shape the nodal cross section of interest is created at a height of around 6 meter.

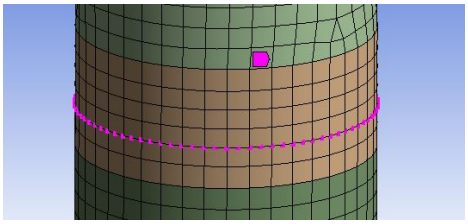

Figure 5.2: Example of a nodal cross section.

This selection of nodes can also be extracted to a text or excel file containing a single column. This column contains all the selected node numbers. The file containing the information about the nodal deformation is now compared with the file containing the node numbers of the cross section. This results in the deformation of the cross sections, as plotted in Figure 5.3.

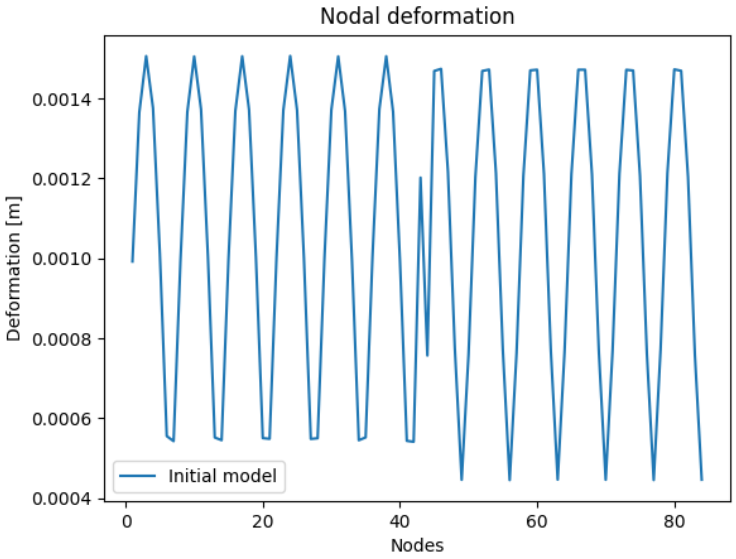

Figure 5.3: Nodal deformation of the cross section.

Figure 5.3 clearly shows harmonic shape of the mode shape. However, it is easy to notice that the mode shape shown in Figure 5.1 has a circumferential wave number of 3 and the vibration shown in Figure 5.3 has 12 peaks. This is happens because of two reasons. The first reason is that Ansys provides the absolute nodal deformation, resulting in the negative part of the vibration also being shown as a peak in the graph, effectively doubling the amount of peaks. The remaining 6 peaks are cause by how the nodes where created in Ansys. The example model of Figure 5.1 mainly consists of conical sections modelled with quadratic shell elements. These elements have a node at each corner and also have a mid-span node. The node numbers given to these nodes are not in the same order as the nodes appear along the cross section. Ansys first assigns node numbers to the corner nodes and only assigns node number to the mid-span nodes after. The consequence is that when the nodes are presented in numerical ordering the nodes circulate the cross section twice, which causes another doubling of the peaks. The shift from corner nodes to mid-span nodes can be seen halfway the graph shown Figure 5.3. The order of the nodes can also cause other problems, as will be shown in Section 5.1.3.

5.1.2 Orientation of the eigenmodes

The second mode vector required for the MAC comparison can be created the same way as the first using the alternate FE model. An alternate FE model was created for this purpose. In this model, simplifications were applied to the lower slip joint. A detailed overview of these simplifications is provided in Section 6.1.1. An eigenmode that is very similar to that of Figure 5.1 is also found in this model. Now that the cross sectional mode vectors for both models are obtained, they are plotted in a single graph, shown in Figure 5.4.

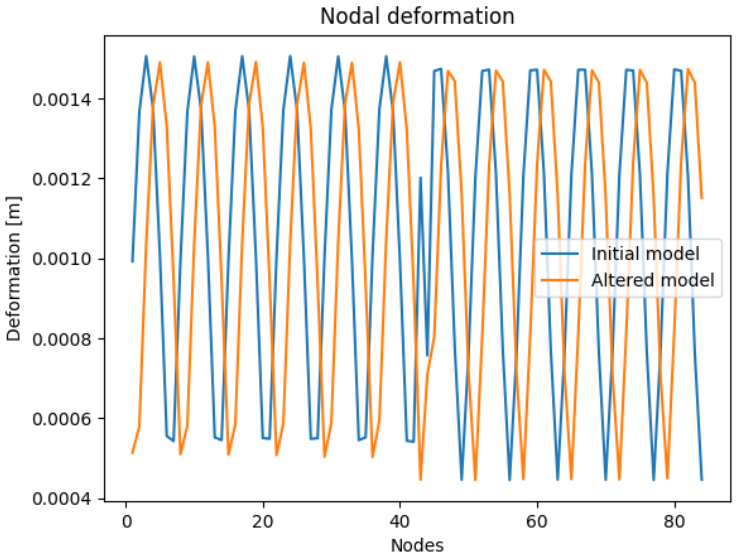

Figure 5.4: Nodal deformation of the original and altered model.

This graph shows that the mode vectors have nearly the same mode shape but are not in phase. This is happens because the location of the initial node of the node vector is not pre-defined and can differ for each FE model. Since the initial node is not defined the phase of the node vector is random. Entering these two mode vectors in the MAC equation 2.3 gives a MAC value of 0.771. There are two ways to deal with the phase of the node vectors. The first is by shifting the node vector one node at the time and assessing the MAC. The best fitting phase can be found by assessing when the MAC has reached a maximum value. This method ignores the orientation of the eigenmode as provided by Ansys. The highest MAC value will be obtained when the node vectors are in phase, which is shown in Figure 5.5. Entering these two mode vectors in Equation (2.3) now provides a MAC value of 0.994.

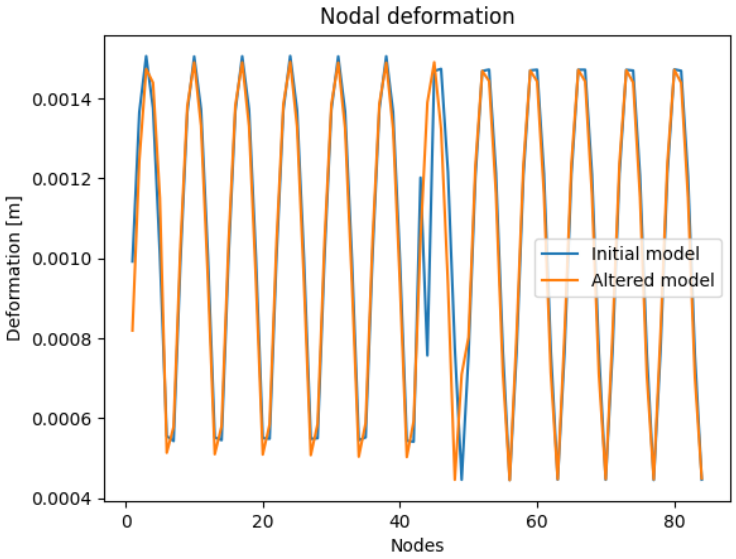

Figure 5.5: Nodal deformation of the original and altered model with correct phase.

The second method two correct the phase of the mode vectors would be to define the starting node of the node vectors. The starting node can be defined based on its geometrical location. In this script the starting node was chosen as the node with the largest X-coordinate. This method does include the orientation of the eigenmode as provided by Ansys. Which method is preferred is dependent on whether or not the orientation of the eigenmode is of interest. The orientation of the eigenmodes are of interest, as explained in Section 3.4. The script will estimate the MAC value using both methods. The script will therefore estimate two MAC values, one that respects the orientation of the eigenmode and one that ignores it and maximizes the MAC by shifting the node vector. Using both methods might provide some insights about the angle in which the modes are oriented.

5.1.3 Sorting the nodes

The order of the nodes in the node vector is important. If the nodes of both vectors are not in the same respective order the resulting MAC value has no meaning. The order of the nodes in the node vector is determined by the node number which is assigned by Ansys. The node vectors of the example of the previous section were already in the correct order by accident. This happened by 'coincidence' as Ansys generated the nodes and node numbers in corresponding order when it meshed the FE models. Unfortunately, this is not always the case for other models. In this section another example model is discussed. This model consists of a rectangular hollow beam and is created as a surface area meshed with shell elements, shown in Figure 5.6a. The eigenmode that will be considered is shown in Figure 5.6b. This eigenmode will be compared with the eigenmode obtained using the same beam model which is rotated by 45 degrees along its length. These models obviously provide the same eigenmodes, as the geometry is exactly the same. However, the rotation mixed the order of the nodes in both models.

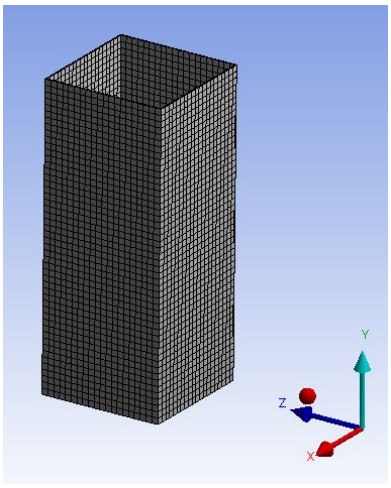

(a) Meshed model

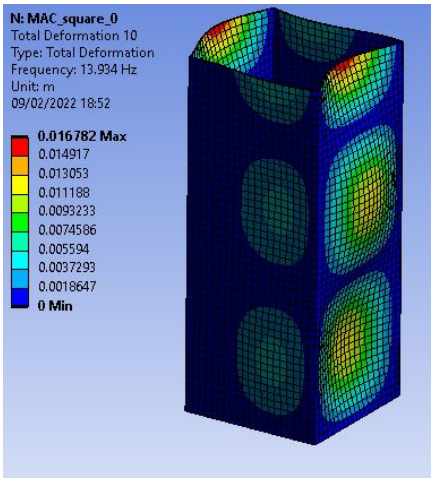

(b) Eigenmode to be compared

Figure 5.6: 2nd example model.

The mode vectors at a cross section near the top of the models were obtained and are shown in Figure 5.7. It is obvious that these mode vectors have no correlation and they can't be used to calculate the MAC value. The nodes of the mode vectors are not in the same order because Ansys generated the nodes in a different way for both models. The order of the nodes have to be corrected to properly compare the mode vectors. The nodes are reordered by post-processing the mode vectors in the python script. The nodes are put in order by starting at the initial node in the node vector. The script than calculates which of the other nodes is located nearest to this node and places the nearest node in the 2nd position. The nearest node is located by using the nodal X,Y,Z-coordinates and Pythagoras' formula. This is done for all the nodes in the mode vector, which reorders the nodes based on their geometrical proximity.

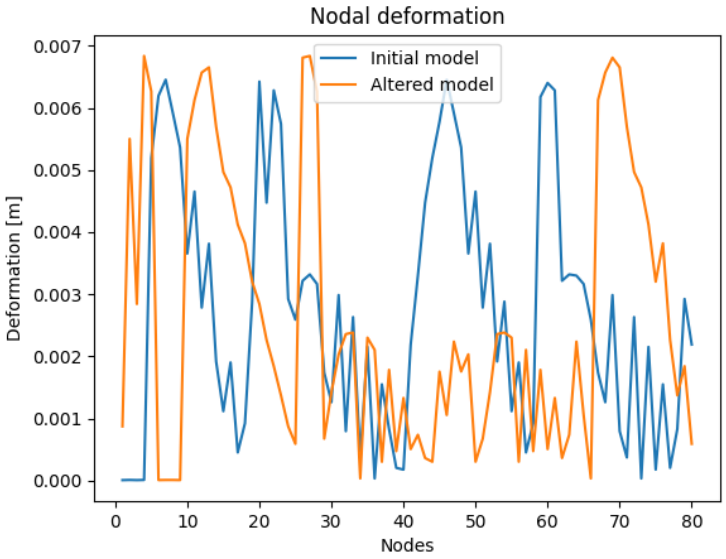

Figure 5.7: Nodal deformation of the cross section of the square model before sorting.

After re-ordering the nodes of the two mode vectors the are again plotted, which is shown in Figure 5.8

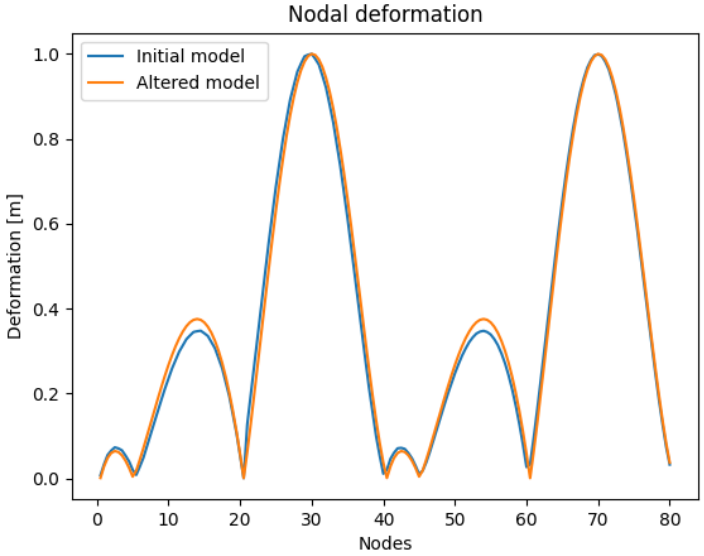

Figure 5.8: Nodal deformation of the cross section of the square model after sorting.

Entering these mode vector into Equation (2.3) provides a MAC value of 0.997 which correctly matches the two eigenmodes.

5.1.4 Interpolation of the nodes

Not only the order of the nodes of the node vector is important, but so is its length. Both node vectors need to have the same number of nodes to be compared. The total number of nodes is dependent on the mesh of the FE model. If both FE models have a similar mesh the could have the same amount of nodes but this is not guaranteed. If the mesh is different both models will likely have a unequal amount of nodes. For example, the second model of the second example, shown in Figure 5.6, is now meshed with a half the original element size. This results in one mode vector having a length of 80 nodes and a second mode vector with a length of 160 nodes. These mode vectors are plotted in Figure 5.9.

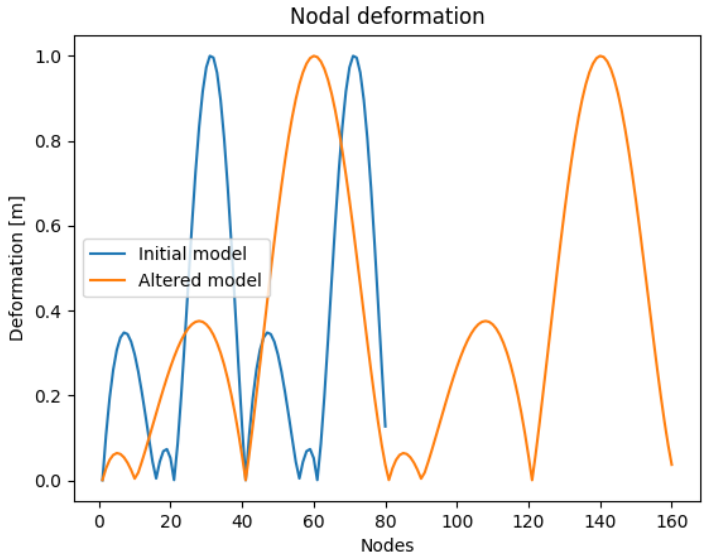

Figure 5.9: Nodal deformation of the cross section with unequal amount of nodes.

The graph shows two similar mode shapes which are of different length. These mode vectors have to be made of the same length before they can be used to calculate the MAC. Both mode vector represent the full cross section of the structure but the second one simply contains more nodes with a smaller division along the cross section. The length of the mode vectors can be changed by interpolating the nodes. In the python script, linear interpolation is applied to the smaller of the two mode vectors, making it the same length as the other mode vector. The resulting mode vectors are shown in Figure 5.10.

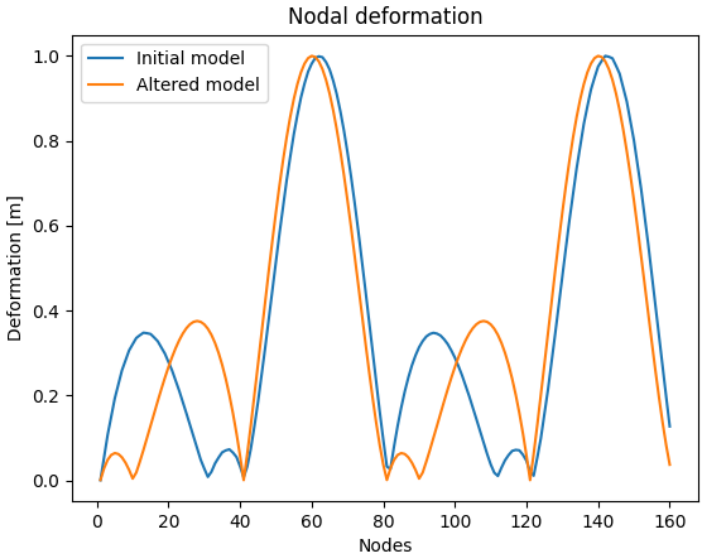

Figure 5.10: Nodal deformation of the cross section after interpolation.

The mode vectors are of the same length and show that the mode shapes are similar but are in the opposite direction of each other. This can happen because the direction of the nodes along the cross section was not yet defined in the sorting part of the script. This can easily be fixed by adding code that checks the direction of the nodes and reverses the mode vectors if necessary.

5.1.5 Scaling the vectors and multiple cross sections

The nodal deformations given in the mode vectors produced by Ansys are not actual measures for the deformation in the structure since they are scaled arbitrary and only specify the mode shape of the eigenmode. Equal scaling between the two models can not be assured. In the python script the mode vectors are all normalized by the highest deformation present in the mode vectors. This normalizes the mode vectors while still keeping the scaling equals between them. The MAC is not affected by the scaling of the mode vectors. This does, however, come with a problem. When two cross sections have a similar mode shape but differ in amplitude they will still provide a MAC value close to 1. An example of this is given in Figure 5.11. In this example, two separate mode vectors are extracted from the same mode in the reference model and the altered model. The mode vector of the reference model is taken at a height outside the region of where the eigenmode is localized.

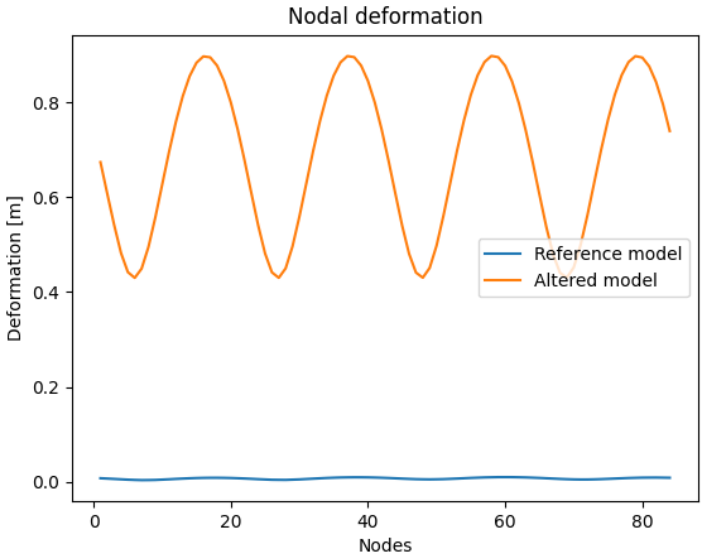

Figure 5.11: Node vectors taken at different heights.

When these two node vectors are used to calculate the MAC they still provide a value of 0.99. This happens because the shape of the mode vectors is the same, the only difference is their individual scaling. Looking closely, Figure 5.11 shows the similarity in mode shape. The mode vectors can be made equal by using the right scaling parameter. This problem with the scale of the mode vectors can be solved by using multiple cross sections at the same time. By using multiple cross sections, the mode vectors can not be scaled arbitrarily any more. This is shown by introducing a second cross section in the previous example. This cross section is taken at the same height for both models, at a region where the eigenmode is localized. The two mode vectors at this height are shown in Figure 5.12. The mode vectors have a similar shape and amplitude and have a MAC value of 1.

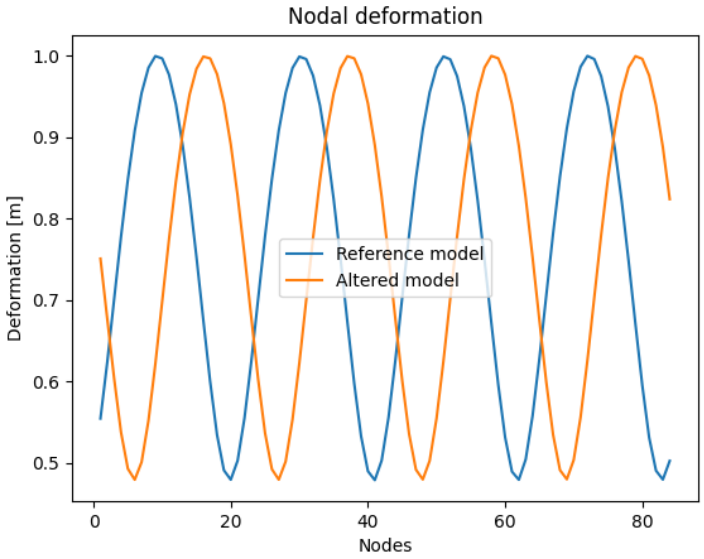

Figure 5.12: Node vectors taken at same height.

By appending the mode vectors belonging to the same model two new mode vectors containing the deformation of both cross section can be created. These new mode vectors are shown in Figure 5.13.

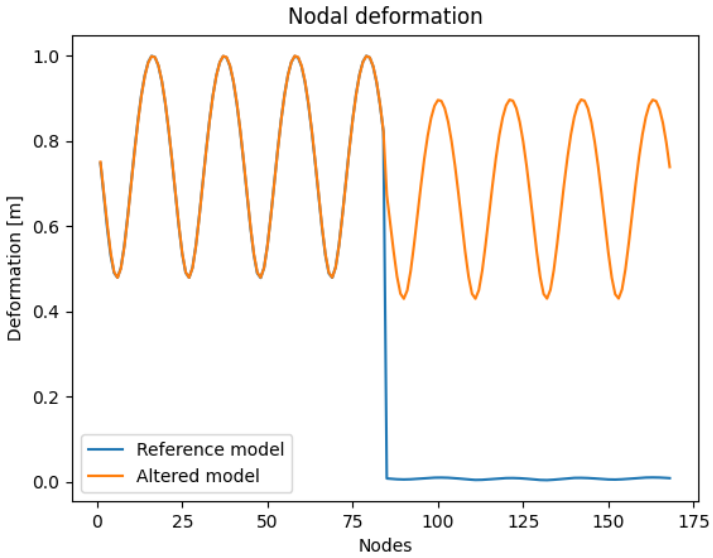

Figure 5.13: Combined node vectors taken two heights.

The figure shows that the mode vector of the reference model includes a cross section that is located outside the region where the eigenmode is localized. Now that the mode vectors are combined, there no longer exists a scaling parameter that can make both vectors similar. These mode vectors now result in a MAC of 0.56, showing that the models do not have the same mode shape and/or relative amplitude.

5.1.6 Cross section selection

It is essential that the right cross sections are selected for the estimation of the MAC of two eigenmodes. The MAC will only contain information about the mode shapes at the selected cross sections. Information about the mode shapes of the eigenmodes outside of these cross sections is lost. The cross sections should therefore be taken at a location of interest. Not only the location of the cross sections is important but also how many are selected. Section 5.1.5 already showed that multiple cross sections are required to fix the scaling of the node vectors. How many cross sections should be included is not yet known. The resulting MAC value is dependent on the amount of cross section used. Whether an added cross section decreases or increases the resulting MAC is dependent on the mode shapes of that cross section. Two similar mode shapes could still obtain a low MAC value when the cross sections are taken at precisely the locations where there are small discrepancies between the mode shapes. Sufficient cross sections should be selected to increase the accuracy of the results. Each added cross section decreases the influence of the other cross sections. This also decreases the influence of outliers, resulting in a more reliable MAC.

The amount of cross section which is sufficient is studied with an example. For this example eigenmode 225 of the reference model is used. This eigenmode was selected because of its short wavelength, which increases the chance of selecting inaccurate cross sections. The second model used is the first simplified model, as presented in Section 6.1.1. The two mode shapes located at the lower slip joint are shown in Figures 5.14a and 5.14b.

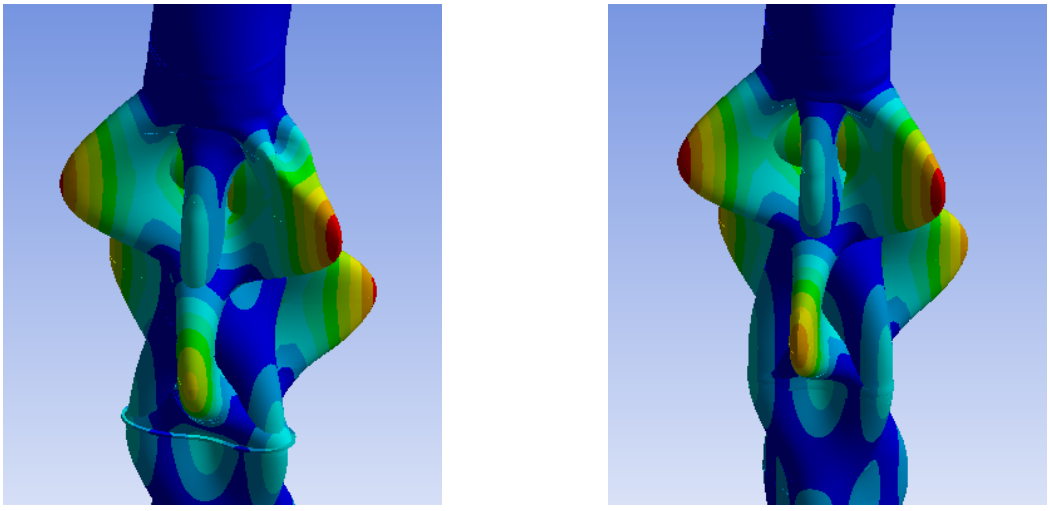

(a) Mode 225 of the reference model

(b) Matched mode of changed model

Figure 5.14: Mode of both models used to study the MAC cross sections.

To estimate the MAC of these mode shapes, ten cross sections are selected along the height of the slip joint, shown in Figure 5.15.

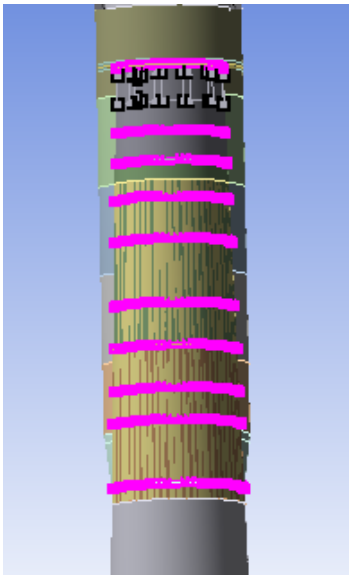

Figure 5.15: Ten cross sections selected at the lower slip joint.

Now, the cross sections are be removed one by one and every time the MAC is calculated. This is done twice. Once removing the cross sections starting from the bottom and once starting from the top. The results are shown in Table 5.1.

Cross sections	10	9	8	7	6	5	4	3	2	1
MAC1	0.89	0.87	0.86	0.86	0.86	0.91	0.94	0.95	0.85	0.97
MAC2	0.89	0.89	0.91	0.92	0.9	0.89	0.93	0.94	0.98	1

Table 5.1: MAC for different amount of cross sections.

This table shows that the MAC convergences to a value around 0.89. The MAC starts to converge around 8-9 cross sections. For the most accurate MAC it would be beneficial to include many cross section. However, adding many cross sections can be challenging. Each added cross section requires a horizontal nodal cross section. It was therefore chosen to set the minimum amount of cross sections to eight. When assessing the MAC it should be kept in mind that a small error is possible, especially for higher order modes.

5.1.7 Limitation to the MAC script

The developed script offers the ability to quantitatively compare local mode shapes. It does so by using node vectors of specified cross sections and calculating the MAC, which indicates the

correspondence between the mode shapes. However, mostly due to the complexity of the FE models, there are some limitations the script. First of all, the script can't be used when assessing the global modes of the structure. The script uses the changes in cross sections to assess the mode shapes. For global modes the cross sections remain mostly unchanged, making the script unreliable. Second, the script can't be used for the initial matching of the eigenmodes. Because of large local similarities between several modes the script can provide high MAC values for multiple modes and thus can't be used to distinguish between those modes. This is further discussed in the next sections. Lastly, the script requires the presence of horizontal nodal cross sections. These are not always present in the FE model. The horizontal nodal cross sections can be guaranteed by applying changes to the FE model, but this can become an relatively extensive task.

5.2 Matching the modes

Before the eigenmodes estimated by a model can be compared to the eigenmodes of a different model they have to be matched, as explained in Section 2.6. The most common way to do this is with the use of a MAC matrix, as explained in Section 2.6.1. Unfortunately, the use of a MAC matrix to match the eigenmodes is not applicable in this research. Using a MAC matrix to match the estimated shell modes would not result in a matrix containing a clear divide between the matching and non-matching modes but a mix of value ranging from 0 to 1, often without revealing a clear match. This happens because there are many similar mode shapes between the estimated eigenmodes. Also, the mode shapes often are not a perfect match due to the changes to the FE model. For this reason there might be multiple mode shapes that have similar MAC values, causing the inability to match with the MAC matrix. The next section discusses a example of similar MAC values.

5.2.1 Example of the MAC matrix

This example discusses the matching of mode 203 of the reference model with a mode estimated by a model with simplifications applied to the lower slip joint. Mode 203 of the reference model is a shell mode with an eigenfrequency of 5.15 Hz, see Figure 5.16.

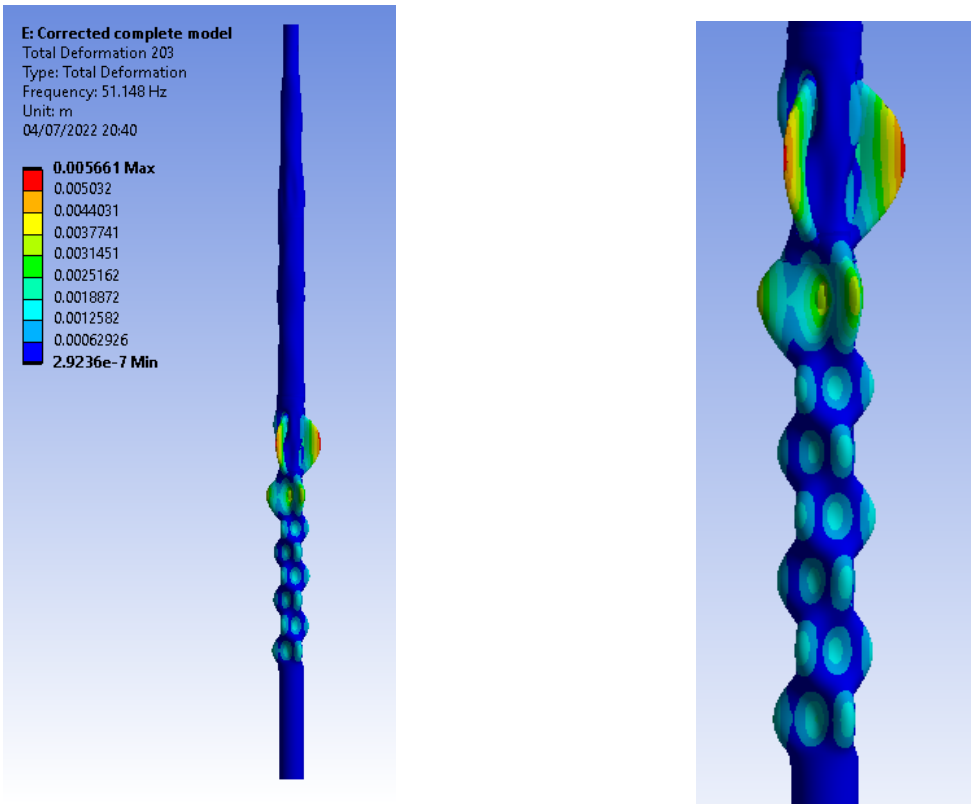

(a) Complete view of shell mode

(b) Zoomed in view

Figure 5.16: Mode 203 of the reference model.

A few shell modes of the simplified model were selected in the same frequency range as this mode, which can be found in Figure A.1. By visually comparing these modes you would likely match mode 203 of the reference model with mode 206 of the simplified model. There is a difference in the mode shape due to the simplification, but it is the best fitting option.

Using these shell modes to calculate the MAC provides the results shown in Table 5.2.

Eigenmode	MAC
203	0.042
205	0.646
206	0.718
207	0.718
208	0.345
216	0.064

Table 5.2: MAC values for the example studied.

This table shows that the mode shape of the shell mode changed significantly, since the highest MAC value present is only 0.718. There are also other MAC values present that are equal or similar to this value. The matching mode can't be selected solely on the MAC. This example shows why a MAC matrix can't be used to match the found shell modes. In this case, the MAC can only be used to provide a quantitative comparison of already matched modes.

5.2.2 Manual matching

Unfortunately, the MAC script developed can't be used to match the modes. There likely exist better methods to match the shell modes, but this lies outside the scope of this thesis. For the lack of a better method, the shell modes will be matched manually. The matching eigenmodes are found by manually comparing the mode shapes of the eigenmodes. There are several strategies to match the eigenmodes. For example, one can look at the location of excitation. It can also be useful to assess the amount of waves present in each of the modes, denoted with the parameters m and n, which are described in Section 2.3. Matching eigenmodes are also usually found within a certain region of eigenfrequencies. Combining these strategies usually leads to being able to match the modes.

Unfortunately, this is a extensive and subjective task which is prone to errors. Therefore, results need to be checked thoroughly. When uncertainties occur during the matching process, the MAC value can be used to provide extra information on the similarity between the mode shapes of the shell modes. Luckily, there is one upside to this story. Problems during the matching process are most likely to occur for shell modes with large changes in their mode shapes. When modes have large differences in their mode shape the simplification applied to the FE model obviously affected that resulting shell mode a lot. Difficulties in the matching process can therefore be seen as a first indication that the simplification had to much of an effect on the results.

5.3 Modes of interest

The FE model of the offshore wind turbine estimates the first 300 eigenmodes of the structure. It would be tedious and inefficient to compare each eigenmode to the matching eigenmode of the changed FE model. Not all eigenmodes are interesting for comparison and will only clutter the results. For example, changes applied to the lower slip joint are likely to have more effect on shell modes localized at this region. For this reason it is helpful to select a few shell modes which are localized around the location where the changes to the FE model are applied. The most preferred option for selecting the eigenmodes would be based on their effectiveness in reducing the friction force in the slip joint, as this is the idea behind this thesis. However, at the current time it is not yet known which eigenmodes that would be. Instead, the eigenmodes will have to be selected based on other criteria.

The first criterion, as was provided as an example, is the location of excitation for the eigenmodes. When local changes are applied to the FE model it is more interesting to select shell modes which are localized around the region where the changes are applied. The second criterion is based on the eigenfrequency of the shell modes. It is likely for the reduction of friction to be dependent on the frequency of the eigenmode. A wide variety in the eigenfrequencies of the selected eigenmodes

is therefore a necessity. The last criterion for the selection is that the shell mode must show a clearly recognizable mode shape. This criterion can be a bit vague but is added because of practical reasons. Section 5.2.2 explained that the shell modes need to matched manually. Matching the eigenmodes manually can become challenging, especially for higher modes with more erratic mode shapes. Eigenmodes that have no clearly recognizable mode shapes should not be included in the modes of interest, as matching them can become too challenging.

Each detail to be studied has a specific selection of shell modes, since each detail has a different location in the structure. Next to the selected global modes, the results will also include the first and second global mode of the structure. These modes are not of great interest for reducing the the friction force within the slip joint, but they are still included for several reasons. The first reason is that these eigenmodes are usually the eigenmodes of interest when assessing the eigenmodes of the structure, as explained in Section 2.5. Most information available on the eigenmodes of wind turbine towers is in regard to their global modes. This means that they can be used as point of reference. The comparison of the global modes might also be of interest for other studies regarding the vibration of offshore wind turbines. A second reason is that the first two global eigenmodes are easy to recognize and match, making them easy and quick to use for initial comparisons. Lastly, these modes span the entirety of the structure and are therefore more likely to be influenced by the simplification studied.

The selection of the eigenmodes that are specific to the location of the detail to be studied will be discussed in their respective sections of Chapter 6.

5.4 Evaluation of the results

The matched eigenmodes can be compared based on the following three results: the eigenfrequencies, the mode shapes with the help of the MAC and the angle of orientation of the mode. These values will be used to discuss whether or not the simplifications applied to the FE model have a large affect on the resulting shell modes. Before this is done it should be discussed how these individual parameters will be evaluated and what limits will be applied to them. How these values will be evaluated is partially based on their role in the decommissioning process.

The eigenfrequency is the most basic result of the three. The eigenfrequency of the mode is important because it is used to set the frequency of the shakers. Luckily, there is some margin in how exact the estimated eigenfrequencies have to be. Changing the frequency of the shakers is relatively easy and most of the time even common practice. Eigenfrequencies are almost never known exactly. When trying to excite an eigenmode, the frequency of the shaker can be tuned to try and find the correct frequency. What error in eigenfrequency should be accepted is still a subjective matter. For practicality, the limit used in this thesis is set to 2 percent. This will result in a maximum error of approximately 1.2 hertz, as the highest modes estimated have an eigenfrequency of around 60 hertz.

The mode shapes of the shell modes will be compared using the MAC. In Section 2.6.1, it was mentioned that often a MAC of greater than 0.9 is accepted for matching modes. However, this value is likely to be too strict for the goal of this thesis. A MAC of 0.9 or higher indicates a very close match between the mode shapes. In this thesis a slightly lower MAC value of 0.8 will be

accepted. This is done because small differences in the mode shapes are to be expected, caused by the simplifications applied to the model. A MAC of 0.9 is therefore to strict. A MAC of 0.8 still indicates a good resemblance between the mode shapes, but is a bit more lenient to small local changes in the mode shapes.

The angle of orientation of the modes can be an important result for the decommissioning of the slip joint, as it can influence the location of the shakers. However, there are some uncertainties regarding this property. It is unclear how this value is determined by Ansys and how it is affected by changes to the model. The angle of orientation is included in the results to gain more insight into this property. However, the angle of orientation will not be used to judge the validity of the simplified models.

Chapter 6

Results

This chapter presents the results of the comparisons of the shell modes found be the reference model and the simplified models. The results of seven separate simplified models are compared to the reference model. Each section presents which simplifications were applied to the FE model and provides the results of the comparison. Section 6.1 includes the simplification and results for the lower slip joint. Section 6.2 presents the simplifications and results for the upper slip joint. Finally, Section 6.3 discusses the results of averaging the wall thickness of the tower for both the lower and upper slip joint.

6.1 The lower slip joint

The lower slip joint is the part of the wind turbine that contains the most details and has the largest interests in relation to the decommissioning phase. It is essential that eigenmodes around this area can be accurately predicted. A section view of the lower slip joint is shown in Figure 6.1. It consists of an outer cylinder and an inner cone which is the part that is in contact with the monopile. For this reason, the inner cone is of greater interest than the outer cylinder when assessing the shell modes. The outer cylinder and inner cone are connected at the top with a horizontal ring, shown in Figure 6.2c. They are also connected at the bottom where the cone and the cylinder touch. Within the slip joint, many stiffener-like parts are present, each having their own function. Some of these parts are presented in Figure 6.2. The outer cylinder and inner cone have a varying wall thicknesses along their height. All these details make the lower slip joint a difficult part to model. This section discusses these details are simplified and how the simplification affects the results of the modal analysis.

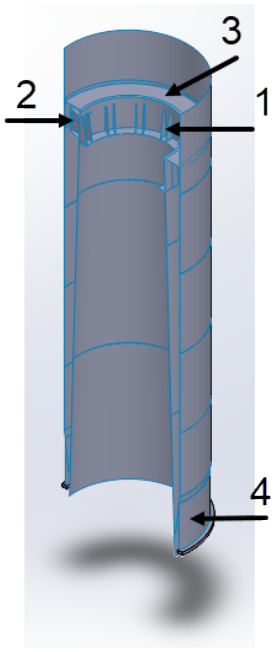

Figure 6.1: Complete model of the lower slip joint including location of the details.

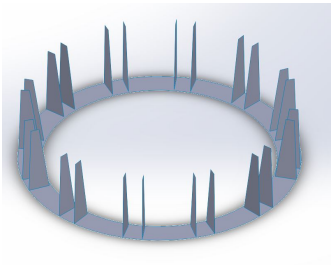

(a) Flanged ring (1)

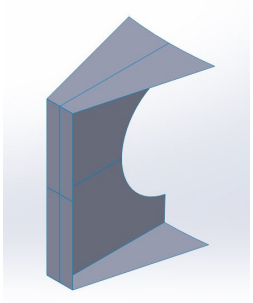

(b) Sled plates (2)

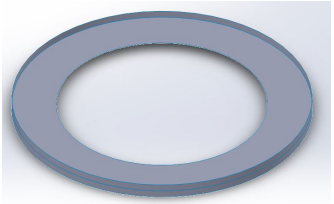

(c) Horizontal ring (3)

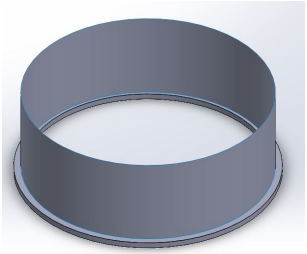

(d) Skirt (4)

Figure 6.2: Four features present in the lower slip joint.

Modes of interest

The modes of interest of the lower slip joint can be found in Appendix A.2. The location of the lower slip joint is indicated with two red dotted lines. These modes were selected based on the criteria given in Section 5.3. The first two modes, as shown in Figures A.2a and A.2b, are the first two global modes of the tower. The other selected modes were chosen based on the selection criteria as discussed in Section 5.3.

MAC cross sections

The cross sections used to determine the MAC for the eigenmodes of interest are shown in Figure 6.3. The cross sections are taken at the inner cone of the slip joint, because it is the main location of interest. The highest modes in the modes of interest had similar wavelengths to the example mode of Figure 5.14a. It was therefore chosen to use eight cross sections.

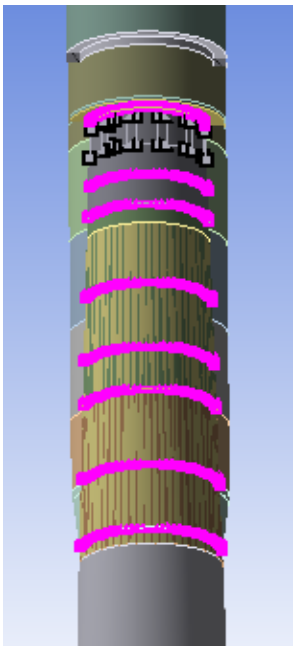

Figure 6.3: Cross sections used for the MAC of the lower slip joint.

6.1.1 Removing stiffener-like features

The first simplified model of the lower slip joint is developed with the goal to study the effects of removing the stiffener-like parts, while keeping the geometry of the inner and outer cylinders mostly the same. This is done by removing three details from the lower slip joint model. These details are the flanged ring, the sled plates between the inner and outer cylinders and the skirt at the bottom. These details are shown in Figure 6.2. A fourth detail, the horizontal ring connecting the inner and

outer cylinders, is altered. The vertical flange of this ring was removed and its dimensions were changed to exactly fit between the inner and outer cylinder of the slip joint. This was done because to simplify the geometry. They required contact definitions and, due to their unique geometries, also required local mesh refinements. The parts are shown in Figure 6.2 and their locations within the lower slip joint are shown in Figure 6.1. With these added changes the new section view of this model of the slip joint is shown in Figure 6.4

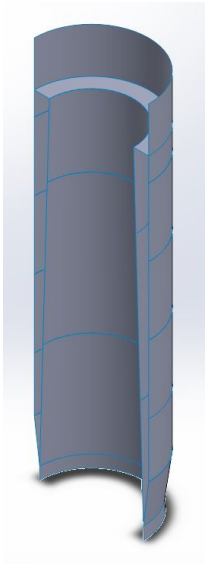

Figure 6.4: First simplified model of the lower slip joint.

Removing stiffener-like features - Results

The resulting eigenfrequencies, MAC values and orientation angles are shown in Table 6.1.

Mode number Reference	Mode number Simplified	Frequency Reference [Hz]	Frequency Alternate [Hz]	Δ Freq [%]	MAC_{opt}	Orientation angle [°]
3	4	0.266	0.266	0	-	-
5	5	1.298	1.305	0.54	-	-
14	14	6.512	6.492	-0.31	1	12
25	26	11.036	10.808	-2.07	0.99	15
37	38	16.472	15.39	-6.57	0.96	14.6
61	56	22.768	21.7	-4.69	0.82	9.73
97	90	31.709	30.272	-4.53	0.99	6
131	128	38.871	37.473	-3.60	0.62	28.5
188	189	49.154	49.243	0.18	0.99	12
203	206	51.148	52.193	2.04	0.72	0
225	222	55.955	55.082	-1.56	0.71	4.9
255	258	60.033	60.607	0.96	1	7.5

Table 6.1: Removing stiffener-like features - Results.

Table 6.1 shows that the simplification does affect the eigenmodes estimated by the FE models. Most of the eigenfrequencies found by the simplified model are lower then those found by the reference model. The reduction in eigenfrequency was expected because the removed details were mostly resembling stringers, which improve the stiffness of the structure. The largest changes in eigenfrequencies happen for mode pairs 37-38, 61-56 and 97-90. These modes have high excitation directly located at the lower slip joint. Modes with excitation near but not on the slip joint show a smaller change in eigenfrequency. These results confirm the importance of the relative location of the simplifications and the eigenmodes.

The largest changes in mode shape are happening for mode 131-128, 203-206 and 225-222. They have a MAC value below 0.8, showing that the simplifications had a large influence on the mode shapes of these modes. The change in mode shape around the slip joint for mode 131-128 and 203-206 can be verified visually in Appendix A.2 and Appendix A.3. These figures show that mode 131-128 extends further along the slip joint and mode 203-206 changes from having a half wave to a full wave along the slip joint. The change in mode shape for mode 225-222 is hard to see visually, which shows the usefulness of the MAC.

The last column of Table 6.1 shows the orientation angle of the eigenmodes. The maximum angle is approximately 15 degrees with the one outlier being mode 131-128. The second mode pair of eigenmode 128 of the simplified model, mode 124, had a orientation angle of only 7.5 degrees but had a MAC value of 0.52, which made it an even worse match with mode 131 of the reference model. These results shows that the orientations of the modes shift when simplification are applied to the FE model. The orientation angles show little correlation with the other results. This indicates that the angle of orientation might not be reliable after simplifications are applied.

6.1.2 Removing the segmented wall thickness

Another detail complicating the modelling of the lower slip joint is the segmented wall thickness. The outer and inner cone of the slip joint have a varying wall thicknesses along their height. As a consequence, the cones have to be modelled with several connected smaller cones. This allows for assigning individual wall thicknesses. This also adds a lot of extra modelling work and can introduces a lot of different errors and/or inaccuracies. It would be beneficial if the wall thickness could be averaged and be applied to the entirety of the respective cone. The original wall thicknesses of the cones are visible in Figure 6.5.

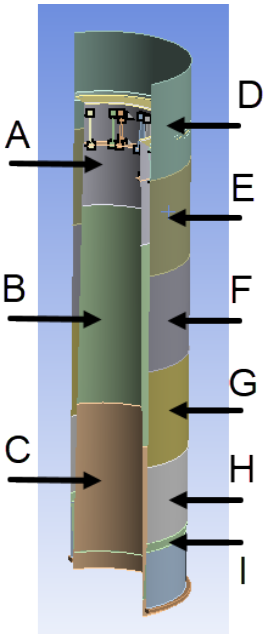

Figure 6.5: Multiple wall thicknesses of the lower slip joint.

The corresponding wall thicknesses can be found in Table 6.2. This table also shows the surface area of the respective parts as these will be used to average the wall thickness. Using the surface area will help average the wall thickness based on the size of the individual cones, as the surface area reflects both the height and diameter of that cone.

Part	Wall thickness [mm]	Surface area [m^2]
A	30	26.58
B	35	55.22
C	30	50.14
D	27	32.84
E	28	32.51
F	29	32.51
G	30	32.51
H	35	25.96
I	30	18.87

Table 6.2: Wall thickness and surface area of the sections.

The average wall thickness for the outer and inner cone are estimated at 29.6 mm and 32.1 mm, respectively. These average wall thicknesses are applied to the FE model and the eigenmodes are estimated. The eigenmodes matching to the eigenmodes of the reference model are shown in Appendix A.4.

Removing the segmented wall thickness - Results

The resulting eigenfrequencies, MAC and orientation angles are shown in Table 6.3.

Mode number Reference	Mode number Simplified	Frequency Reference [Hz]	Frequency Alternate [Hz]	Δ Freq [%]	MAC_{opt}	Orientation angle [°]
3	3	0.266	0.266	0	-	-
5	5	1.298	1.297	-0.077	-	-
14	14	6.512	6.511	-0.015	1	0
25	25	11.036	11.041	0.045	1	4.5
37	37	16.472	16.471	-0.006	1	0
61	61	22.768	22.74	-0.123	1	9.7
97	97	31.709	31.682	-0.085	1	0
131	134	38.871	39.125	0.653	1	4.5
188	190	49.154	49.158	0.008	1	0
203	196	51.148	50.364	-1.533	0.99	4.9
225	225	55.955	55.94	-0.027	0.98	0
255	255	60.033	60.103	0.117	1	0

Table 6.3: Removing the segmented wall thickness - Results.

The resulting eigenfrequencies and MAC values show that the reference model and altered model provide nearly the same estimations for each of the eigenmodes compared. Based on these results, it can be concluded that the averaging of the wall thickness for both the cylinders of the slip joint has little effect on the resulting shell modes. Their are several possible explanation why averaging the wall thickness has little effect on the results. First, the wall thicknesses were already very similar, averaging them lead to only small changes. Second, this type of simplification is likely to have a

more equally divided influence over the slip joint. For example, removing local features are more likely to have local effects, while averaging a wall thickness will influence the entirety of the section to which it is applied. The angles of orientation are also a lot smaller than those in Section 6.1.1, but still not zero for all eigenmodes. This shows that the orientation of a mode can even be affected by small changes in the FE model, even when the eigenfrequencies and mode shapes are nearly identical. According to this study, this type of simplification may be applied without having a large influence on the shell modes of the structure.

6.1.3 Simply replaced lower slip joint.

The simplifications of the previous two sections were applied to the lower slip joint. In both cases the lower slip joint is an individual part that is later inserted into the assembly of the complete FE model. Instead of creating a separate model for the lower slip joint and the monopile, this section will discuss the possibility of merging these models. It can be beneficial to merge these models together, since the lower slip joint and the monopile are connected as a bonded contact. This results in a simpler combined model. A cross section of this model is shown in Figure 6.6.

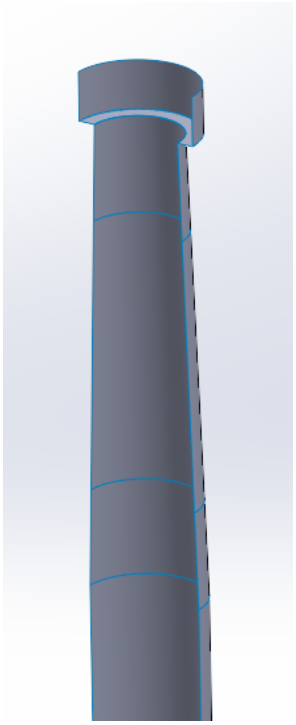

Figure 6.6: Model of the combined lower slip joint and monopile.

In this model, the lower slip joint and monopile are merged into a single model consisting of a single cylinder like part. The outer cylinder of the slip joint is removed and the inner cone is merged with the monopile. It was chosen to remove the outer cylinder and respect the geometry of the

inner cone, because the inner cone is actually the slip joint, while the outer cone is not. Because the geometry of the inner cone is respected, there is a sudden jump in cylinder diameter at the top of the slip joint. Here, the joint is connected to the tower with a horizontal ring, which is the same as in the reference model. All other details of the lower slip joint are removed. The initially overlapping part of the slip joint and monopile is given a wall thickness equal to the combined wall thickness of both parts. For the wall thickness of the inner cone of the lower slip joint the average value of 32.1 mm is used. Section 6.1.2 showed this had little effect on the results of the modal analysis. The monopile has a wall thickness of 40 mm at this height, resulting in a combined wall thickness of 72.1 mm.

Simply replaced lower slip joint - Results.

The eigenmodes of the model are estimated and are matched to those of the reference model, shown in Appendix A.5. The resulting eigenfrequencies, MAC and orientation angles are shown in Table 6.4.

Mode number Reference	Mode number Simplified	Frequency Reference [Hz]	Frequency Alternate [Hz]	Δ Freq [%]	MAC_{opt}	Orientation angle [°]
3	3	0.266	0.07	-73.68421	-	-
5	5	1.298	1.294	-0.308	-	-
14	15	6.512	6.214	-4.576	1	0
25	26	11.036	10.808	-2.066	1	4.5
37	39	16.472	16.746	1.663	0.99	14.6
61	59	22.768	22.311	-2.007	0.94	19.5
97	92	31.709	31.364	-1.088	0.95	9
131	125	38.871	38.269	-1.549	1	4.5
188	174	49.154	48.349	-1.638	0.99	0
203	199	51.148	53.306	4.219	0.73	4.9
225	236	55.955	59.287	5.955	0.51	9.7
255	231	60.033	58.508	-2.540	1	4.5

Table 6.4: Simply replaced slip joint - Results.

This table shows interesting results. First of all, the large difference in eigenfrequency for the first global mode. This reduction in eigenfrequency is caused by the simplifications of the slip joint. After removing the outer cylinder of the slip joint the only part connecting the slip joint and the tower is the horizontal ring. This part is susceptible to the bending moments present in the global modes. Figures A.8a and A.8b shows that this part starts to act as a hinge in the global modes. Due to the location of this hinge, the eigenfrequency of the first global mode is much more affected than the second global mode.

The eigenfrequencies of the local shell modes also show some difference between the reference and simplified model. The largest differences are around 6 percent. Mode pair 14-15 has a difference in eigenfrequency of 4.58 percent. Mode pairs 203-199 and 225-236 have an increase in eigenmode of 4.2 and 6 Hz, respectively. Both mode pairs also have MAC values below 0.8 which means that the simplification had a large effect on these two modes. The angles of orientation between the eigenmodes has a maximum of 19.5 degrees and again look to have no correlation to the rest of the

results.

These results show that for this simplification, the eigenfrequencies were affected for both low and high frequency shell modes. The mode shapes were affected far more for high frequency shell modes than the low frequency shell modes. The mode shapes of high frequency shell modes can be more susceptible to local changes in the model than lower frequency modes.

6.2 The upper slip joint

The upper slip joint is a simpler construction than the lower slip joint. It does not include an inner and outer cylinder. It only consists of a single cone, which is placed over a second cone located at the top of the tower. The rotor nacelle assembly is connected to the top of the upper section of the slip joint. Figure 6.7 shows three figures of the upper slip joint.

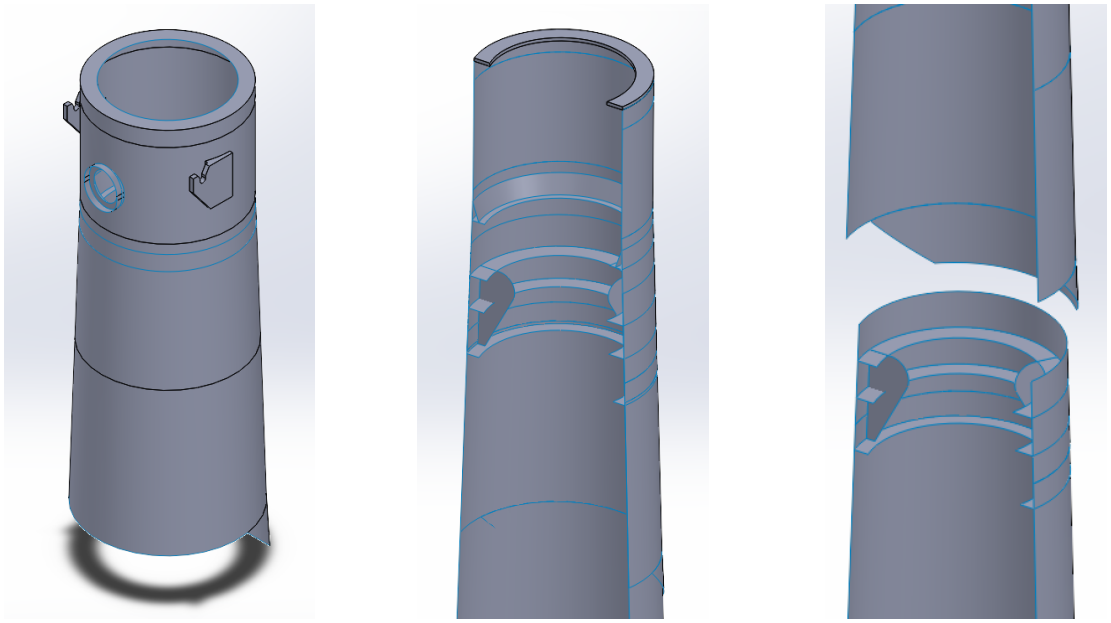

(a) The top section. (b) Internal view. (c) Disconnected slip joint.

Figure 6.7: The upper slip joint.

The upper section of the upper slip joint is shown in Figure 6.7a. The inside of the slip joint can be seen in Figures 6.7b and 6.7c. These figures show the inner details of the slip joint, consisting of horizontal pressure rings and three vertical support plates.

Modes of interest

Next, the modes of interest for assessing the shell modes at the upper slip joint were selected. Selection of these modes was more difficult than for the lower slip joint. There were more complicated eigenmodes with non-symmetric mode shapes located at the upper slip joint, especially for the higher modes. Selecting these modes would result in the difficulties during the matching process. The final selection of eigenmodes is shown in Appendix A.6. Two of the selected modes, mode 208 and 275, shown in Figures A.7d and A.7f, have non-symmetric mode shapes and might be difficult to match. It was chosen to include these modes for two reasons. First, most other higher shell modes had the same difficult mode shapes. Including higher shell modes would therefore always result in problems with matching. Second, it can be interesting to see if these modes can be matched and if they can, how they are affected by the changes in the FE model.

MAC cross sections

Now that the upper slip joint is of interest, new cross sections for the MAC estimation have to be selected. Again, eight cross sections along the height of the slip joint are selected, which are shown in Figure 6.8.

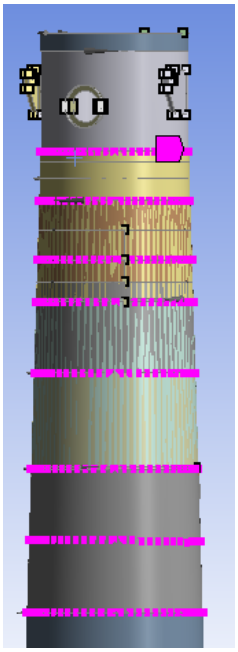

Figure 6.8: Cross sections used for the estimation of the MAC for the upper slip joint.

6.2.1 Removing the pressure ring

The upper slip joint is a lot simpler than the upper slip joint. Nevertheless, it includes some details which can complicate the creation of the FE model. One of those details is the pressure rings and vertical plates located inside the lower cone of the joint. Removing these features from the model simplifies the modelling of the upper slip joint. The pressure rings and vertical plates, as installed in the tower, are shown in Figure 6.9. It can be seen that this feature includes many smaller details.

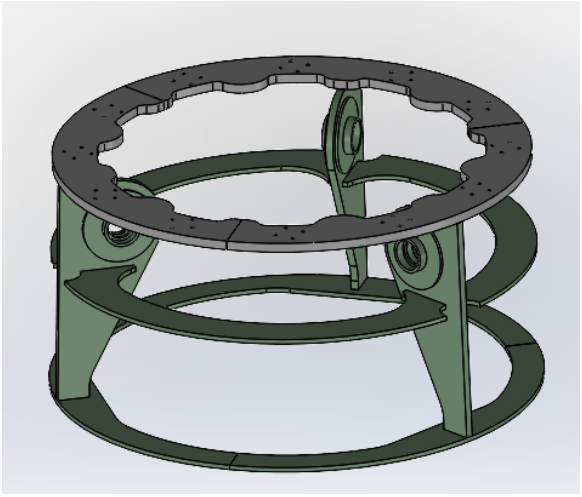

Figure 6.9: Pressure rings and vertical plates as installed in the tower.

The simplified FE model is created by duplicating the reference model and removing the pressure rings and support plates. The simplified model is used to estimate the eigenmodes of the tower. The eigenmodes were matched with those of the reference model. During the matching process, it already became clear that some of the eigenmodes had a large difference in mode shape. This complicated the matching of these modes. An eigenmode was matched with a 'most likely' mode when there was no clear match for the eigenmode. This was a difficult and subjective task, but it was done so the MAC could be calculated. When assessing the results of these modes it should be kept in mind that these modes were not able to be properly matched. There were two modes that were too difficult to match, which were modes 115 and 259 of the reference model. These modes are marked with an * in the results. This method was not ideal, as will be discussed in Section 7.2. The matched eigenmodes are shown in Appendix A.7.

Results - Removing the pressure ring

The resulting eigenfrequencies, MAC and orientation angles are shown in Table 6.5.

Mode number Reference	Mode number Simplified	Frequency Reference [Hz]	Frequency Alternate [Hz]	Δ Freq [%]	MAC_{opt}	Orientation angle [°]
3	3	0.266	0.267	0.38	-	-
5	5	1.298	1.298	0.00	-	-
12	12	6.056	5.961	-1.57	0.96	17.4
27	27	13.086	12.368	-5.49	0.93	11.6
46	41	17.9	16.82	-6.03	0.9	0
59	59	22.457	21.98	-2.12	0.97	0
90	90	30.13	30.088	-0.14	0.98	5.8
115*	103*	35.156	32.116	-8.65	0.68	12.4
192	193	49.706	49.71	0.01	0.72	5.8
206	215	52.762	54.122	2.58	0.92	18.6
259*	263*	61.355	61.444	0.15	0.88	0
275	260	63.552	61.045	-3.94	0.75	6.2

Table 6.5: Removing the pressure ring - Results.

The results show that many of the eigenmodes were affected by the removal of the pressure rings and support plates. Mode pairs 27-27 and 46-41 both had a difference in eigenfrequency of more than 5 percent and have a MAC of roughly 0.9. This shows that the simplification doesn't only affect higher shell modes. There are 3 mode pairs with a MAC value below 0.8, which all are higher modes. One of these mode pairs was a mode that was difficult to match as a result of the large difference in mode shape, which is reflected by the MAC. It is interesting that the other ill-matched mode pair has a MAC of 0.88. Apparently, for this eigenmode, the mode shape within the slip joint itself was not greatly affected by the simplification. Another interesting thing to notice is the increase in eigenfrequency for mode pair 206-215, while eigenfrequencies of other modes stayed equal or decreased. A reduction in eigenfrequency would be expected, since the removed detail likely had a stiffening effect on the structure. The increase in eigenfrequency for mode pair 206-215 could indicate that these modes are incorrectly matched, even though their mode shapes are very similar. Combined with the ill-matched modes, this shows that the matching of higher eigenmodes can be difficult and prone to errors. Again, the angle of orientation doesn't provide much information about the effects of the simplification. It is still included in the results for the sake of continuity. The results indicate that the pressure rings and support plates provide stiffness to the slip joint and removing them does impact the estimation of the shell modes.

6.2.2 Simple upper slip joint

The second simplification to be assessed is developed with an idea similar to that of Section 6.1. In the reference model, the upper and lower section of the slip joint are developed individually and connected after. It would be easier if the slip joint can be developed using a single cylinder with a combined wall thickness. In Section 6.1.3, the inner stiffener-like parts were also ignored, which resulted in relatively inaccurate results. Section 6.2.1 showed that removing the pressure ring resulted in deviating results. It was therefore chosen to include the pressure ring in this second simplified model of the upper slip joint. The two hooks and the man hole, which can be seen in Figure 6.7a, are not included in this model. A cross section of the simple upper slip joint model is shown in Figure 6.10.

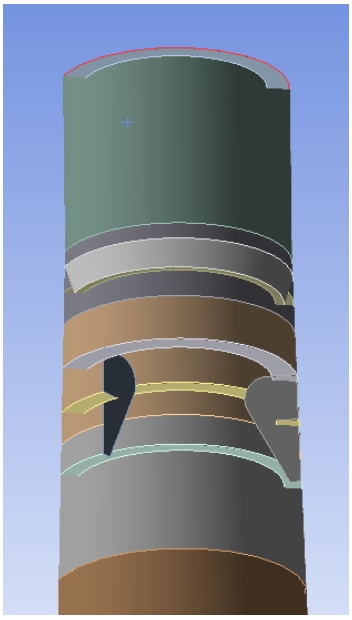

Figure 6.10: Simple upper slip joint model.

After this model was used in the modal analysis, the eigenmodes were matched to those of the reference model. The matched eigenmodes can be found in Appendix A.8.

Results - Simple upper slip joint

The results of the comparison of the eigenfrequencies and mode shapes of the modes of interest are shown in Table 6.6.

Mode number Reference	Mode number Simplified	Frequency Reference [Hz]	Frequency Alternate [Hz]	Δ Freq [%]	MAC_{opt}	Orientation angle [°]
3	3	0.266	0.266	0.00	-	-
5	5	1.298	1.299	0.08	-	-
12	12	6.056	6.052	-0.07	1	11.6
27	27	13.086	13.073	-0.10	0.99	5.8
46	46	17.9	17.916	0.09	0.99	0
59	61	22.457	22.687	1.02	0.99	5.8
90	91	30.13	30.436	1.02	0.99	0
115	116	35.156	35.255	0.28	0.96	0
192	191	49.706	49.694	-0.02	0.94	0
206	212	52.855	53.628	1.46	0.89	6.2
259	269	61.355	62.85	2.44	0.44	6.2
275	272	63.552	63.453	-0.16	0.97	0

Table 6.6: Simple upper slip joint - Results.

The results show that most of the eigenmodes are affected little by the simplification of the upper slip joint, with the exception of mode pair 259-269. For other mode pairs the differences in eigenfrequencies are at most 1.5 percent and the MAC values are nearly all higher than 0.9. Mode pair 259-269 had a difference in eigenfrequency of 2.44 percent and a MAC of 0.44, which indicates that the mode shapes are not similar around the upper slip joint. These modes are apparently not comparable. Efforts were made to check whether the mode was incorrectly matched, but a better fitting mode could not be found. It can be concluded that a mode similar to mode 259 of the reference model couldn't be found in the results of the simplified model. It is unclear why this mode was unrecognizable and the other modes weren't. Looking at the other shell modes, it can be seen that they have little difference in their eigenfrequencies and mode shapes. This indicates that this simplification has potential to be applied. The angles of orientation also have a relatively low error in comparison with previously obtained results.

6.3 Averaging the wall thickness

The tower of the wind turbine gradually decreases in wall thickness as the height increases. The lower part of the monopile has a wall thickness of 65 mm, while there are parts with a wall thickness of 14 mm in the upper tower. Each jump in wall thickness requires an individual part within the assembly of the tower. An example of this is shown in Figure 6.11.

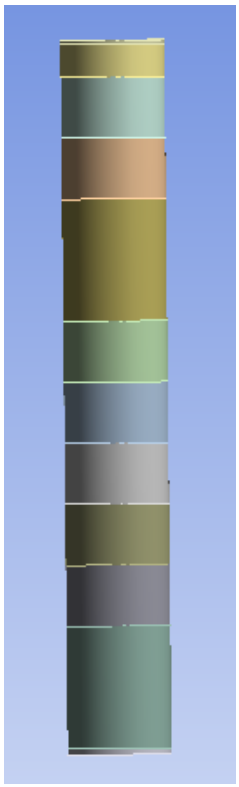

Figure 6.11: Middle section of the reference model.

This figure shows the middle section of the tower, which consist of multiple parts with an unique wall thickness. Each jump in wall thickness is often small, usually consisting of only 1-2 mm. It would be very convenient if the wall thicknesses could be averaged within individual sections of the tower. The simplification of averaging the wall thicknesses of the tower is the topic of this section.

The averaging of the wall thickness was already done in Section 6.1.2, where only the lower slip joint was assessed. The wall thickness was average based on the surface area of each section. The results showed little difference between both models, which is an indication that it possibly can be applied to other sections of the tower as well. For this simplification of the reference model, four section of the tower will be given an average wall thickness. These four sections are the upper section of the tower, the middle section of the tower, the outer cylinder of the lower slip joint and the monopile. The average wall thickness for the outer cylinder was already calculated to be 29.6

mm in Section 6.1.2. The wall thicknesses and surface areas of the other three sections are shown in Tables 6.7 to 6.9.

t_{wall} [mm]	$A_{sur}[m^2]$
17	10.85
14	12.6
14	13.74
14	21.51
14	80.22
15	49.48
16	106.75

Table 6.7: Upper section.

t_{wall} [mm]	$A_{sur}[m^2]$
17	17.68
18	32.72
19	32.72
20	65.44
21	32.72
22	32.72
23	32.72
24	32.72
25	32.72
26	65.77

Table 6.8: Middle section.

t_{wall} [mm]	$A_{sur}[m^2]$
40	99.82
40	39.19
55	20.59
55	115.74
60	52.78
65	130.56
65	80.55
60	52.78
55	25.93
55	79.63

Table 6.9: Monopile.

The average wall thickness with respect to the surface areas is shown in Table 6.10.

Section	Average wall thickness [mm]
Upper section	15
Middle section	21.9
Lower slip joint	29.6
Monopile	55.8

Table 6.10: Average wall thickness of the sections.

These changes in wall thickness affect the whole structure. Therefore, both the lower and upper slip joint will be assessed for their changes in eigenfrequencies and modes shapes. The modes of interest and MAC cross sections as selected for both slip joints will be reused for assessing the averaged wall thickness.

6.3.1 Averaging the wall thickness - Lower slip joint

The modes of interest that were selected for the lower slip joint can be found in Appendix A.2. The MAC cross sections can be seen in Figure 6.3. The modes estimated by the new model with averaged wall thicknesses are now matched to those of the reference model. The matched modes can be found in Appendix A.9. The resulting eigenfrequencies, MAC values and orientation angles are shown in Table 6.11.

Mode number Reference	Mode number Simplified	Frequency Reference [Hz]	Frequency Alternate [Hz]	Δ Freq [%]	MAC_{opt}	Orientation angle [°]
3	3	0.266	0.261	-1.88	-	-
5	5	1.298	1.261	-2.85	-	-
14	14	6.512	6.313	-3.06	0.99	13.5
25	25	11.036	11.08	0.40	0.99	6.75
37	42	16.472	17.543	6.50	0.99	4.86
61	62	22.768	23.044	1.21	0.98	4.86
97	99	31.709	31.379	-1.04	0.99	0
131	136	38.871	40.569	4.37	0.95	4.5
188	179	49.154	46.66	-5.07	0.97	0
203	211	51.148	52.511	2.66	0.53	0
225	223	55.955	55.568	-0.69	0.65	14.6
255	262	60.033	60.54	0.84	0.93	4.5

Table 6.11: Averaging the wall thickness - Lower slip joint - Results.

The differences in the eigenfrequencies show that this type of simplification can influence any type of mode, as global modes and lower and higher shell modes were affected. The global modes are affected more than they were with most of the other simplifications. The largest change in eigenfrequency happened for mode pair 37-42. An explanation for this could be that this mode shows is less localized around the lower slip joint than any of the other modes and is therefore affected the most by the change in wall thickness. There were two modes that experienced a large change in mode shape due to the simplifications. This were modes 203 and 225 of the reference model, which are higher frequency modes. The mode shapes of the lower frequency modes remained mostly unchanged. Most of the modes were affected in some way by the averaging of the wall thickness, showing that this simplification should not be applied without extra evaluation.

6.3.2 Averaging the wall thickness - Upper slip joint

The assessment of the eigenmodes located at the upper slip joint is also done with the same modes of interest and MAC cross sections as used in Section 6.2. The modes of interest can be found in Appendix A.6 and the MAC cross sections are shown in Figure 6.8. The eigenmodes of the simplified model matching those of the reference model can be found in Appendix A.10. The results of the comparison of the eigenmodes are shown in Table 6.12.

Mode number Reference	Mode number Simplified	Frequency Reference [Hz]	Frequency Alternate [Hz]	Δ Freq [%]	MAC_{opt}	Orientation angle [°]
3	3	0.266	0.261	-1.88	-	-
5	5	1.298	1.261	-2.85	-	-
12	12	6.056	6.053	-0.05	1	5.8
27	27	13.086	13.031	-0.42	1	0
46	46	17.9	18.015	0.64	1	0
59	61	22.457	22.637	0.80	0.99	0
90	94	30.13	30.397	0.89	0.99	17.4
115	119	35.156	35.346	0.54	0.99	6.2
192	205	49.706	51.091	2.79	0.98	0
206	218	52.855	53.678	1.56	0.96	6.2
259	267	61.355	61.975	1.01	0.98	0
275	277	63.552	63.584	0.05	0.98	12.4

Table 6.12: Averaging the wall thickness - Upper slip joint - Results.

The results in this table show that the eigenmodes located around the upper slip joint are affected far less than those around the lower slip joint. The mode shapes of the shell modes are mostly unchanged. The largest change in eigenfrequency happens for mode 192 of the reference model, which is only a difference of 2.8 percent. It is interesting to see that the shell modes around the upper slip joint are far less affected than shell modes at the lower slip joint. It is likely that the modes of the upper slip joint are less affected because of its location within the structure. The upper slip joint is located at the boundary of the sections where the changes are applied, while the lower slip joint is located in the middle of those sections.

Chapter 7

Conclusion & discussion

7.1 Conclusion

The goal of this thesis was to research how simplifications applied to an FE model of an offshore wind turbine connected with a slip joint affected the estimation of local shell modes. The main research question reads:

How do simplifications applied to a finite element model of a wind turbine connected with a slip joint affect the estimation of the structures high frequency shell modes using modal analysis?

It is tried to answer this question with the development of a reference model of a wind turbine connected with a slip joint and comparing the results of a modal analysis with the results obtained from simplified models. The simplifications applied to the reference model in this thesis can be divided into three categories. The first category is the removal of stiffener-like features of the model, as was done in Sections 6.1.1 and 6.2.1. The second category consists of the simplification of the model of the slip joint. Here, the slip joint is modelled as a continuous cone which was given the combined wall thickness of the originally overlapping cones. This type of simplification was applied in Sections 6.1.3 and 6.2.2. The third category is the averaging of the wall thickness of multiple sections, which was applied in Sections 6.1.2 and 6.3.

The following seven simplified models were assessed in this thesis:

- Lower slip joint: Removing stiffener-like features.
- Lower slip joint: Removing the segmented wall thickness.
- Lower slip joint: Simply replaced slip joint.
- Upper slip joint: Removing the pressure ring.
- Upper slip joint: Simply replaced slip joint.
- Average wall thickness: lower slip joint.
- Average wall thickness: upper slip joint.

Of the seven simplified models studied, only three lead to reasonable accurate in the results and were acceptable for the case study investigated in this thesis. These three simplified models were:

- Lower slip joint: Removing the segmented wall thickness.
- Upper slip joint: Simply replaced slip joint.
- Average wall thickness: upper slip joint.

Removal of stiffener-like features had to much of an affect on the stiffness of the structure and therefore the estimated shell modes. The use of simple models for the slip joints had mixed results. The simplifications applied to the model of the lower slip joint were too large and had much affect on the estimation of the shell modes. The upper slip joint has simpler geometry, which meant that the simplification applied were smaller. Most of the estimated shell modes were mostly unaffected by the simplification except for one. That shell mode could not be found in the results of the simplified model, showing that caution is needed. The third category, averaging the wall thickness, showed the most potential. When applied locally, the the shell modes were estimated with reasonable accuracy. When applied to multiple sections of the tower, the shell modes localized around the lower slip joint were affected more than shell mode localized around the upper slip joint, showing that this simplification also needs to be applied with care.

The most important findings resulting from the comparison of the reference model and simplified models can be summarized as:

- The largest difference in eigenfrequency for any of the simplification was 8.65 percent, with the exception of the large change in the eigenfrequency of the first global mode in Section 6.1.3.
- For most of the simplified models, only a few of the shell modes experienced a large difference in eigenfrequency and/or mode shape. The remaining shell modes remained mostly unchanged. This shows that a simplification doesn't have not affect every shell mode of the structure.

- The change in eigenfrequency seemed to be independent on the order of the eigenmode. Some of the lower eigenmodes could contain as much error in eigenfrequency as the higher modes, percent wise. This was not the case for the mode shapes of the eigenmodes. The difference between mode shapes of lower modes was often far smaller than for the higher modes. Eigenmodes with an eigenfrequency below 20 Hz never obtained a MAC value below 0.9, indicating high consistency between the mode shapes of the reference model and simplified models. Higher modes often obtained MAC values below 0.8, indicating that the simplification had a large affect on those mode shapes.
- The angle of orientation was included because it can be a interesting parameter for the decommissioning of the wind turbine. However, the results did not show any correlation between the FE model used and the angle in which the eigenmodes were oriented.

The main research question can be answered as follows:

Each detail or feature present in a wind turbine has a unique influence on the estimation of its shell modes. The simplifications studied in this thesis had a varying effect on the resulting eigenfrequencies and mode shapes of the wind turbine. The change in eigenfrequencies seemed to be independent of the eigenfrequency of the modes. The mode shapes of high frequency shell modes were affected more than those of low frequency shell modes. Of the seven simplified models studied, there were only three that stayed within set limits of the eigenfrequency and mode shape.

7.2 Discussion

In this thesis, the eigenmodes of a wind turbine connected with a slip joint were estimated by using a reference model in a modal analysis. The results of the reference model were compared to results from simplified models. Seven individual simplifications were assessed for their influence on the estimation of the shell modes of the structure. The results of these comparisons provide insight into whether these model simplifications can be applied when estimating the shell modes of a wind turbine tower. One can judge whether or not the simplifications are viable based on the required accuracy of the results. The limits used in this thesis were a 2 percent difference in eigenfrequency and a MAC of greater than 0.8. Especially the limit of 2 percent change in eigenfrequency is fairly strict.

Unfortunately, it is difficult to make more general statements about the use of simplified models when assessing shell modes. This is mainly caused by the fact that each model and simplification is unique. Therefore, the estimation of the shell modes are also effected in unique ways. Concluding whether or not a potential simplification is a viable option can be very difficult without assessing the results of a more detailed model, which partially defeats the purpose of using simplified models. It is difficult to quantify a simplification, which makes it challenging to compare results obtained from one simplified model with those of another. This also makes it difficult to provide any expectations on the results of a simplified model.

This thesis estimated the shell modes of the wind turbine tower using modal analysis. As previously mentioned, modal analysis is a great tool to make first estimations about the shell modes of the structure, but is not sufficient to study the whole decommissioning process of the slip joint. More advanced models are required to study this process. These models will also provide a more explicit indication on which shell modes to investigate and how the decommissioning process would be affected by the use of simplified models.

Several other observations were made when developing the models and assessing the results. In the matching process, eigenmodes of the reference model and simplified models were matched manually. Some of the eigenmodes were difficult to recognize and match. The inability to match the modes was both a problem and an indication that the simplified models had affected the mode shapes. Some of the modes were matched with uncertainty and were marked as ill-matched mode pairs. Every ill-matched mode pair had a low MAC, showing the low correspondence in mode shape. Initially, it was assumed that every mode had to be matched so the eigenfrequencies could be compared. However, it would likely have been a better approach to exclude difficult to match shell modes and mark them as not recognized. If a model had unrecognized shell modes it could have been concluded that the applied simplification had to much effect on the results of the analysis.

Another observation also has to do with the matching process. The comparisons made in this thesis only assessed a few selected eigenmodes. These modes were selected because they were thought to be favourable for decommissioning, matching and later comparison. Evaluation of these modes already led to difficulties in the matching process. It is likely that the results of the analysis would have contained far greater errors if other less favourable eigenmodes were to be included.

The angle of orientation was included in the results because it is an interesting parameter for the decommissioning phase of the wind turbine. It quickly became clear that the angle of orientation of the eigenmodes had little consistency between models or even modes. Small changes in the model would have unexpected seemingly random effects on the orientation of the modes. This shows that the orientation angle as shown in the results is unreliable.

7.3 Recommendations

This sections provides recommendations for future research regarding the estimation of eigenmodes of a wind turbine tower.

- One of the largest simplifications applied in the reference model of the wind turbine is the bonded contact within the slip joints. This was a necessary assumption because the FE model was required to be linear be used in a modal analysis. Attempts to obtain more realistic vibration characteristics of the joint during decommissioning would require another type of non-linear analysis. It could be interesting to evaluate the differences between the results of the modal analysis applied in this thesis and the results of a more realistic non-linear analysis.
- In this thesis the modes are matched manually, which is time consuming job and can lead to errors. It was chosen to match the modes manually since the use of a MAC matrix had its own difficulties, which were not tackled in this thesis. Developing an alternative approach to manual matching of the eigenmodes would speed up the comparison of different models and would decreases the chance of errors being made.
- The results did not show any consistency in the orientation of the eigenmodes. If the orientations of the eigenmodes are of interest further research into this subject is required.
- The reference model used in this thesis is not properly validated. The simplified models showed that small modelling choices can have relatively large effects on the shell modes. Modelling choices made during the development of the reference model are therefore also likely to have affected the shell modes resulting from this model. Efforts into validation of the reference model would provide much insight into the modelling of wind turbine connected with a slip joint.
- A final recommendation is for additional research in how the boundary conditions of the tower affect the shell modes of the structure. The soil boundary condition and hydrodynamic added mass were included with simple models. It would be interesting to study the effects that different modelling choices for these boundary conditions would have on the results of the modal analysis.

Bibliography

[1] *Correlation for Design of Laterally Loaded Piles in Soft Clay*, volume All Days of *OTC Offshore Technology Conference*, 04 1970. OTC-1204-MS.

[2] *Analysis of Laterally Loaded Piles in Sand*, volume All Days of *OTC Offshore Technology Conference*, 05 1974. OTC-2080-MS.

[3] Ahmer Ali, Raffaele De Risi, and Anastasios Sextos. Seismic assessment of wind turbines: How crucial is rotor-nacelle-assembly numerical modeling? *Soil Dynamics and Earthquake Engineering*, 141:106483, 2021.

[4] Djillali Amar Bouzid, Subhamoy Bhattacharya, and Lalahoum Otsmane. Assessment of natural frequency of installed offshore wind turbines using nonlinear finite element model considering soil-monopile interaction. *Journal of Rock Mechanics and Geotechnical Engineering*, 10(2):333–346, 2018.

[5] RP2A-WSD API. American Petroleum Institute Recommended Practice for Planning, Designing and Constructing Fixed Offshore Platforms—Working Stress Design. *Washington: American Petroleum Institute*, 2007.

[6] L. Arany, S. Bhattacharya, S. Adhikari, S.J. Hogan, and J.H.G. Macdonald. An analytical model to predict the natural frequency of offshore wind turbines on three-spring flexible foundations using two different beam models. *Soil Dynamics and Earthquake Engineering*, 74:40–45, 2015.

[7] Laszlo S. Arany, Subhamoy Bhattacharya, John H.G. Macdonald, and Stephen John Hogan. Design of monopiles for offshore wind turbines in 10 steps. *Soil Dynamics and Earthquake Engineering*, 92:126–152, 2017.

[8] Erfan Asnaashari, Andy Morris, Ian Andrew, Wolfgang Hahn, and Jyoti K. Sinha. Finite Element Modelling and In Situ Modal Testing of an Offshore Wind Turbine. *Journal of Vibration Engineering Technologies*, 2018.

[9] P. Boeraeve. Introduction to the Finite Element Method (FEM). *Institut Gramme*, 2010.

[10] C. E. Brennen. A Review of Added Mass and Fluid Inertial Forces. 1982.

[11] Alessandro Cabboi. Private contact, June 2020.

[12] Alessandro Cabboi, Thijs Kamphuis, Evert van Veldhuizen, Maxim Segeren, and Hayo Hendrikse. Vibration-assisted decommissioning of a slip joint: Application to an offshore wind turbine. *Marine Structures*, 76:102931, 2021.

[13] Paul Dallyn, Ashraf El-Hamalawi, Alessandro Palmeri, and Robert Knight. Prediction of Wear in Grouted Connections for Offshore Wind Turbine Generators. *Structures*, 10:117–129, 2017.

[14] Fateh Ferroudji. Numerical modal analysis of a 850 kw wind turbine steel tower. *International Review of Applied Sciences and Engineering*, 12(1):10 – 18, 2021.

[15] Hans D. Fridman and Pascal Levesque. Reduction of static friction by sonic vibrations. *Journal of applied physics*, 30(10):1572–1575, 1959.

[16] Douglas Godfrey. Vibration reduces metal to metal contact and causes an apparent reduction in friction. *ASLE transactions*, 10(2):183–192, 1967.

[17] Adrien Jacomet, Ali Khosravifardshirazi, Iman Sahafnejad-Mohammadi, Mahdieh Dibaj, Akbar Javadi, and Mohammad Akrami. Analysing the Influential Parameters on the Monopile Foundation of an Offshore Wind Turbine. *Computation*, 9, 06 2021.

[18] Ming Li and Shuming Gao. Estimating defeaturing-induced engineering analysis errors for arbitrary 3D features. *Computer-Aided Design*, 43(12):1587–1597, 2011.

[19] Domenico Lombardi, Subhamoy Bhattacharya, and George Nikitas. Chapter 17 - Physical Modeling of Offshore Wind Turbine Model for Prediction of Prototype Response. In Trevor M. Letcher, editor, *Wind Energy Engineering*, pages 353–374. Academic Press, 2017.

[20] Ali Mehmanparast, Saeid Lotfian, and Vipin Sukumara Pillai. A Review of Challenges and Opportunities Associated with Bolted Flange Connections in the Offshore Wind Industry. *Metals*, 10:732, 06 2020.

[21] Anton V. Mobley, Michael P. Carroll, and Scott A. Canann. An Object Oriented Approach to Geometry Defeaturing for Finite Element Meshing. In *IMR*, pages 547–563. Citeseer, 1998.

[22] John Nicholas Newman. *Marine hydrodynamics*. The MIT press, 2018.

[23] Miroslav Pastor, Michal Binda, and Tomáš Harčarik. Modal Assurance Criterion. *Procedia Engineering*, 48:543–548, 2012. Modelling of Mechanical and Mechatronics Systems.

[24] Francesco Petrini, Hui Li, and Franco Bontempi. Basis of design and numerical modeling of offshore wind turbines. *Structural engineering mechanics*, 36:599, 11 2010.

[25] Raffaele Risi, Subhamoy Bhattacharya, and Katsuichiro Goda. Seismic performance assessment of monopile-supported offshore wind turbines using unscaled natural earthquake records. *Soil Dynamics and Earthquake Engineering*, 109:154–172, 03 2018.

[26] M.L.A. Segeren and K. W. Hermans. Experimental investigation of the dynamic installation of a slip joint connection between the monopile and tower of an offshore wind turbine. 2014.

[27] Karl Terzaghi. Evalution of Conefficients of Subgrade Reaction. *Géotechnique*, 5(4):297–326, 1955.

[28] Delft Offshore Turbine. SJOR - PUBLIC REPORT. 2016.

[29] B. van der Tempel, J. Lutje Schipholt. The Slip-Joint Connection,Alternative connection between pile and tower. *DOWECreport-F1W2-JvdT-03-093/01-P, Dutch Offshore Wind Energy-Converter project 2003*, 2003.

[30] Det Norske Veritas. Dnv-os-j101 design of offshore wind turbine structures, 2011.

[31] Chong Wang and Joseph Lai. Prediction of natural frequencies of finite length circular cylindrical shells. *Applied Acoustics - APPL ACOUST*, 59:385–400, 04 2000.

[32] Huan Wang and Keith Williams. Vibrational modes of thick cylinders of finite length. *Journal of Sound and Vibration*, 191(5):955–971, 1996.

[33] E. Winkler. Die Lehre von der Elasticitaet und Festigkeit: mit besonderer Rücksicht auf ihre Anwendung in der Technik für polytechnische Schulen, Bauakademien, Ingenieue, Maschinenbauer, Architecten, etc. *H. Dominicus*, 1867.

[34] Torben K. Wolf, Kristian L. Rasmussen, Mette Hansen, Hanne Ravn Roesen, and Lars Bo Ibsen. Assessment of p-y Curves from Numerical Methods for a non-Slender Monopile in Cohesionless Soil. (024), 2013.

Appendix A

Appendix

A.1 Modes selected for the MAC matching example

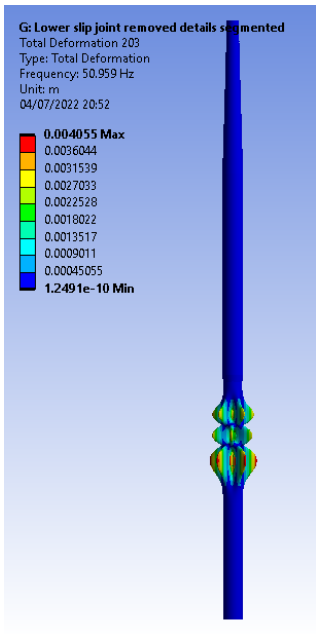

(a) Eigenmode 203

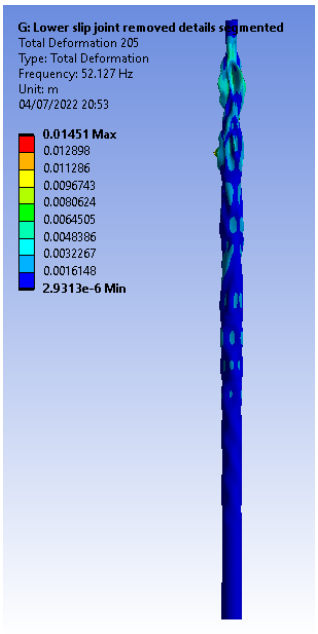

(b) Eigenmode 205

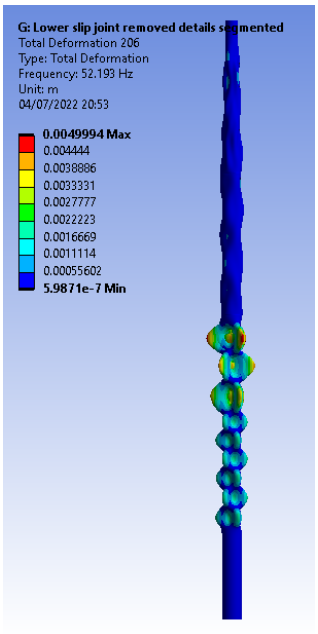

(c) Eigenmode 206

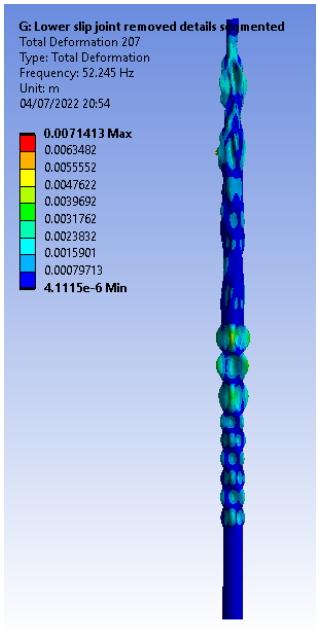

(d) Eigenmode 207

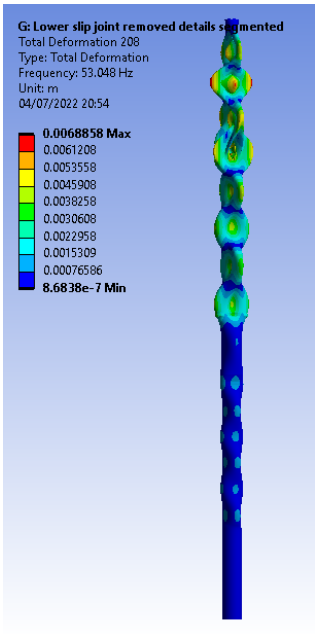

(e) Eigenmode 208

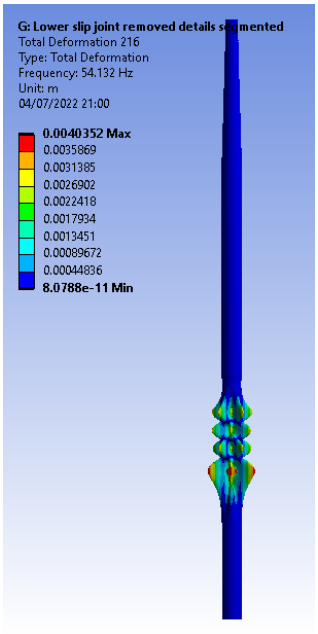

(f) Eigenmode 216

Figure A.1: Modes selected for the MAC matching example

A.2 Modes of interest lower slip joint

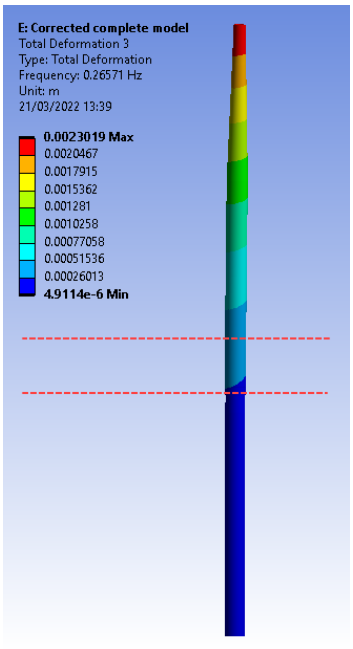

(a) Eigenmode 3

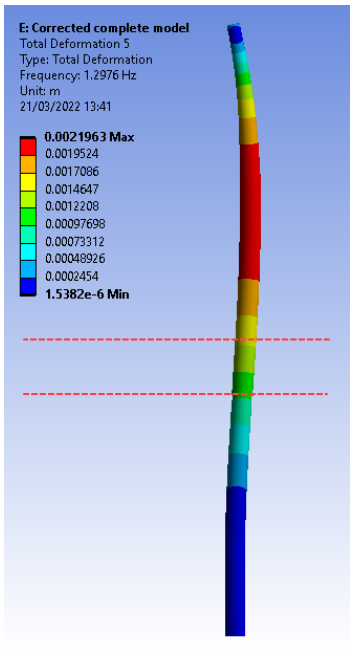

(b) Eigenmode 5

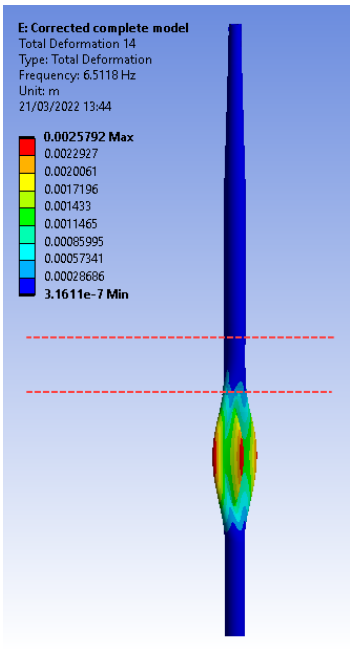

(c) Eigenmode 14

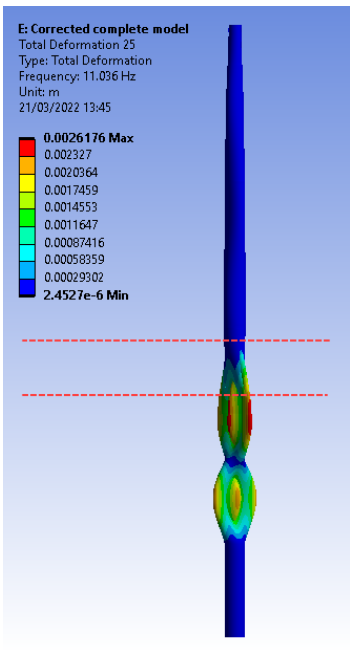

(d) Eigenmode 25

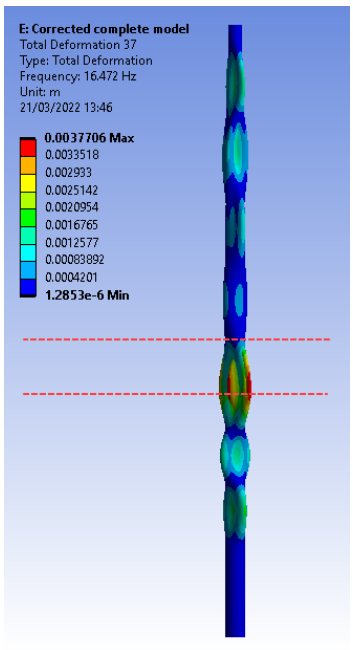

(e) Eigenmode 37

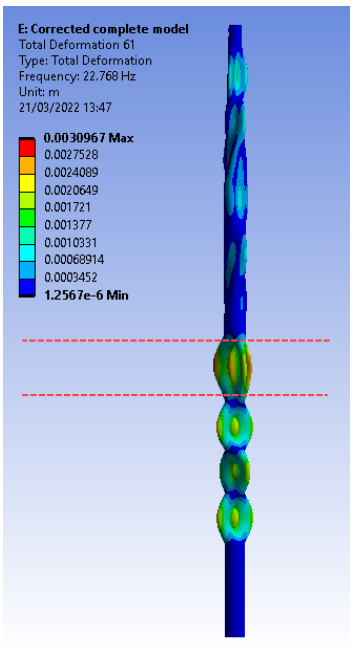

(f) Eigenmode 61

Figure A.2: Reference model: modes of interest 1-6

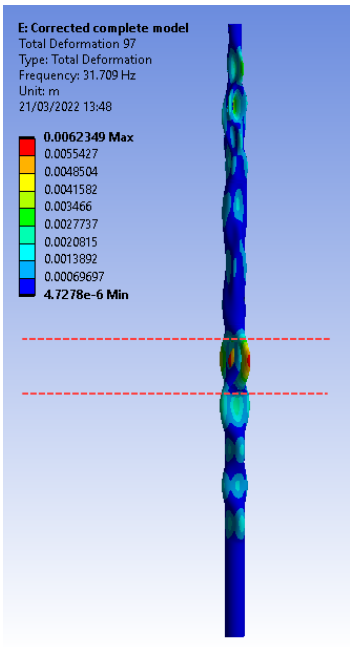

(a) Eigenmode 97

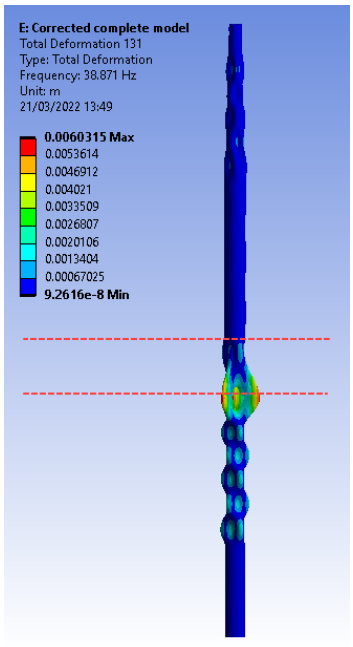

(b) Eigenmode 131

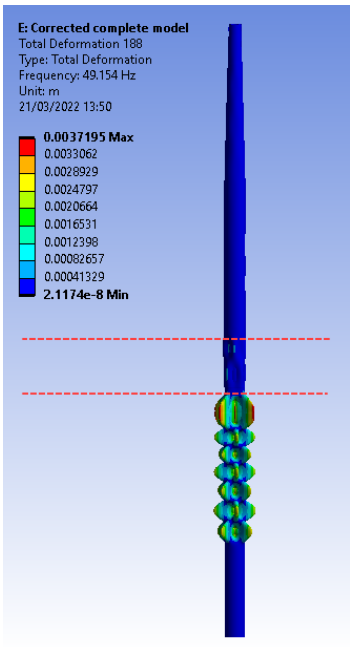

(c) Eigenmode 188

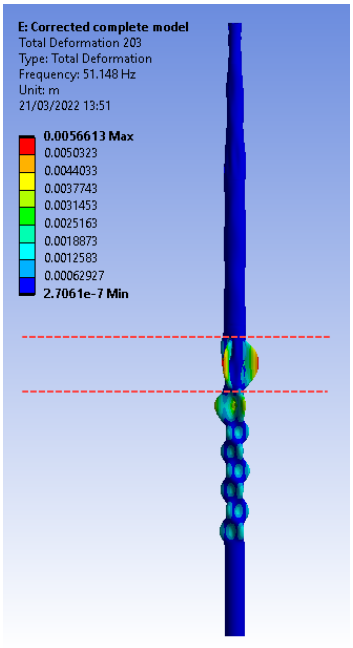

(d) Eigenmode 203

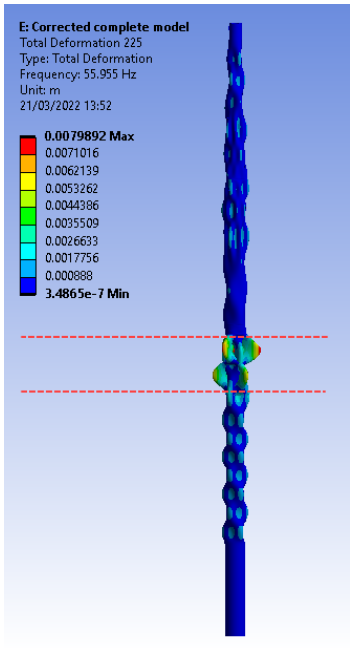

(e) Eigenmode 225

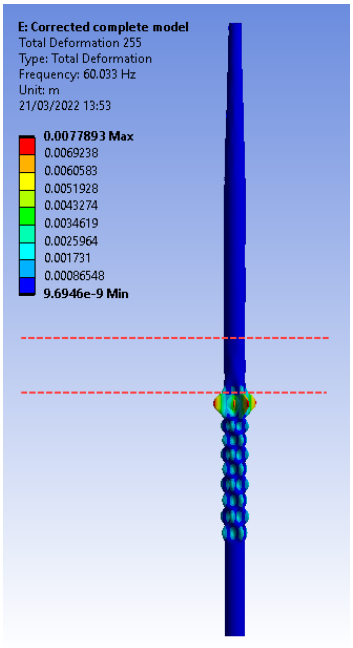

(f) Eigenmode 255

Figure A.3: Reference model: modes of interest 7-12

A.3 Matched modes first simplified model

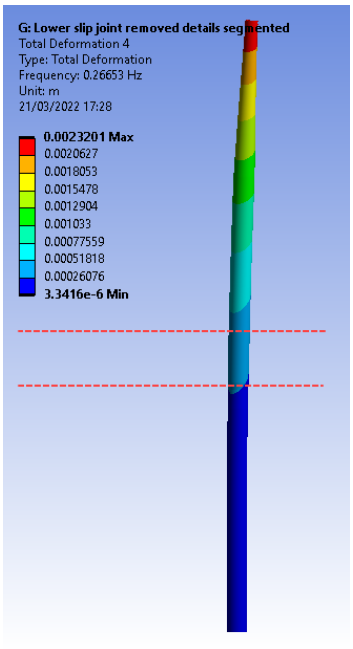

(a) Eigenmode 4

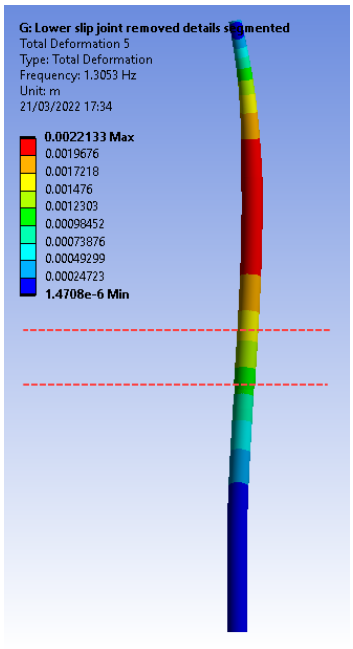

(b) Eigenmode 5

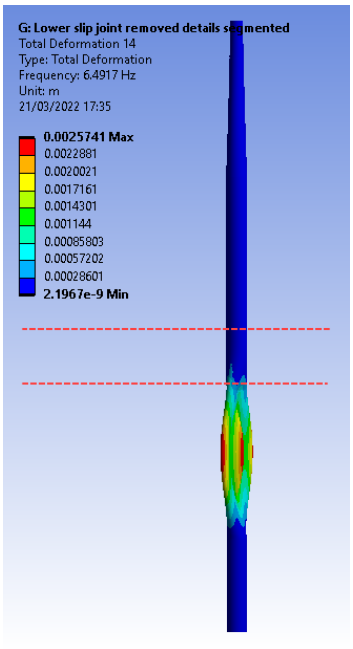

(c) Eigenmode 14

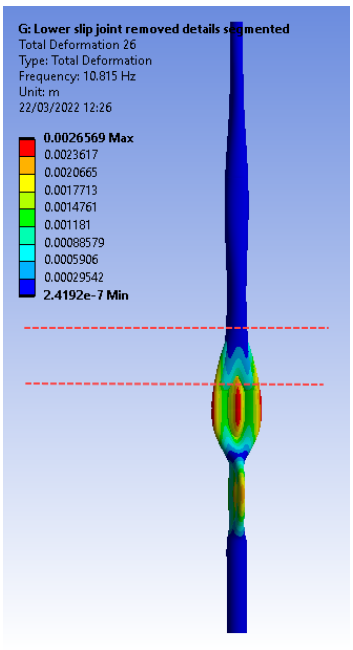

(d) Eigenmode 26

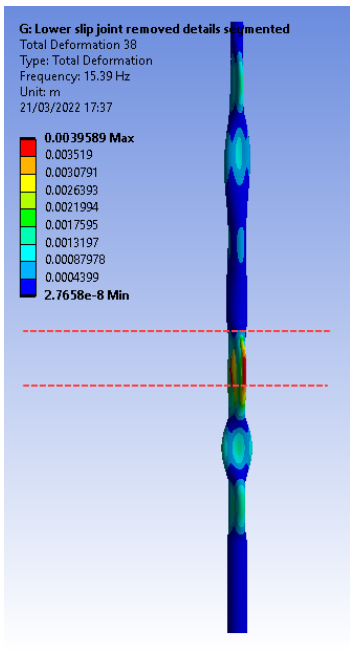

(e) Eigenmode 38

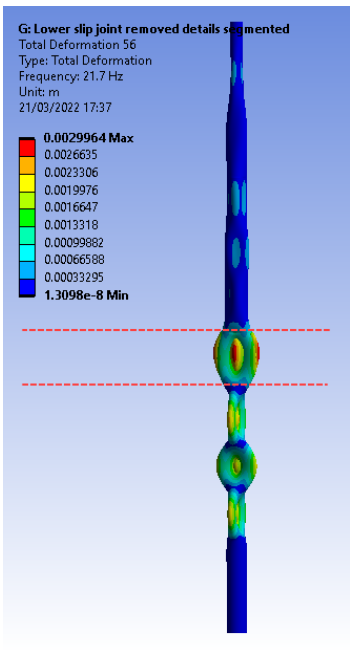

(f) Eigenmode 56

Figure A.4: Matched modes first simplified model 1-6

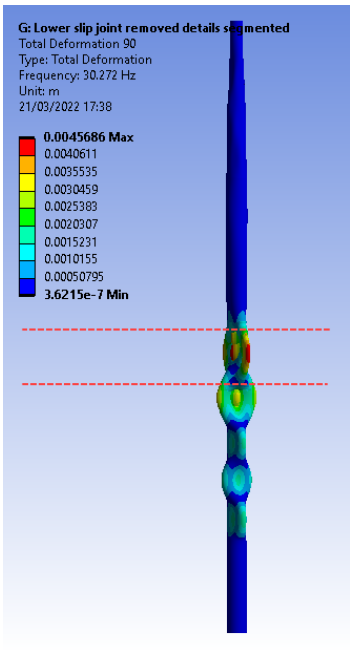

(a) Eigenmode 90

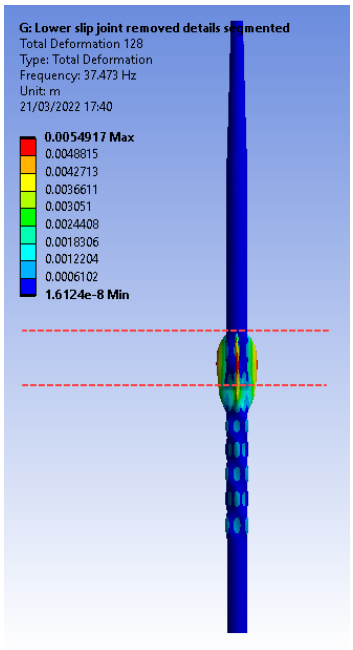

(b) Eigenmode 128

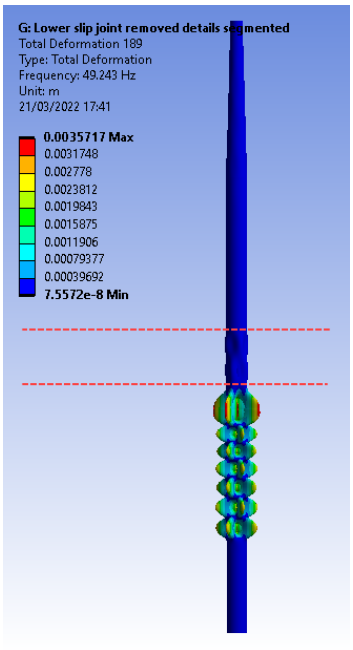

(c) Eigenmode 189

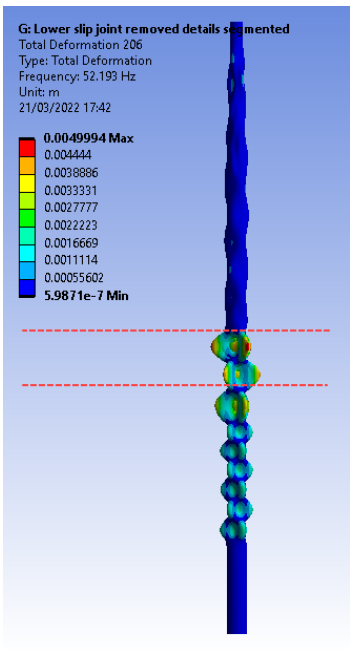

(d) Eigenmode 206

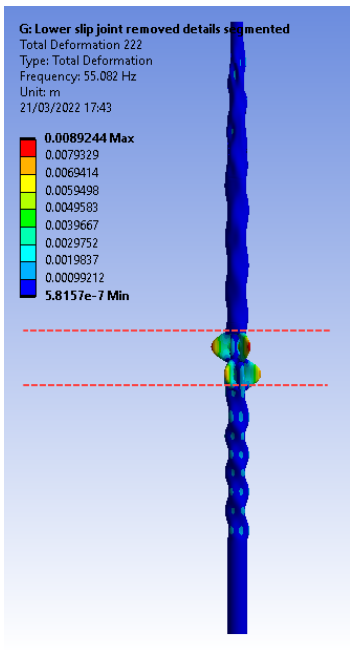

(e) Eigenmode 222

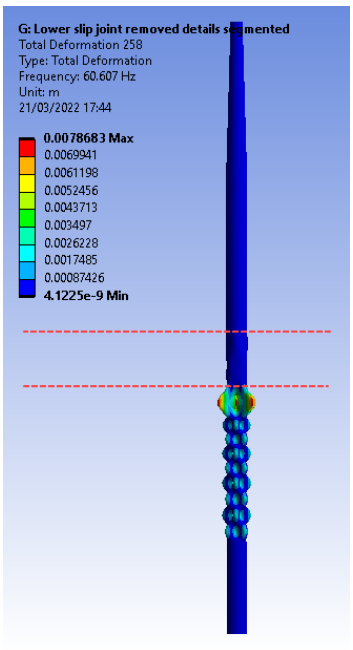

(f) Eigenmode 258

Figure A.5: Matched modes first simplified model 7-12

A.4 Matched modes - Removing the segmented wall thickness

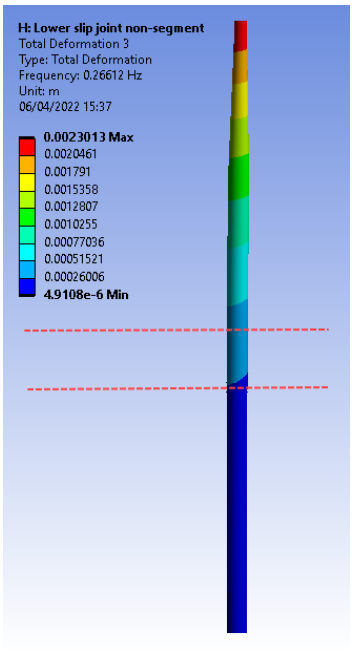

(a) Eigenmode 3

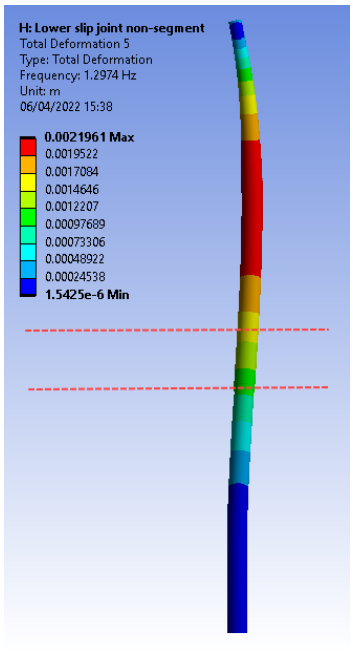

(b) Eigenmode 5

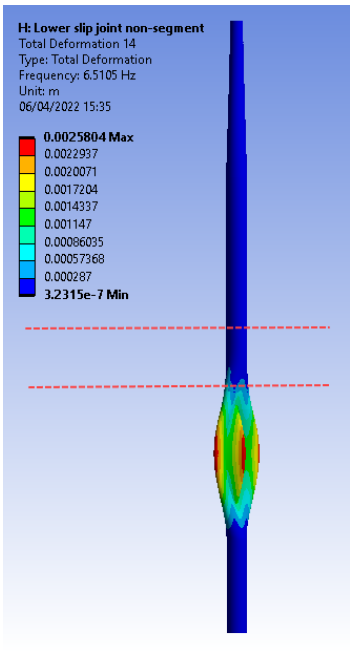

(c) Eigenmode 14

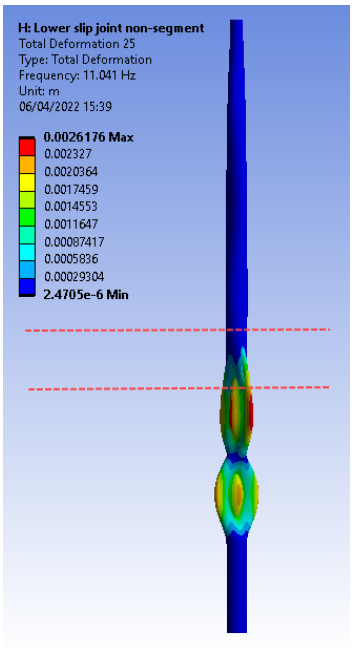

(d) Eigenmode 25

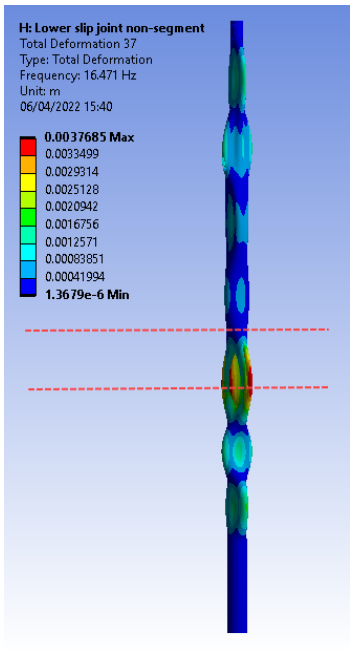

(e) Eigenmode 37

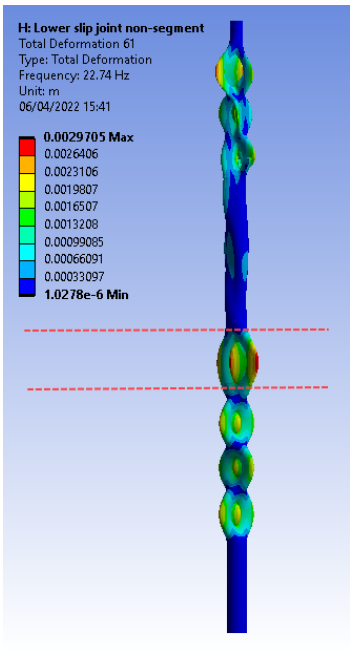

(f) Eigenmode 61

Figure A.6: Matched modes: modes of interest 1-6

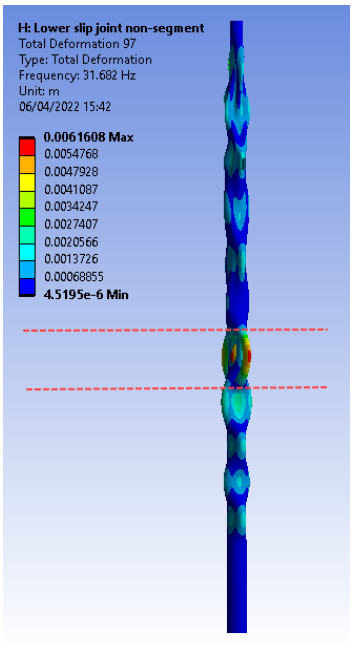

(a) Eigenmode 97

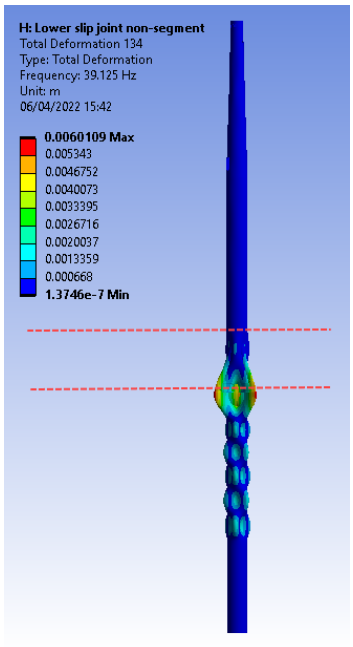

(b) Eigenmode 134

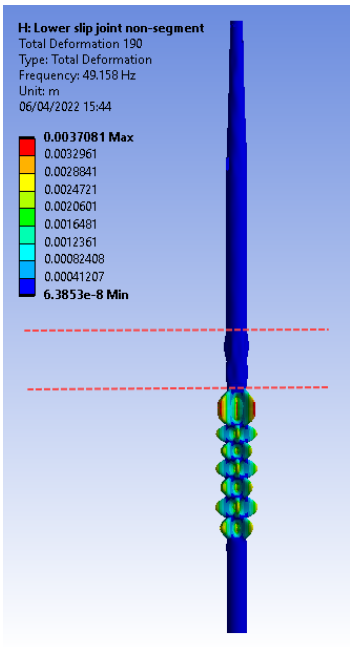

(c) Eigenmode 190

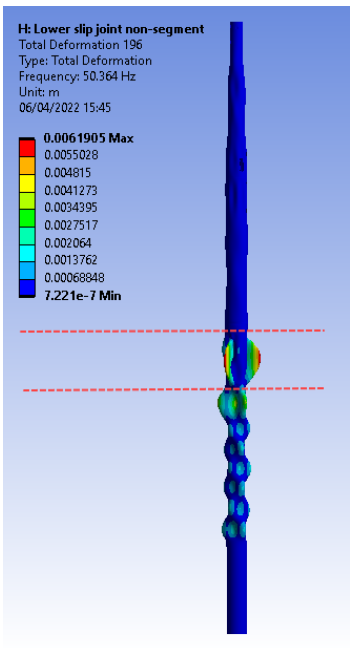

(d) Eigenmode 196

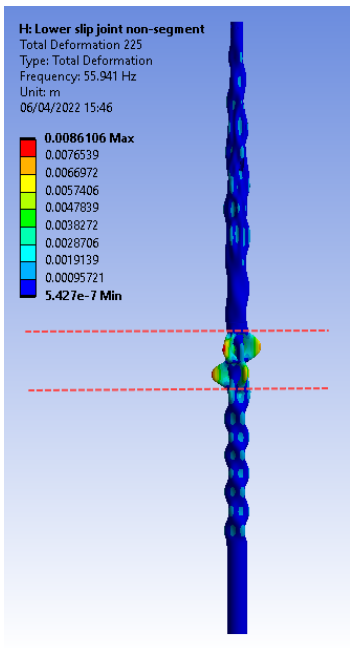

(e) Eigenmode 225

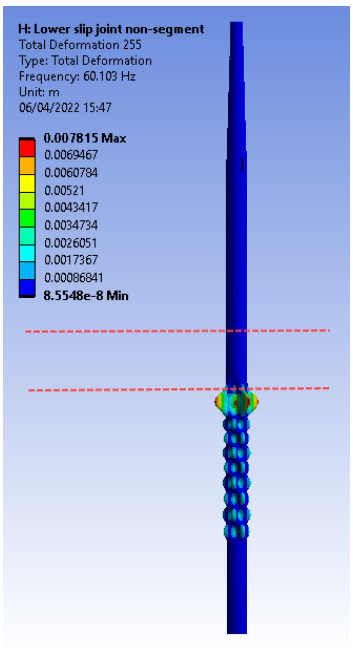

(f) Eigenmode 255

Figure A.7: Matched: modes of interest 7-12

A.5 Matched modes - Simply replaced slip joint

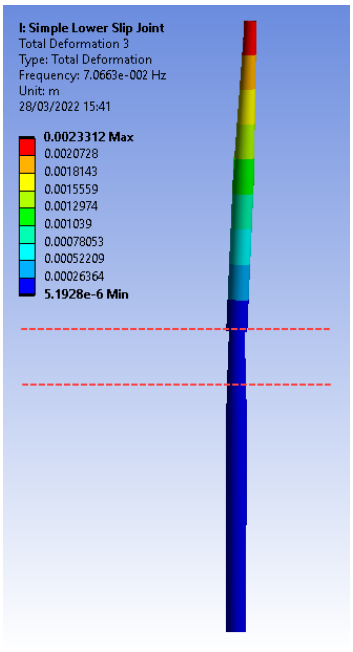

(a) Eigenmode 3

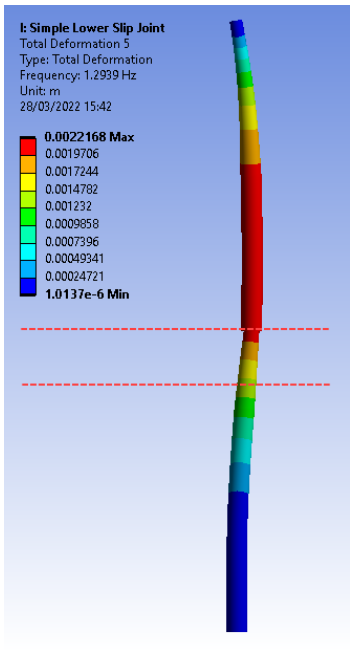

(b) Eigenmode 5

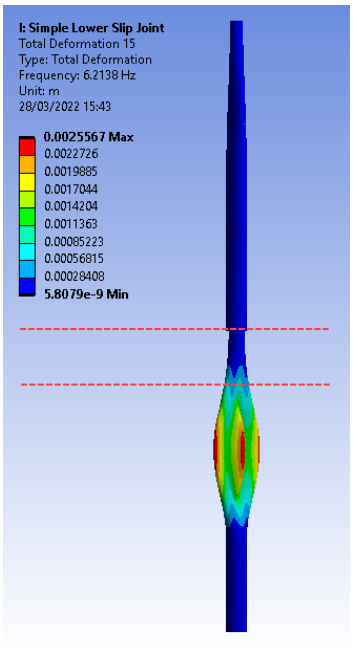

(c) Eigenmode 15

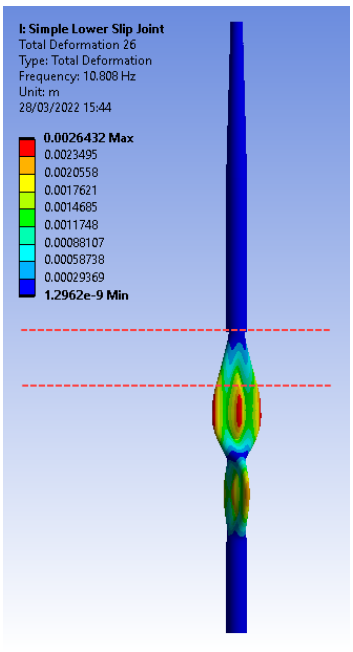

(d) Eigenmode 26

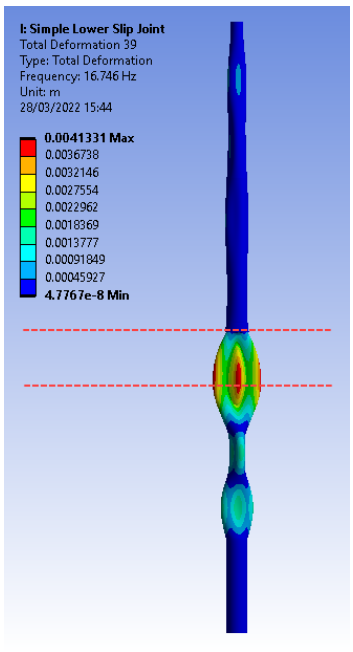

(e) Eigenmode 39

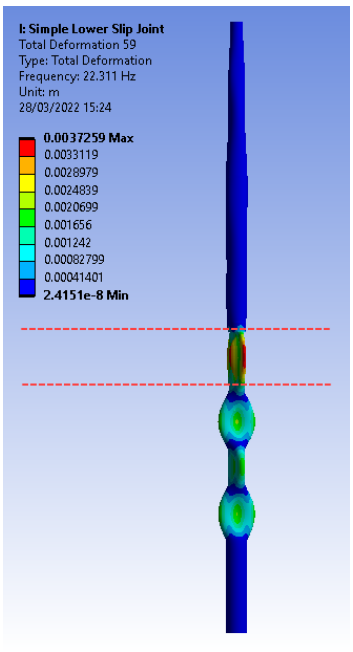

(f) Eigenmode 59

Figure A.8: Matched modes first simplified model 1-6

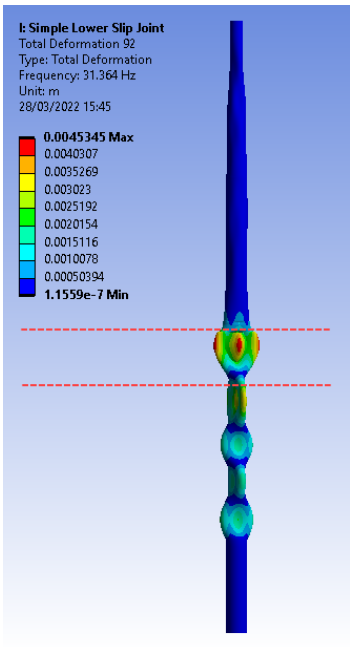

(a) Eigenmode 92

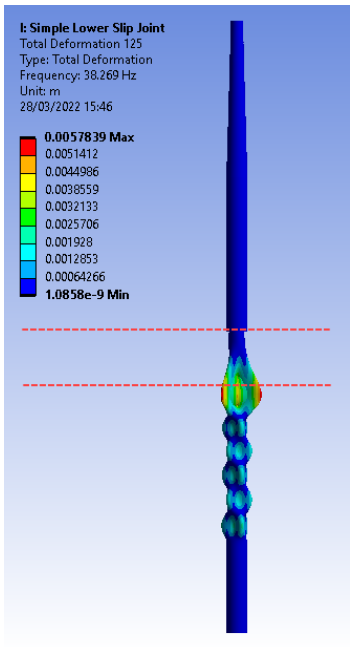

(b) Eigenmode 125

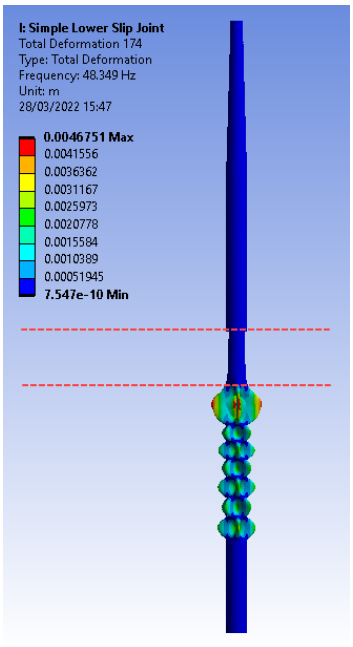

(c) Eigenmode 174

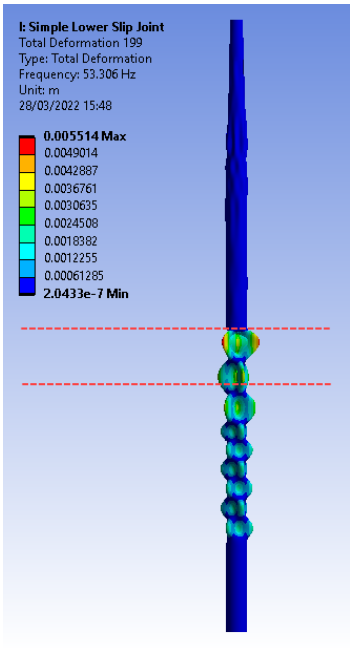

(d) Eigenmode 199

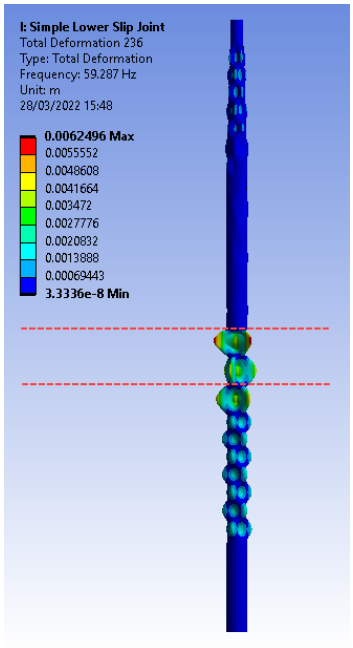

(e) Eigenmode 236

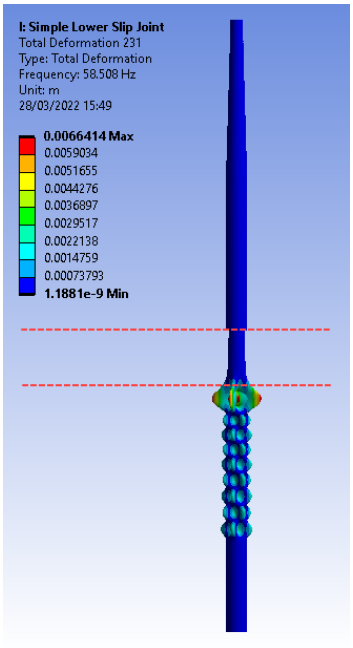

(f) Eigenmode 231

Figure A.9: Matched modes first simplified model 7-12

A.6 Modes of interest lower slip joint

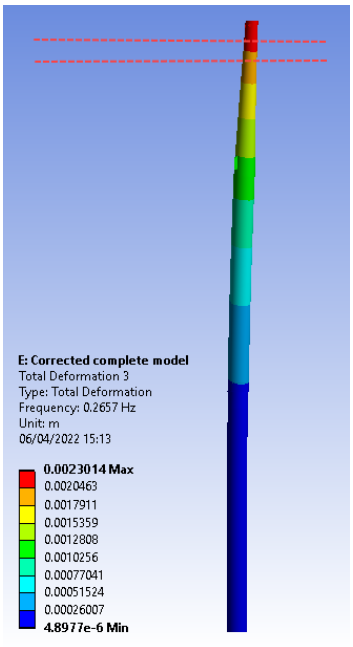

(a) Eigenmode 3

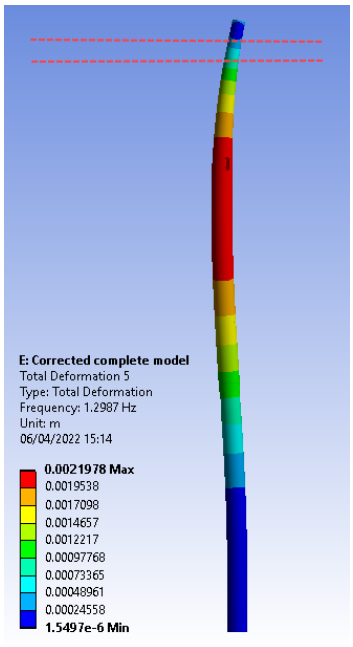

(b) Eigenmode 5

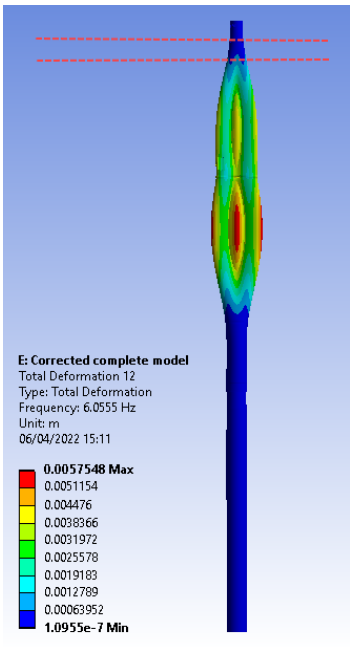

(c) Eigenmode 12

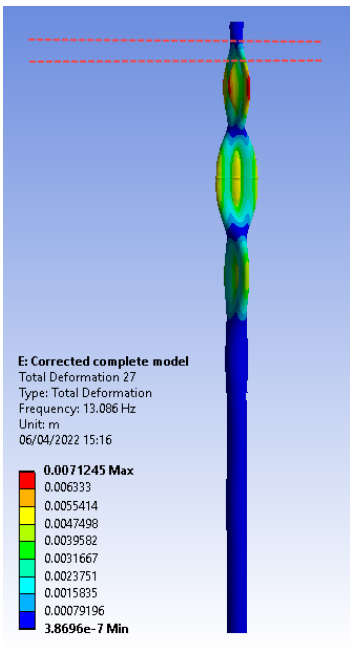

(d) Eigenmode 27

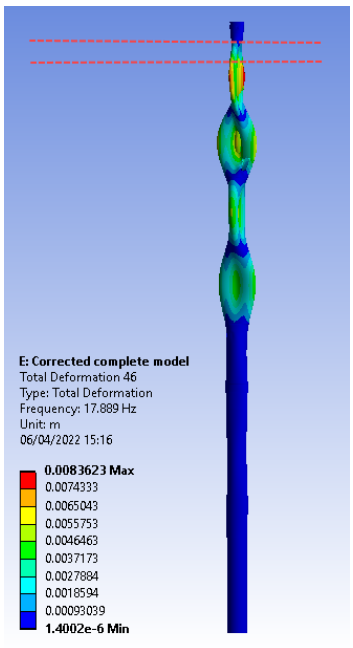

(e) Eigenmode 46

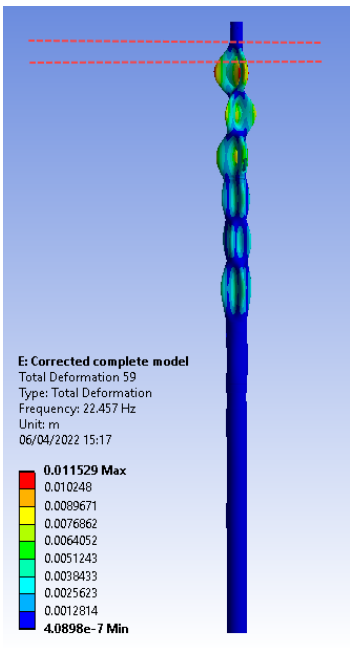

(f) Eigenmode 59

Figure A.10: Upper slip joint: modes of interest 1-6

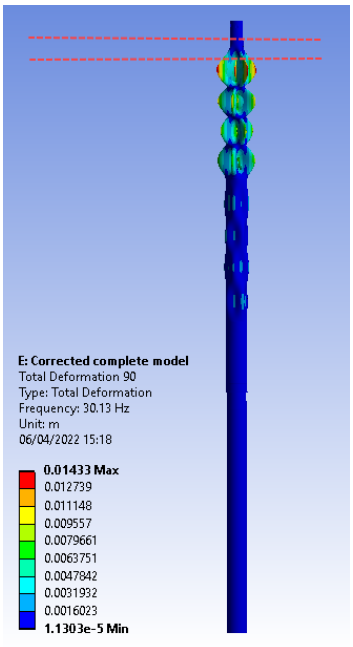

(a) Eigenmode 90

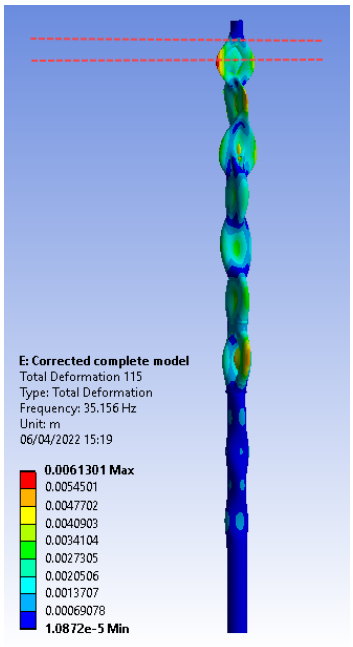

(b) Eigenmode 115

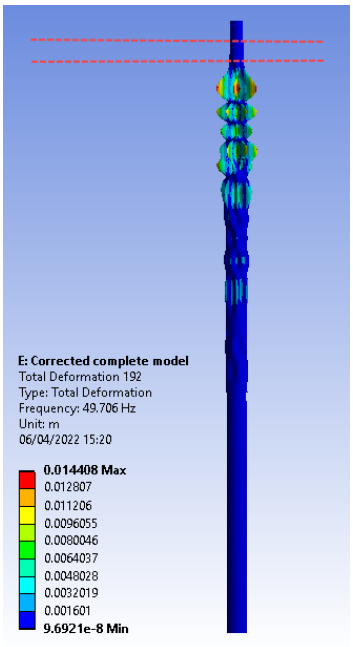

(c) Eigenmode 192

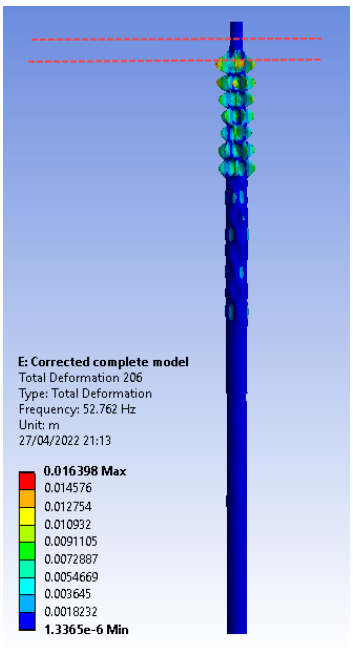

(d) Eigenmode 206

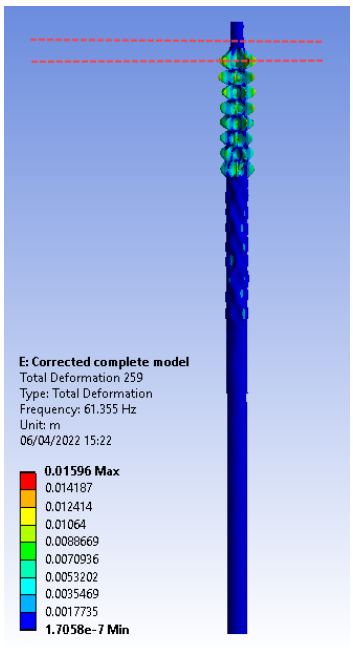

(e) Eigenmode 259

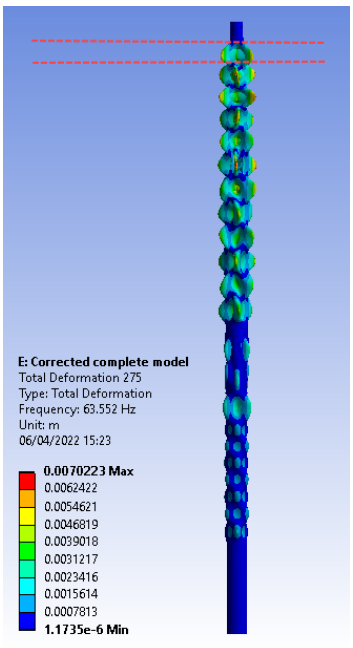

(f) Eigenmode 275

Figure A.11: Upper slip joint: modes of interest 7-12

A.7 Matched modes - Removing the pressure ring

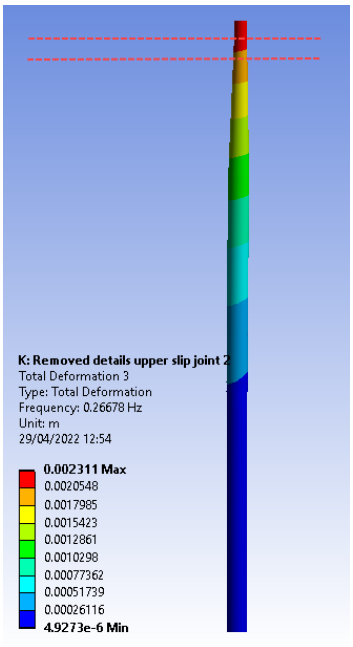

(a) Eigenmode 3

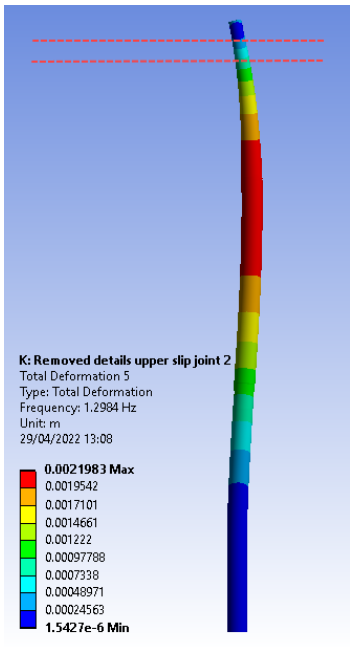

(b) Eigenmode 5

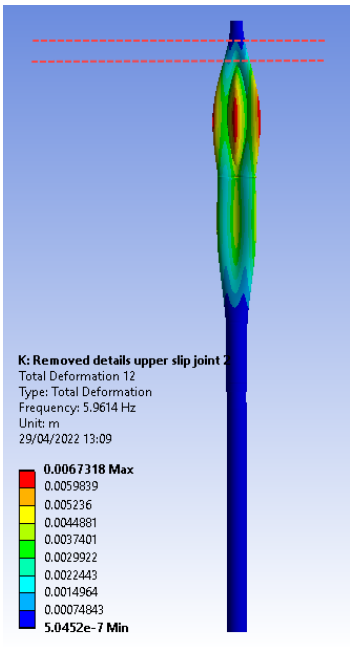

(c) Eigenmode 12

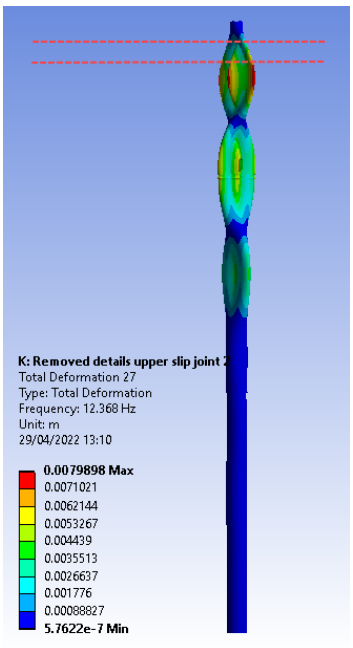

(d) Eigenmode 27

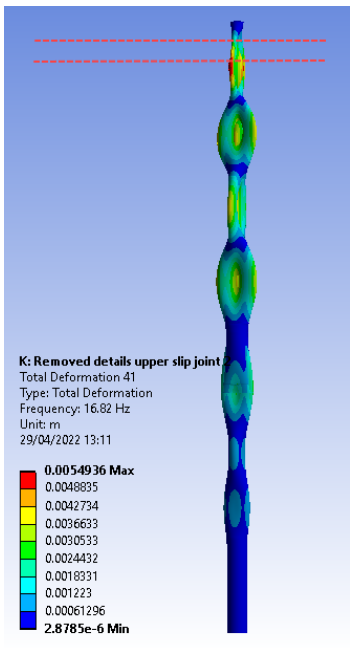

(e) Eigenmode 41

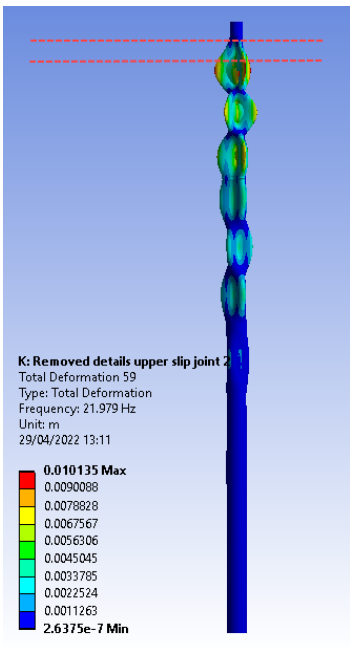

(f) Eigenmode 59

Figure A.12: Removing the pressure ring: matched modes 1-6

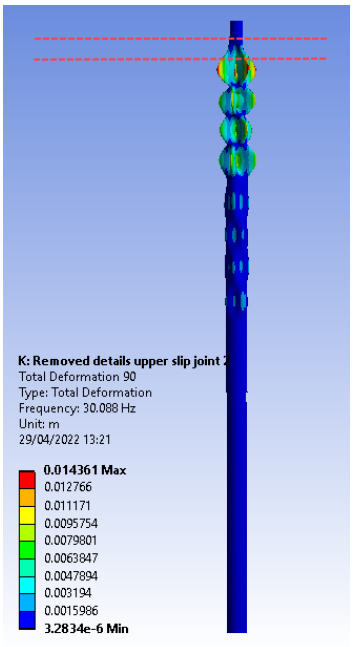

(a) Eigenmode 90

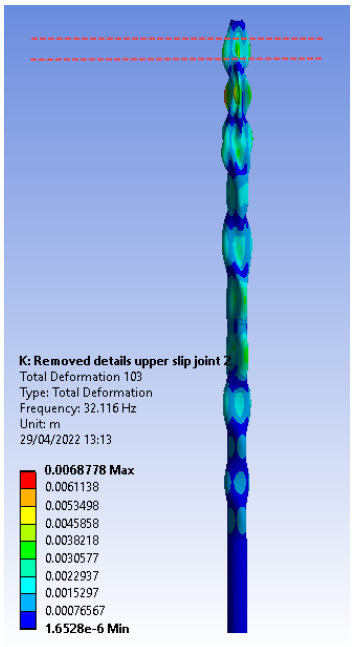

(b) Eigenmode 103

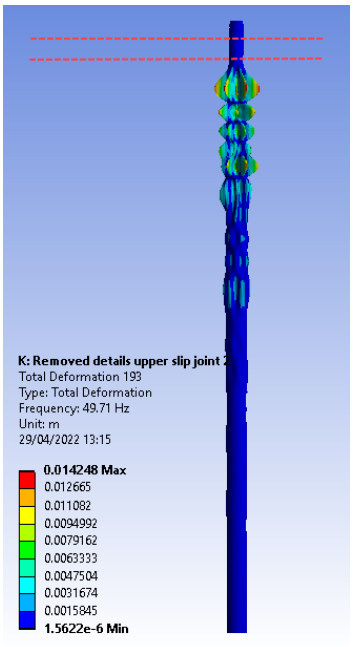

(c) Eigenmode 193

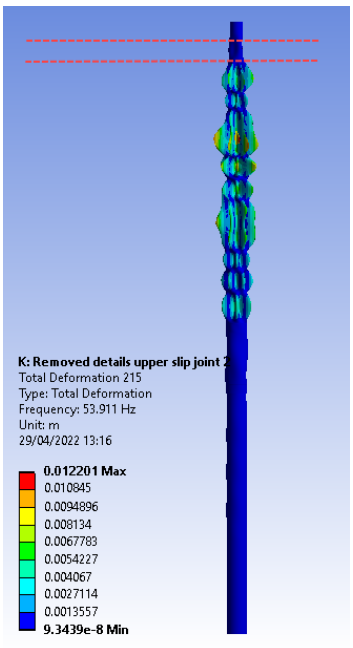

(d) Eigenmode 215

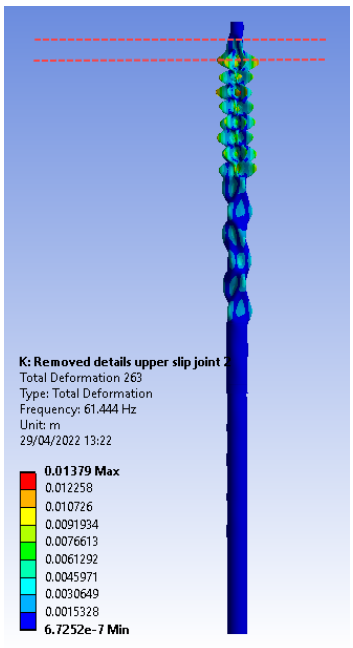

(e) Eigenmode 263

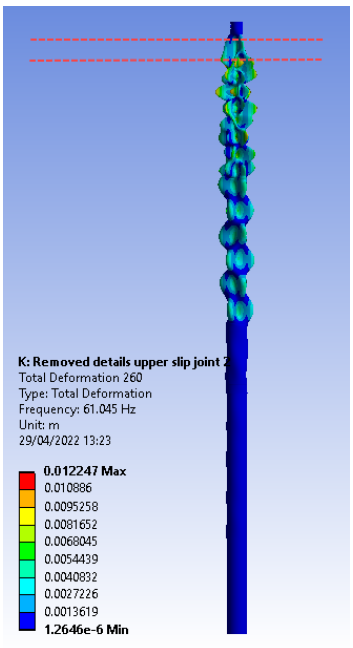

(f) Eigenmode 260

Figure A.13: Removing the pressure ring: matched modes 7-12

A.8 Matched modes - Simple upper slip joint

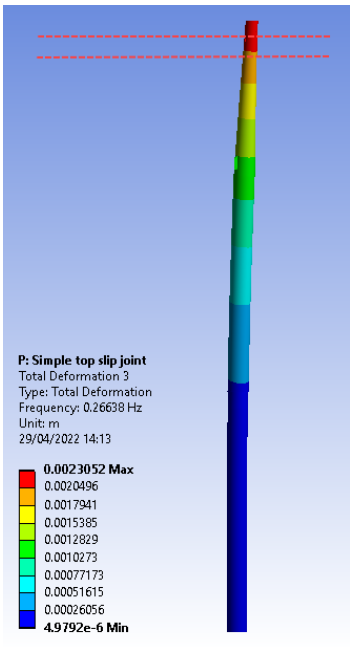

(a) Eigenmode 3

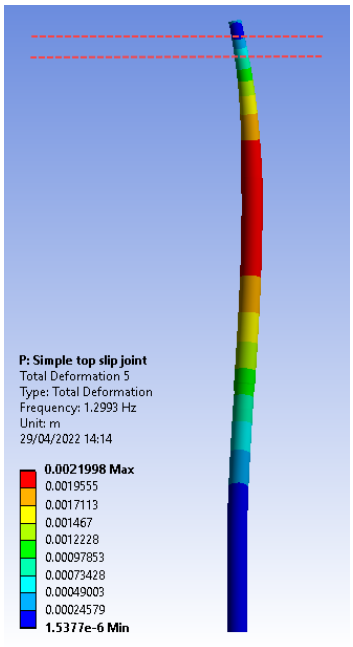

(b) Eigenmode 5

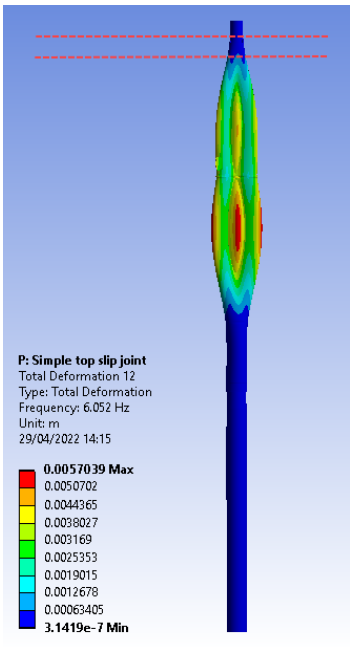

(c) Eigenmode 12

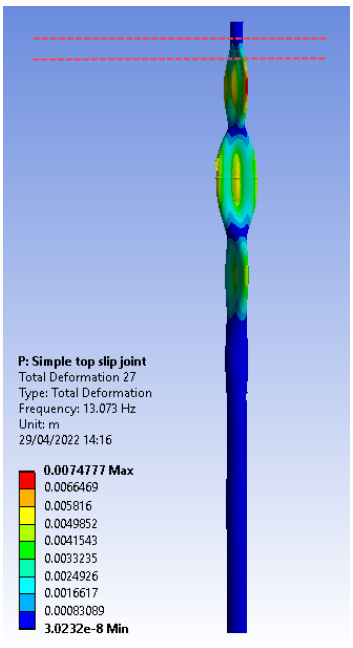

(d) Eigenmode 27

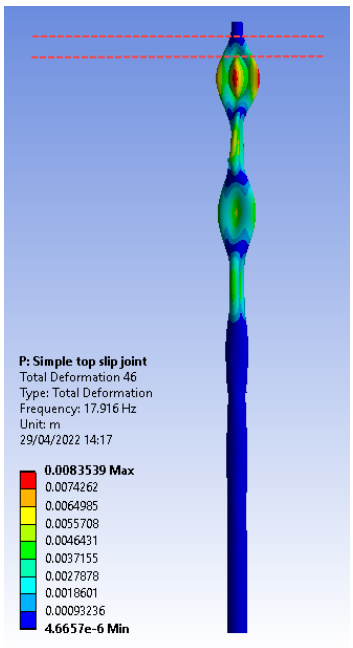

(e) Eigenmode 46

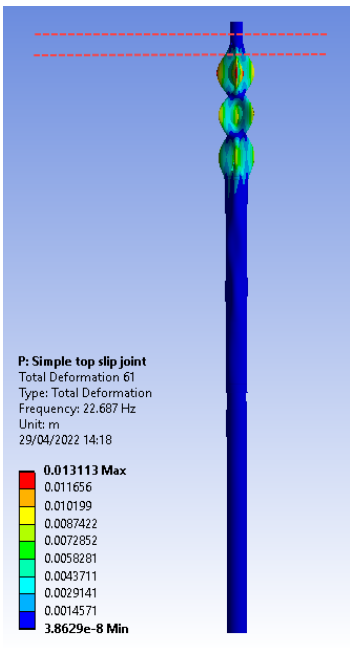

(f) Eigenmode 61

Figure A.14: Simple upper slip joint: matched modes 1-6

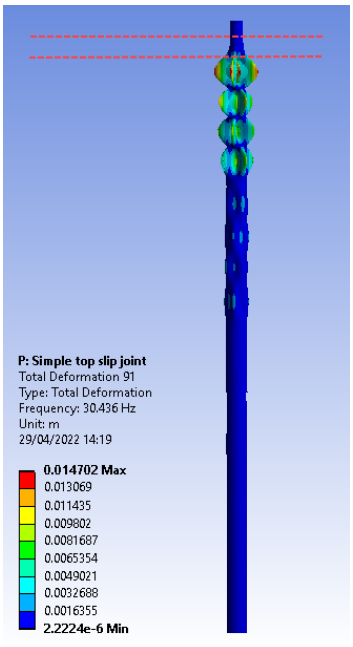

(a) Eigenmode 91

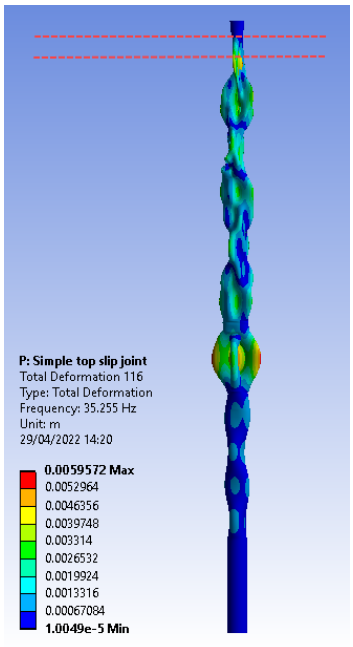

(b) Eigenmode 116

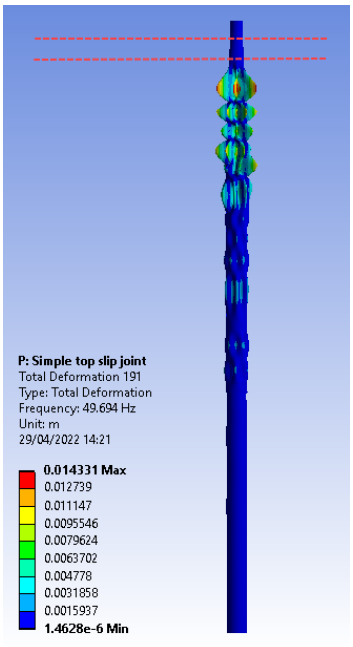

(c) Eigenmode 191

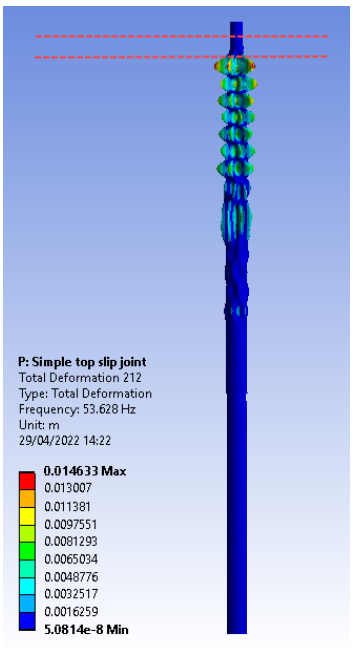

(d) Eigenmode 212

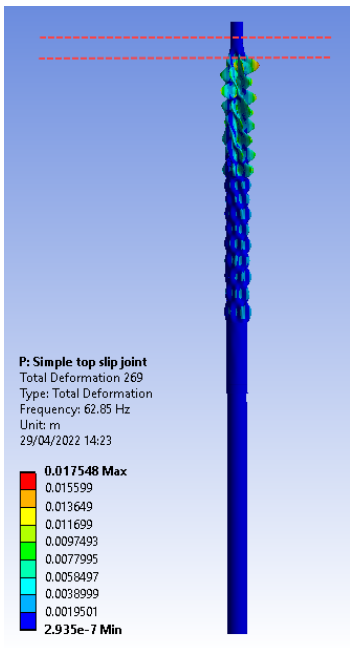

(e) Eigenmode 269

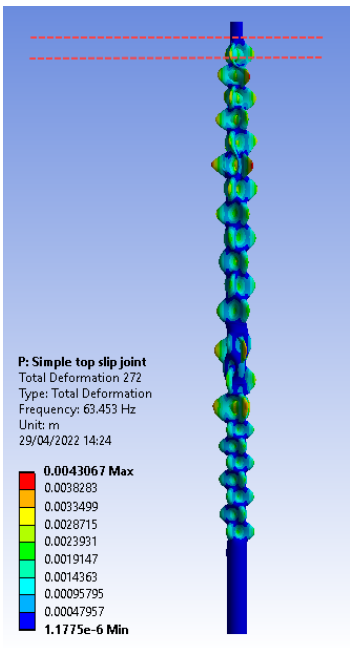

(f) Eigenmode 272

Figure A.15: Simple upper slip joint: matched modes 7-12

A.9 Matched modes - Average wall thickness - Lower slip joint

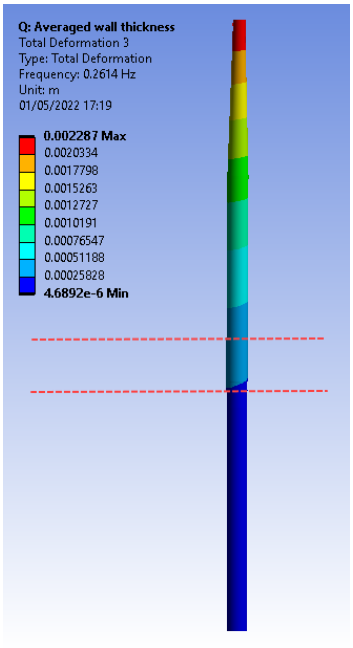

(a) Eigenmode 3

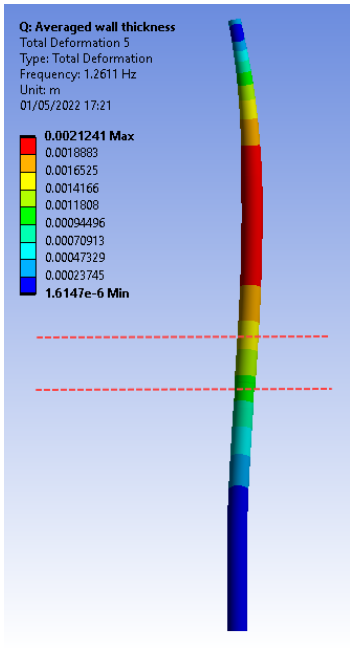

(b) Eigenmode 5

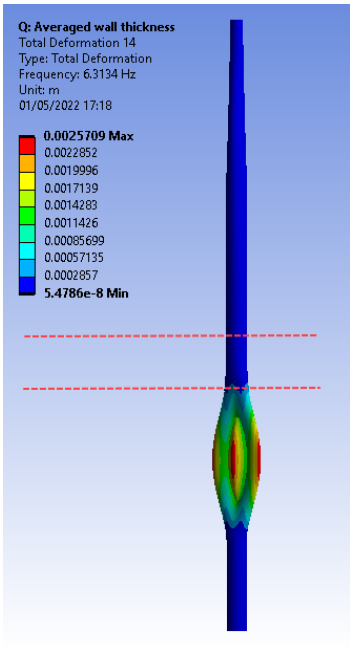

(c) Eigenmode 14

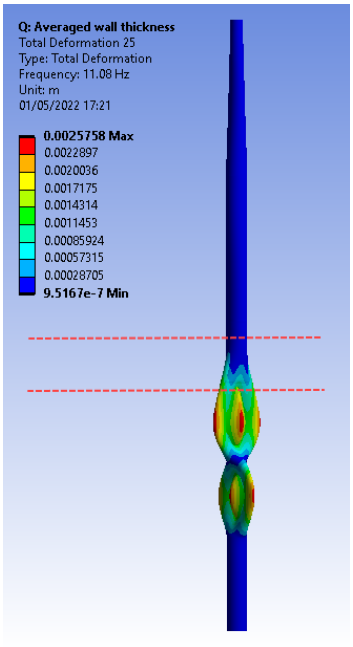

(d) Eigenmode 25

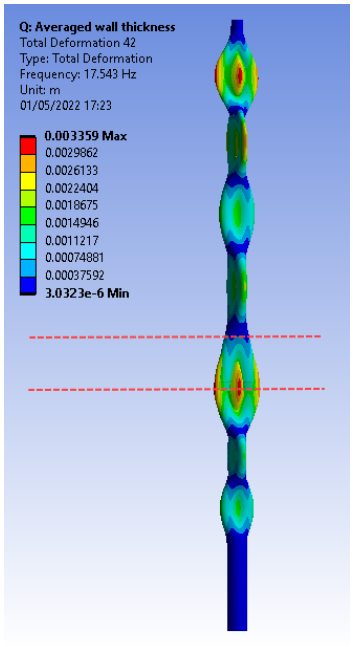

(e) Eigenmode 42

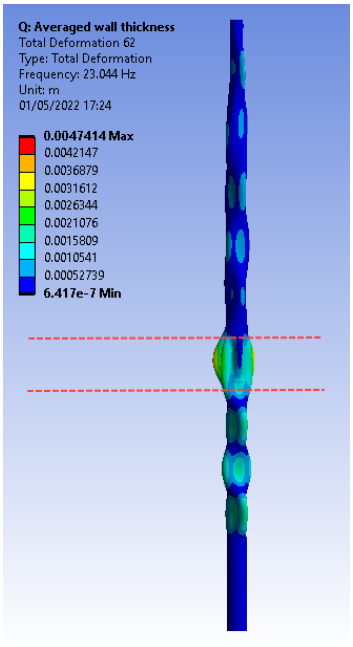

(f) Eigenmode 62

Figure A.16: Average wall thickness, Lower slip joint: matched modes 1-6

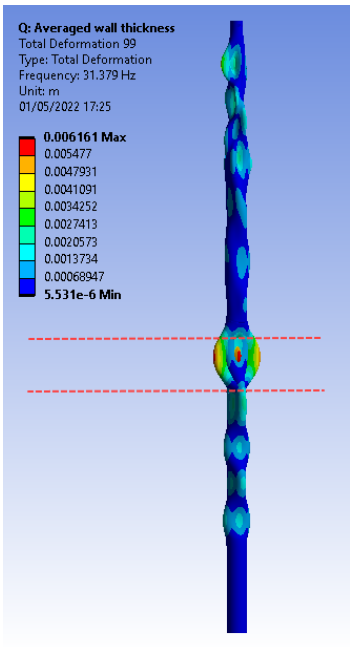

(a) Eigenmode 99

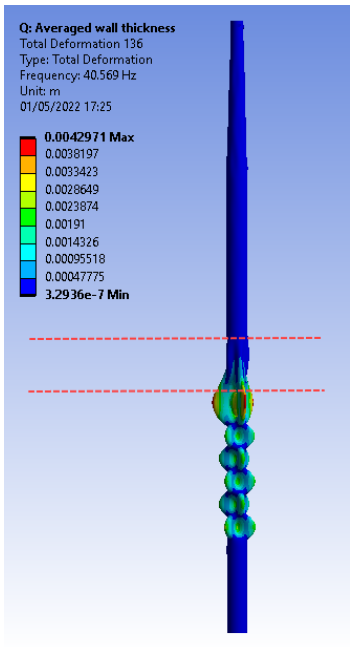

(b) Eigenmode 136

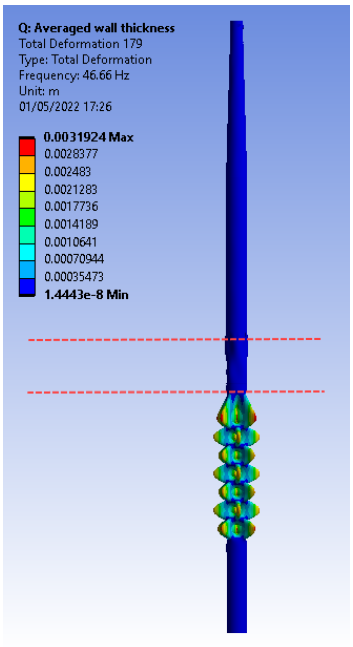

(c) Eigenmode 179

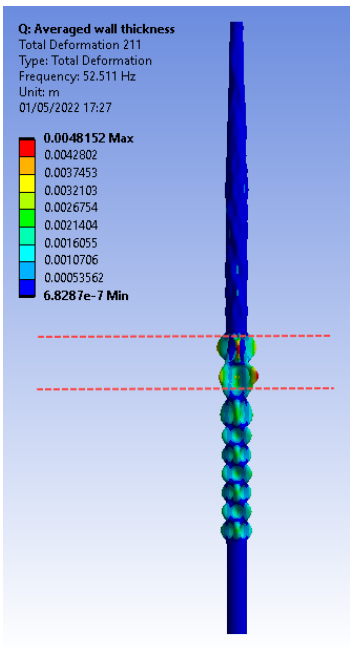

(d) Eigenmode 211

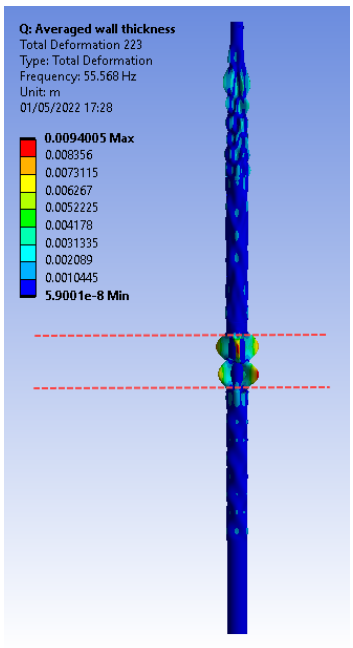

(e) Eigenmode 223

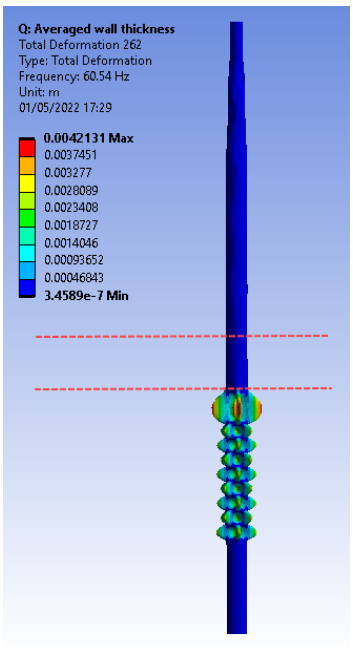

(f) Eigenmode 262

Figure A.17: Average wall thickness - Lower slip joint: matched modes 7-12

A.10 Matched modes - Average wall thickness - Upper slip joint

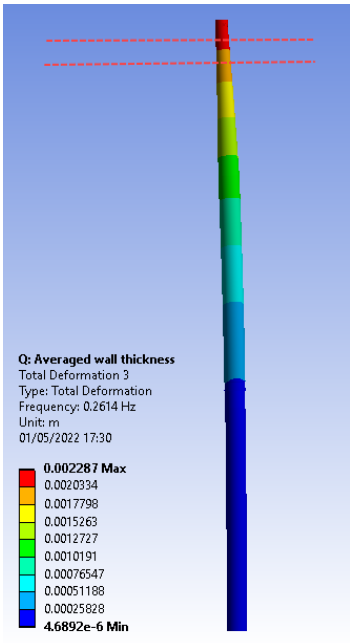

(a) Eigenmode 3

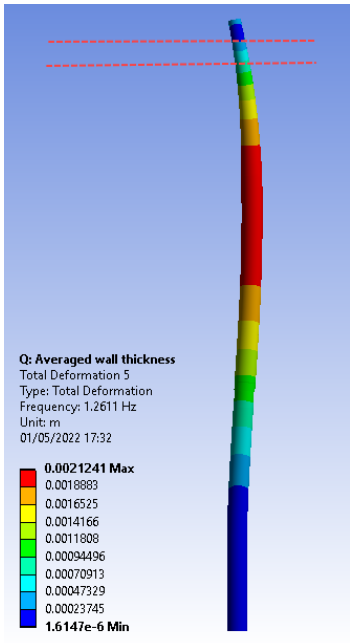

(b) Eigenmode 5

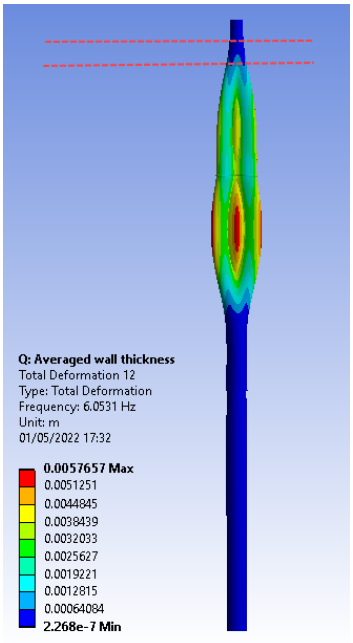

(c) Eigenmode 12

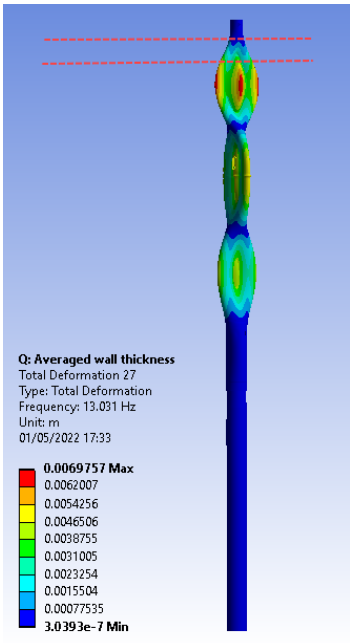

(d) Eigenmode 27

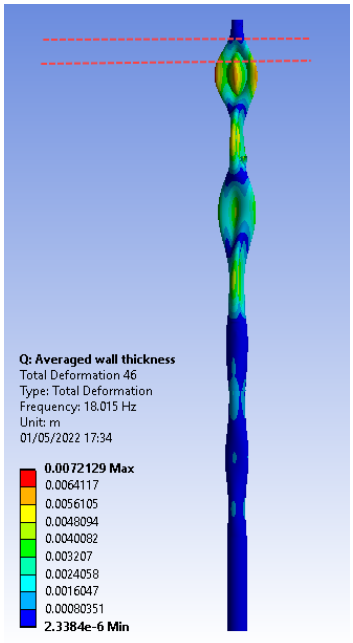

(e) Eigenmode 46

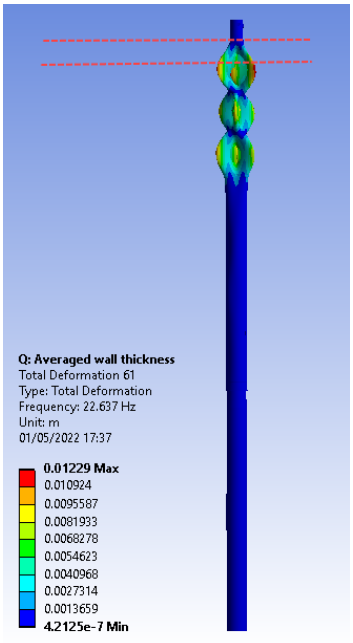

(f) Eigenmode 61

Figure A.18: Average wall thickness - Upper slip joint: matched modes 1-6

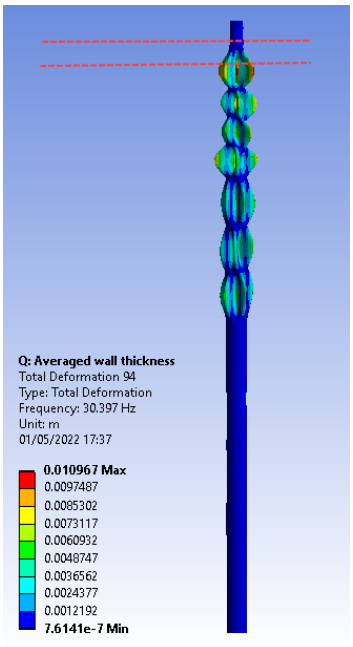

(a) Eigenmode 94

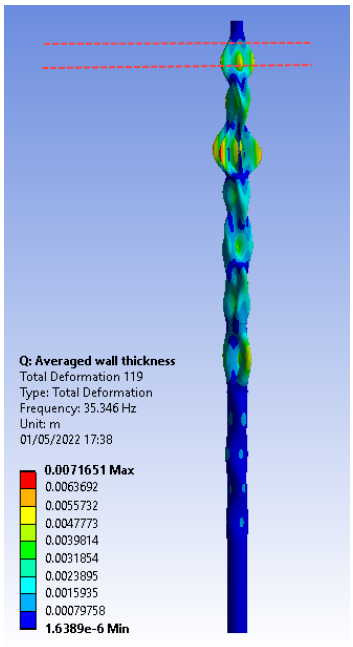

(b) Eigenmode 119

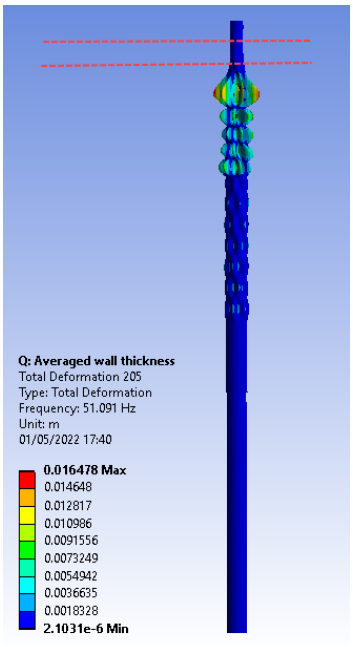

(c) Eigenmode 205

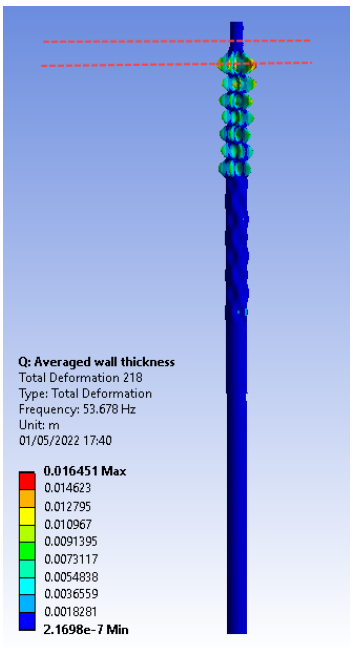

(d) Eigenmode 218

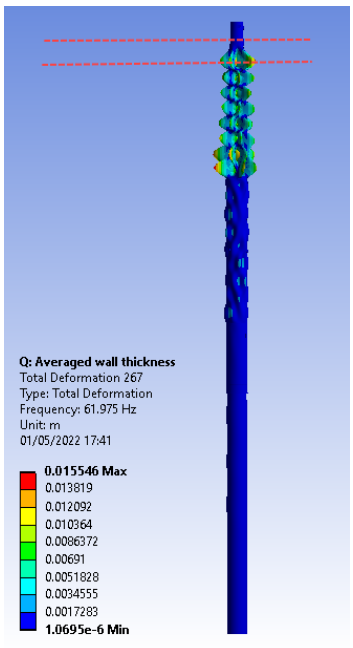

(e) Eigenmode 267

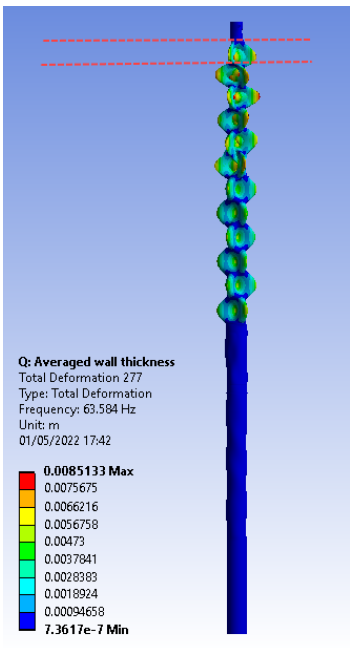

(f) Eigenmode 277

Figure A.19: Average wall thickness - Upper slip joint: matched modes 7-12